POLITECNICO
MILANO 1863

SCUOLA DI INGEGNERIA INDUSTRIALE
E DELL'INFORMAZIONE

Dual Modulator based SSB Transmitter for Optical Metro and Access Networks

Tesi di Laurea Magistrale in
Telecommunication Engineering - Ingegneria delle Telecomunicazioni

Author: **Stefano Gaiani**

Student ID: 970290
Advisor: Prof. Pierpaolo Boffi
Co-advisors: Prof. ssa Paola Parolari, Prof. Alberto Gatto
Academic Year: 2021-22

Abstract

During the last years we are witnessing a huge traffic increase in the metro and access network, so it is fundamental to adopt new technological approaches able to properly manage the data flux. At the same time, one wants to minimize costs, energy consumption and complexity as much as possible. For this reason, the research has focused its attention in finding solutions that guarantee high performance with simple implementation.
In this thesis work we initially introduced the most interesting of simplified solutions available in the literature to increase the performance in terms of capacity and reach for metro and access network applications. Then, we focused on the so called dual modulator scheme and we performed a deep and detailed analysis. This approach is very simple, since it is composed by the cascade of a Directly Modulated Laser (DML) and an intensity modulator. However, we believe that the dual modulator presents big potentials: it is versatile, it is suitable for the multicarrier modulation (such as DMT) employment and for the generation of Single-Sideband signals (more robust to the chromatic dispersion accumulated during the fiber propagation) and it allows to reduce cost, energy consumption, complexity and bulk. The main dual modulator architecture developed in literature is constituted by a DFB combined with an Electro-Absorption Modulator (EAM). Nevertheless, we propose an interesting alternative exploiting the VCSEL as a coherent light source, having comparable quality to the DFB, but reduced cost and consumption, and a Mach-Zehnder (MZ) modulator that, in the proper conditions, works better than an EAM.
For this reason, in this work we discuss this new proposal in detail, starting from a theoretical point of view and then simulating its performance. This latter one is divided into a signal generation part and a signal detection part and, in doing so, we have compared the different realizations achieved with VCSEL and DFB as source, and EAM and MZ as modulator. This investigation is based on a simulator developed in Matlab®, where we tried to set as much degrees of freedom as possible for all the signal aspects (generation, propagation and detection). The simulative results confirm the effectiveness of the proposed dual modulator realized by means of VCSEL and MZ to improve the performance and increase the transported capacity in typical metro and access network applications.

Keywords: Metro and access network, Directly Modulated Laser (DML), Dual modulator, SSB signals, Amplified and un-compensated networks

Abstract in lingua italiana

Negli ultimi anni si sta assistendo ad un enorme incremento del traffico dati sulla rete metro e di accesso, quindi è necessario adottare nuovi approcci tecnologici che riescano a gestire il flusso di dati a dovere. Allo stesso tempo, però, si vogliono minimizzare i costi, i consumi, l'ingombro e la complessità il più possibile. Per questo motivo, la ricerca si è concentrata nel cercare delle soluzioni che garantiscano prestazioni elevate con una semplice implementazione.
In questo lavoro di tesi andiamo inizialmente a introdurre le proposte più interessanti presenti in letteratura per migliorare le prestazioni delle reti metro e di accesso in termini di capacità e distanza. Dopodichè, passiamo ad un'analisi più profonda e dettagliata della soluzione basata sul cosiddetto modulatore duale, il quale è un'architettura molto semplice composta dalla serie di un Laser Direttamente Modulato (DML) e un modulatore di intensità (IM). Questo approccio è molto allettante perchè esso è versatile, è adatto all'uso di modulazioni multicarrier (come per esempio DMT) e alla generazione di segnali Single Sideband (SSB) (particolarmente robusti alla dispersione cromatica associata alla propagazione in fibra) ed è in grado di abbattere costi, consumi, complessità ed ingombro. Il modulatore duale principalmente sviluppato in letteratura è costituito da un laser DFB seguito da un Modulatore a Elettro-Assorbimento (EAM) . Tuttavia, noi proponiamo un'alternativa che sfrutta un VCSEL, sorgente di qualità comparabile ad un laser DFB ma molto più piccola ed innovativa, e un modulatore Mach-Zehnder che, nelle opportune condizioni, lavora meglio di un EAM.
In questo lavoro abbiamo discusso in dettaglio questa nuova proposta, partendo da un approccio teorico e poi passando ad uno studio delle sue prestazioni. Quest'ultimo è suddiviso in una parte relativa alla generazione del segnale e una relativa alla rivelazione ed è stato fatto un confronto approfondito tra varie soluzioni basate su VCSEL o DFB come DML e su EAM o MZ come IM. Tutto ciò è stato possibile grazie allo sviluppo di un simulatore Matlab® che concedesse una certa libertà di scelta per quanto riguarda generazione, propagazione e rivelazione del segnale. I risultati simulativi confermano l'efficacia del modulatore duale proposto VCSEL-MZ per migliorare le prestazioni e aumentare la capacità e la distanza raggiungibile in tipiche applicazioni per la rete metro e d'accesso.

Parole chiave: Network metro e di accesso, Laser Direttamente Modulato (DML), Modulatore duale, Segnali SSB, Network amplificati e non-compensati

Contents

Introduction

The optical network is a reality that has strongly developed during the last couple of decades and it has more or less completely replaced the copper wires technology in the wired communications context. Such big success has been possible thanks to the continuous technological progresses and to the innovations in various fields, above all optical fibers, photonic devices, optoelectronic devices and electronic hardwares. Within the optical network, we can distinguish two main levels:

- the core network;
- the "outer" network, this one including the metro network and the access network.

These two network types are very different one from each other and, as a consequence, require a completely different technology both at the transmission stage and at the detection stage. In particular, the technology used in the core network is much more sophisticated because of two main reasons:

- the core network must manage a huge data flow;
- it constitutes the network skeleton, so if there is a failure in the network inner part, the outer part is affected too.

For the metro and access network, instead, the technology is much simpler and limited. This happens because, at these network levels, one addresses to cities, companies and people. Therefore, the main goals to be pursued should be five fundamental "*less*":

- less energy consumption;
- less complexity;
- less bulk/occupied space;
- less resource waste;
- less cost.

There are also other similar aims that one should consider, but they are more general: these five are the most important for the metro and access network. Due to this mindset,

it's a natural consequence that the technology is more limited. At the same time, one clearly wants to maximize the performance at the metro and access level as much as possible, in order to try to get as close as possible to the core network one. This concept has become more and more a main question over time, until nowadays. In fact, we are witnessing an exponential increment of data traffic in the network at an access and metro level. This is due to the development and the diffusion of audiovisual streaming applications (*e.g* YouTube® and Netflix®) and applications with a strong "real-time" requirement to properly work (like online gaming or video calling, where the lag is really undesired). In both cases, we are speaking about data-hungry applications, which load the network with a lot of traffic. Therefore, there are two conflicting requirements: a simple, cheap and integrable technology that, however, should guarantee a high-level performance. The proposals made during the years are many and the research results are numerous and various.

In this thesis work, we are going to present and discuss the main proposals and then we will focus on an approach (called "*dual modulator*"), that looks very promising, as it is able to satisfy the five previous *less*, together with this, adds also other features that allow to obtain a capacity and reach improvement for the optical network. Since this is quite a new topic on which there is still an active research, we are going to treat a "simplified" condition, so we will work with just one optical channel (that means we won't consider the Wavelength Division Multiplexing (*WDM*) approach, even if it is extensively used nowadays in the optical network), we will use a single mode fiber, we will assume a Point-to-Point (*P2P*) link, etc... Obviously, all these new features can be introduced and studied in the future.
This essay is organized in 6 chapters as follows:

CHAPTER 1: introduction of the IM-DD system and coherent detection, discussion about all the problems related to the two solutions and finally presentation of the main performance improvement proposals for an IM-DD system found in the research bibliography.

CHAPTER 2: general analysis of the dual modulator approach for applications in IM-DD systems with brief discussions about concepts related to this device and that will be employed in the following chapters (DMT modulation, semiconductor lasers and SSB signals).

CHAPTER 3: theory development for a dual modulator structure, where will be presented the main model parameters (with their definition) and the fundamental algorithms

starting from a simple single harmonic case and then moving to a DMT signal context.

CHAPTER 4: demonstration by means of simulations of the generation algorithms previously discussed both for the single sinusoid and for the DMT signal with a comparison among different solutions.

CHAPTER 5: dual modulator application in a metro and access network level with a detailed performance evaluation for different cases and with different variables and parameters. The study is carried out with a Matlab® simulator.

CHAPTER 6: final thesis sum up, conclusions and future developments.

1 | IM-DD systems

The continuous demand for bandwidth and data rate due to data-hungry applications is stressing more and more the optical network and it can be managed just with the adequate technology. Focusing on the access and metro level, the most diffused approach for the information transmission in the current network is the so called Intensity Modulation - Direct Detection (*IM-DD*). As the name says, on the transmitter side the information is encoded through an intensity modulation (or an amplitude modulation if preferred) in the light, typically emitted by a laser . On the receiver side, instead, we have a simple direct detection process, where the light just impinges on a single-ended photodiode (*SE-PD*), which is able to convert the optical power and generate a photocurrent, that is used to recover the transmitted data with a Digital Signal Processing (*DSP*) algorithm. Examples of modulations that can be used in this context are the On-Off Keying Return-Zero and the On-Off Keying Non-Return-Zero (*OOK-RZ* and *OOK-NRZ* respectively) and the M^{th}-order Pulse Amplitude Modulation (*M-PAM*), where M is the number of symbols of the constellation. Figure 1.2a and Figure 1.2b respectively represent the constellations associated to these modulations. The big advantages of an IM-DD system are

- the extreme simplicity in the architecture and hardware implementation;
- the elements' compactness (that, in other terms, means the possibility of integration);
- the components' low cost (thanks to the large-scale production with a simple procedure);
- the low energy consumption.

On the other hand, the big problem that we have to face is that the performance of this kind of system is limited by some factors (the constituent elements bandwidth, the optical fiber dispersion, the exploitation of the only light intensity in the modulation process, etc...) and we are reaching that limit, beyond which is very complicated to get some new improvements.
Therefore, we can think to completely change the network technology in order to em-

ploy the other type of detection that is available in the today's network, as to say the coherent detection. This technology has been borrowed from the Radio-Frequency (RF) communications and it is relatively new in the optical fiber field, but the intense studies and developments have led to a reinforcement of this technique. The coherent detection is a fundamental cornerstone in the current optical network. In fact, it is used for those links that have to support and transport a huge capacity, in the order of $Tbit/s$ (these kind of connections are called backbone links or back-haul links). This result is achievable because, in the coherent detection, we can exploit all the three light degrees of freedom:

- the amplitude (or equally the intensity);
- the phase;
- the polarization.

This allows us to get a better information encoding and, consequently, a better information transmission with an equal number of optical pulses sent. The term *coherent* is not chosen casually, because it indicates that, at the receiver, we must be able to retrieve the phase of the optical signal that is received: we can use the phase in the information encoding just if we can get this information back, otherwise this operation is totally nonsense. Therefore, we cannot use the same simple receiver described for the direct detection, since a photodiode provides a quantity that is proportional just the signal power. In the receiver of a coherent detection system, instead, we must completely change our point of view: we have to think in terms of electric field (characterized by amplitude and phase). For sure, this leads to a big modification of the device. The receiver that is able to implement the desired function in the most generic way possible is called Phase Diversity - Coherent Detection (PhD-CD) receiver and its block diagram is reported in Figure 1.1a. This kind of receiver is much more complicated. In fact,

- it is able to distinguish two orthogonal polarizations;
- the number of components that must be used is much greater than what we have in a direct detection receiver;
- the signal processing after the revelation is more complex with respect to the direct detection case.

Nevertheless, this device performs much better than a simple direct receiver. For example, it allows the chromatic dispersion compensation, something that is not available in the other detection case. Even more important, we can employ complex modulations, where the term *complex* means that, in a Gauss plane, the constellation symbols don't lie anymore just on the real axis, but they have both a real and an imaginary part. Examples

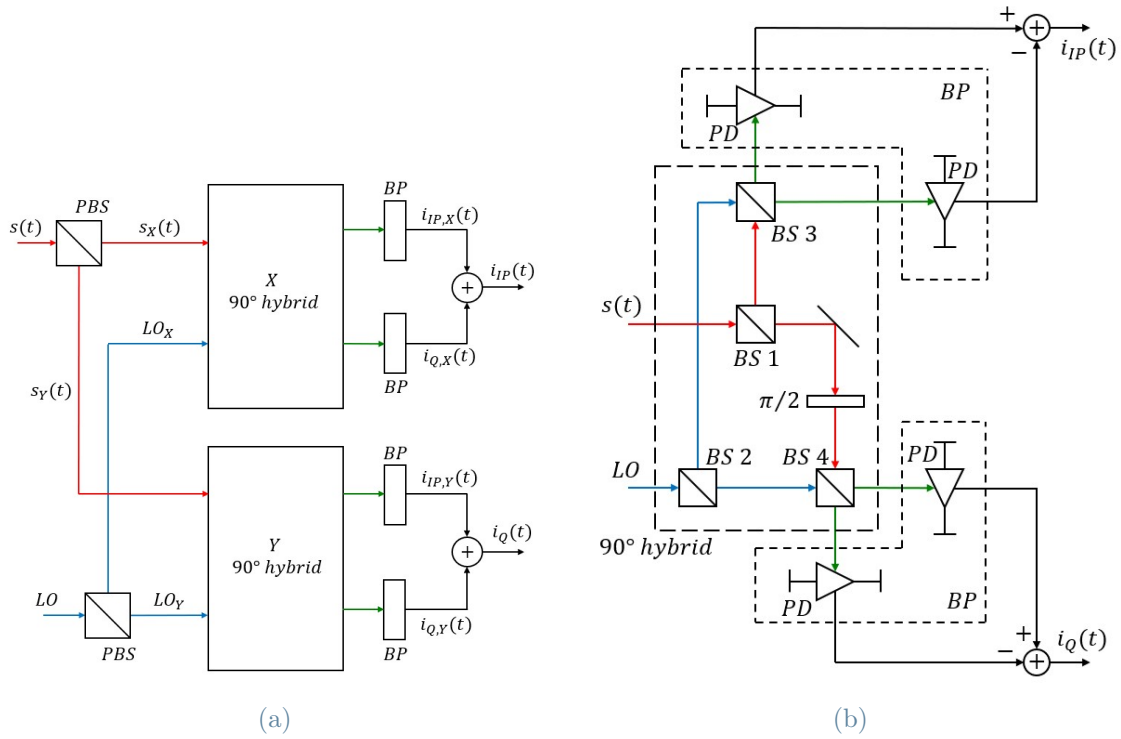

Figure 1.1: ***(a)*** *Block diagram of a Phase Diversity - Coherent Detection receiver;* ***(b)*** *Implementation of a 90°-hybrid and balanced photodiodes (PD = SE-PD).*
Red lines are associated to the signal; Blue lines are associated to the LO; Green lines are associated to the mixed light.

of such modulations are the M^{th}-order Phase Shift Keying (*M-PSK*) and the M^{th}-order Quadrature Amplitude Modulation (*M-QAM*) (examples of constellations associated to these kind of modulations are represented in Figure 1.2c and Figure 1.2d respectively). This is possible considering that, as we said, the main function carried out by a coherent detection receiver is the phase recovery of the signal electric field and the blocks involved in this operation are the *90°-hybrid* (which is in turn constituted by other elements) and the Local Oscillator (*LO*). The LO is a high power laser that works in the Continuous Wave regime (*CW regime*). Figure 1.1b, instead, shows the implementation of the 90°-hybrid and we see that it basically consists of four Beam Splitters (*BS*) and a $\pi/2$ waveplate. The BSs are needed to split in two equal contributions both the incoming signal and the LO (BSs 1 and 2) and then to mix them (BSs 3 and 4). In this way, there is a beating between the LO and the signal that reinforces the signal itself. Using this procedure, we would get just the In-Phase (*IP*) component of the signal (at BS 3), but we wouldn't have any information on the Quadrature (*Q*) component. However, here is where the wave-plate becomes fundamental: it introduces a $\pi/2$ phase shift to one of the signal replicas

coming out from BS 1, so that the beating occurring at BS 4 is now between the LO and the signal Q-component and this allows to recover this signal contribution. After the two mixings, the results are detected not by a SE-PD, but by a Balanced Photodiode (*B-PD*). The structure of such element is shown again in Figure 1.1b and it is quite simple: there are just two SE-PDs that collect the mixed light coming out from the two output ports of BSs 3 and 4. Nevertheless, because of a property of the BS as device, these outputs exhibit a π phase shift. Therefore, when we sum the two generated photocurrents, we obtain the cancellation of the DC component, which doesn't contain any information. So, we basically obtain a photocurrent around the zero mean value and proportional to the incoming optical signal. Then, the photocurrents for the IP and Q components are used in the following receiver DSP to recover the information carried by the optical signal. The PhD-CD receiver allows to apply all this procedure at the same time to a couple of orthogonal polarizations (for example the vertical and the horizontal ones), as the device includes two Polarizing Beam Splitters (*PBS*). A PBS can be modelled as a 4-port optical circuit (two input ports and two output ports) that is able to separate two orthogonal polarizations, sending them to the two different outputs. So, if we separate the X-component and the Y-component of the field both for the signal and for the LO, we can retrieve the phase of the two polarizations separately and, consequently, improve the system performance. However, note how many components we have introduced during this description of the PhD-CD receiver, which implies cost, complexity, impossibility on integration (especially PBSs are very bulky elements) and high energy consumption. Moreover, the phase recovery requires a phase locking operation for the signal optical carrier, that can be very complicated to be realised.

Considering that at a metro and, above all, access level one must address directly to customers (companies and common people), all these negative characteristics have restrained the access and metro optical network development towards coherent detection and the approach that is still implied in most of the case is the IM-DD one. On the other side, as we said, we must face a performance limitation problem. For this reason, people have recently started to carry out studies aimed at joining the great simplicity of an IM-DD scheme with the performance associated to coherent detection, in order to improve the performance of such system. During the last years, lots of research branches have been followed and the produced bibliography is extremely rich (obviously some fields have been studied more extensively than others). The two main courses of action taken in the research have been focused one side on a simplification/improvement at a structural level (that means acting on components) for transmitter and receiver and, on the other side, on an algorithm research at a DSP level (especially for the receiver). Obviously, some approaches have been focused on the first task, some others on the second task and

yet others on both of them, but the final objective has always been the improvement of an IM-DD system performance. In the following sections, we are going to examine the various proposals that, to our mind, are the most interesting ones.

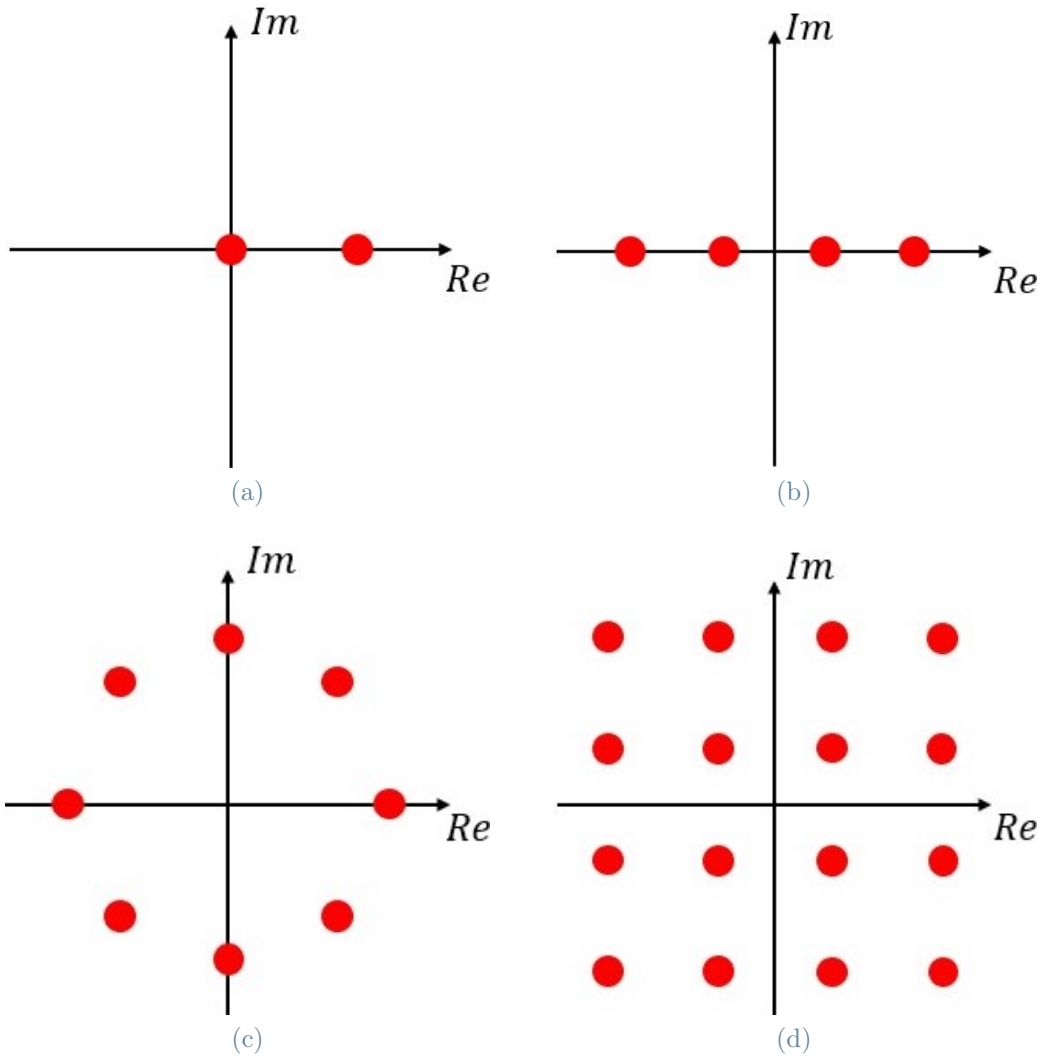

Figure 1.2: *Modulation constellations for* ***(a)*** *OOK (both RZ and NRZ),* ***(b)*** *4-PAM,* ***(c)*** *8-PSK,* ***(d)*** *16-QAM.*

1.1. Transmitter simplification

For what concerns the transmitter side, the research has been mainly working on the components of the transmitting device and on a DSP manipulation of the transmitted signal. The starting point is constituted by a transmitter able to generate a signal with both an IP component and a Q component for sure and then, if possible, able to work with

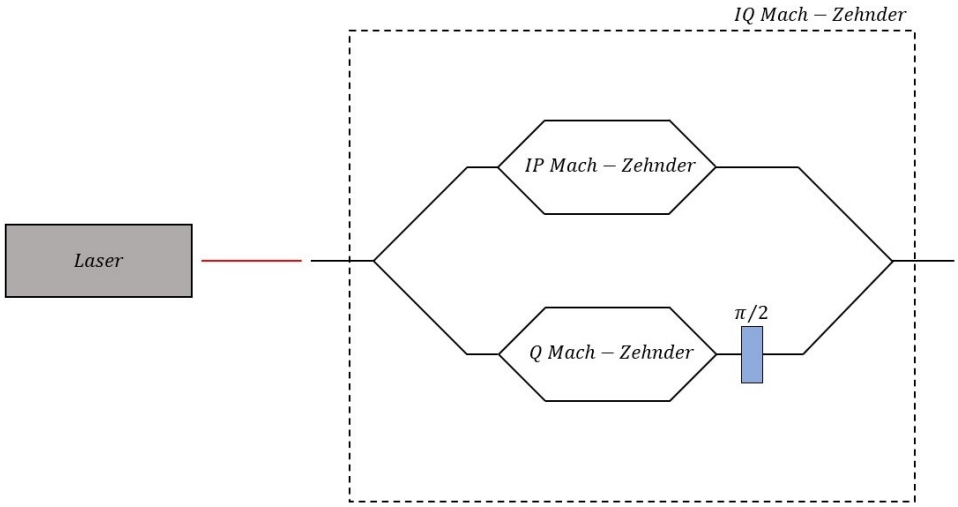

Figure 1.3: *Example of single polarization IQ transmitter for an IM-DD system.*

two orthogonal polarizations. Considering, for sake of simplicity, the single polarization case, the typical structure of a transmitter for a coherent detection system is shown in Figure 1.3. The device is made by two elements. The first one is a laser, which acts as a high coherence light source at the desired wavelength (ordinarily 1.55 μm) and works in the CW regime. For this reason, we have an Externally Modulated Laser (*EML*), which means that the laser light is modulated by a second device and not directly by the laser itself. This element is an external light modulator, that, in the most generic case possible, is both an amplitude modulator and a phase modulator and it is able to realize the symbols of a complex modulation constellation (like a M-QAM one). A traditional example of such device is the IQ Mach-Zehnder (*MZ*) modulator, which exploits two nested MZ modulators to produce both an IP and a Q component for the signal electric field. As much as the performance of this device is very good, we have exactly the same problems highlighted before, so cost, bulk, integration impossibility and energy consumption. Moreover, if we want to exploit two orthogonal polarizations, we have to use another identical device and this makes things even worse. Recently, lots of proposals have been promoted to improve the situation and, among all of them, we think that the most interesting ones are

- the use of Directly Modulated Lasers;
- the introduction of coding and pre-coding;
- the exploitation of Electro-Absorption Modulators.

1.1.1. Directly Modulated Lasers

The usage of Directly Modulated Lasers (*DMLs*) in transmitters certainly represents a very big system simplification, since part of the light modulation (so part of the information encoding) can be assigned to the laser. As a consequence, at least potentially, we can avoid to exploit complicated external modulators, like the previous IQ MZ modulator. As we will discuss in Section 2.2, the lasers used in the optical communications are semiconductor lasers, because they are technologically advanced devices and they are very tiny, so they can be easily integrated on a chip. This means that the laser direct modulation is obtained through the bias current modulation (Subsection 2.2.1). The introduction of a DML at the transmitter brings a lot of interesting advantages about:

- it reduces the cost of the device;
- it reduces the energy consumption;
- it shows lower Insertion Loss (*IL*) with respect to an EML, which means a lower light wastefulness.

These pros are accompanied by the fact that a DML is, in a certain sense, the natural choice for the transmissions based on a pure amplitude modulation (OOK, M-PAM, etc...). In fact, we can adjust the power level at the laser output depending on the symbol just with a simple modulation of the bias current, so without any external modulator. Finally, a DML is quite adaptable, because it can work both with single-carrier modulations and with advanced modulations. However, we must consider the topic in its entirety. First of all, we have to understand if a DML can be suitable to work with complex modulations (M-PSK, M-QAM, etc...). Then, we have to keep into account that the operation regime of a DML is very different with respect to the CW regime of an EML. This aspect requires a deep analysis, that will be developed in Subsection 2.2.1. The DML introduction proposal has been quite successful during the years: the bibliography regarding this solution is very rich ([1]-[12]. In all these studies, the DML employment is justified in the same way that we have just done, but then the proposals are the most different.

1.1.2. Coding and pre-coding

Another research field that has been developed is the use of coding and pre-coding at the transmitter side. The difference between the two terms is very subtle. With coding we mean an operation where the signal that we want to send is basically not modified: at most it goes through operations like a sign change or a complex conjugation, which

change the signal but its structure and shape stay unvaried. With pre-coding, instead, we mean the application of a certain algorithm to the signal, that emerges with a certain transformation in its shape with respect to the input. However, in order to obtain some results in this sector, people have tried to borrow the concepts from other fields, like the RF communications.

In this sense, the main example is for sure the proposal of the Alamouti coding employment ([14]-[16]). In this working scheme we use one possible couple of orthogonal polarizations (for example horizontal and vertical polarizations) to transmit two replicas of two signals $s_1(t)$ and $s_2(t)$ at two different time instants t_1 and t_2. The replicas differ just for small details, like a complex conjugate operation. Then, at the receiver we have the reconstruction of the two signals at the end of the second detection using appropriated algorithms. This proposal is very interesting for sure, because the receiver able to recover the information is much simpler than the PhD-CR receiver, both in terms of elements (number and size) and in terms of DSP. Moreover, this coding can be realized both in the time domain and in the frequency domain. In this latter case, the two time instants are substituted by two frequencies f_1 and f_2, possibly orthogonal to avoid any interference. Finally, the Alamouti coding is quite flexible, as it can be used in several contexts without any particular issue. However, we have also to say that this algorithm introduces a 50% redundancy in transmission (that means inefficiency) and the receiver still has its own LO (that means energy consumption).

In the same way, another algorithm studied for applications in the optical network is the Discrete Fourier Transform-Spread (*DFT-Spread*) pre-coding. This approach is mainly used in the contest of advances orthogonal modulations like the Discrete Multi-Tone (*DMT*) modulation (sometimes also named Orthogonal Frequency Division Multiplexing, *OFDM*) ([12], [13]). We will discuss DMT and its generation procedure in Section 2.1 and Section 3.2. For the moment, it is important to know just that a symbol for such modulation is generated starting from a vector in the frequency domain. Usually, this vector is passed in the time domain though the Fourier transform and the result of this operation is the signal to be transmitted. In the DFT-Spread pre-coding, instead, before this passage we apply a matrix transformation to the frequency vector, which modifies it and, in turn, the time domain signal. The matrix elements are pure phase terms and represent the sinusoids of a Fourier series (hence the algorithm name). The most important advantage is that the resulting time signal shows a lower Peak-to-Average Power Ratio (*PAPR*) with respect to the basic case, that is the signal power peaks are less accentuated with respect to the signal average power. This signal change carries lots

of advantages, among which we have

- a better working condition for the electrical amplifiers at the transmitter side, which results into a lower energy consumption and a better efficiency;
- a lower impact of non-linear effects (like the Kerr effect and the Raman scattering) during the signal propagation along the optical fiber.

Together with the DFT-Spread algorithm, we can cite another pre-coding technique called Orthogonal Circulant Matrix (OCT) algorithm ([12]). Conceptually speaking, this method is absolutely similar to the DFT-Spread one. The difference is constituted just by the pre-coding matrix, which still contains pure phase terms, but they are determined following a different procedure. On one hand, the DFT and the OCT operation are an advantage, but on the other hand they mean an increased complexity of the transmitter DSP. Apart from the matrix application, the remaining part (components and procedures) of the transmission system stays unchanged in both cases.

1.1.3. Electro-Absorption Modulators

An Electro-Absorption Modulator (EAM) is an intensity modulator realized in the semiconductor technology. This element is simply a semiconductor waveguide having a $100 - 200\ \mu m$ length able to act on the incoming light amplitude/intensity. The physical effect exploited to reach this goal is the so called Franz-Keldysh effect, which is related to the electro-absorption phenomenon of a semiconductor. In a few words, it consists in a semiconductor bandgap variation depending on the applied electric field. This bandgap variation directly determines the material absorption, since the lower the bandgap is, the more electrons can be excited from the valence band to the conduction band thanks to a photon absorption. In the considered case, we can exploit this effect because an EAM

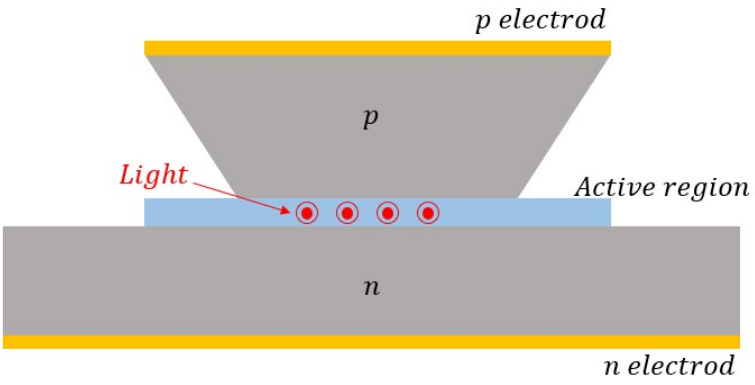

Figure 1.4: *EAM frontal section.*

is a waveguide indeed, but it is built such that we have a pn junction, as shown in Figure 1.4. Consequently, applying a suitable electrical signal (in particular a voltage signal) to the junction, we are able to control the material absorption in time. Therefore, an EAM allows to modulate the light intensity with basically a semiconductor absorption modulation and this happens with a very tiny device, a simple working principle and a very cost-effective solution. These are the main advantages that make the EAM modulator so interesting nowadays, so much so the research has concentrated on this device a lot ([2]-[10]). However, there are also some cons that will be discussed in the following chapters.

1.2. Receiver simplification

Passing now to the system receiver side, basically all the proposed solutions are concentrated on the simplification of the hardware part and a complication of the software part of the device. In particular, the first one is based on the elimination of the various PBSs and BSs, while the latter one works on the DSP after the light detection. The studies have been devoted to the development of algorithms able to combat the direct detection problems and, obviously, recover the transmitted information. In particular, the most critical aspect of the direct detection approach is the Signal-Signal Beat Interference ($SSBI$), even more than the issues pointed out in the previous discussion. The SSBI problem is caused by the beating between the signal and itself, which, with respect to the signal-carrier ones, is definitely an undesired product of the detection process. In fact, the SSBI is detrimental for the receiver sensitivity and, as a consequence, it must be limited as much as possible. Two of the earliest proposals to face this problem are the iterative SSBI-Cancellation ($SSBI$-C) algorithm and the Square-Root ($SQRT$) algorithm. The SSBI suppression performances of these algorithms are not particularly good for a certain number of reasons, which has led to the development of other procedures.

One of these algorithms is the so called Kramers-Kronig (KK) algorithm ([17]). The KK algorithm is a procedure that allows to retrieve the input signal spectrum, but this is possible just with some specific kind of signals, that are the so called Single Sideband (SSB) signals or Vestigial Sideband (VSB) signals. The SSB signal concept will be presented in Section 2.3. This algorithm is very interesting because it is extremely flexible and versatile:

- it can be used both in the single-mode transmission context and in the multi-mode transmission case, so it can operate with different kinds of optical fiber ([18]);

- speaking about the receiver structure, it can be employed both with a very simple hardware implementation (for instance, just a photodiode) and with a more complicated receiver hardware ([18]);
- it can be used with "basic" modulations, like a M-PAM ([19]), with complex modulations, like M-QAM ([11]) and with advanced orthogonal modulations, like DMT ([6]);
- it can be applied with pre-coding algorithm at the transmitter ([12]) and/or with other DSP algorithms at the receiver side ([20]);
- it allows the chromatic dispersion compensation before the detection DSP.

Along with these features, as we have said, the KK algorithm is fundamental in the detection process for high level IM-DD systems based SSB signals or VSB signals, which have attracted much attention in the last years. Unfortunately, all these nice characteristics go along with some problems. The most relevant one is for sure the upsampling operation on the detected photocurrent. This passage is necessary to recover the signal spectrum properly and it also helps in terms of noise reduction. The upsampling factor typically employed is 3, that is not very big but implies, at the same time, a superior DSP stress and more energy consumption. Another problem is that there must be a certain equilibrium between the signal power and the carrier power, otherwise the algorithm completely fails in its reconstruction task. Because of all these positive and negative features, the KK algorithm has been the subject of intense studies and developments during years. The research has been aimed exactly at the improvement of the basic procedure or, in other words, the improvement of the algorithm efficiency, even at the cost of the introduction of reasonable approximations. The focus of these advancements is an alleviation of the DSP and this has lead to several similar proposals ([21]-[24]).
Another remarkable solution is the Decomposition and Cancellation (*DCA*) algorithm ([25]). This DSP procedure is an evolution of the SQRT algorithm and, with respect to the SSBI-C algorithm and the KK algorithm, it turns out to be a low complexity algorithm without the necessity of a data upsampling and where all the SSBI contributions are considered. In [25] it is shown that this algorithm operates well, but, to be fair, the KK algorithm performs much better with equal symbol rate: the performance is comparable when the DCA algorithm symbol rate is half the KK algorithm symbol rate. Therefore, the DCA algorithm is a valid replacement of the KK algorithm for relatively low data rate links. However, the DCA performance is much better than the SSBI-C and the SQRT one, even with the same symbol rate, which makes this algorithm interesting.

Along with these solutions where we the focus has been on the software part, there have been some simplification attempts of the receiver's hardware part. Nevertheless, the research extent in this sense has been much minor than the one for the software part and, indeed, the literature regarding this filed is quite poor. In [26] we find a first attempt, but it doesn't represent a big improvement: there is a little reduction of the receiver components number, but we still have the presence of PBSs. The proposal in [27] is more interesting and is an actual implementation simplification, but the number of elements is still quite high, there is the presence of a LO (which means energy consumption) and the DSP after the signal detection is rather complex. This suggests why the research has focused more on the algorithm study than on the receiver implementation.

2 | The dual modulator scheme

Among all the proposals presented in Chapter 1, the DML employment solution is extremely interesting for what concerns the improvement of an IM-DD system transmitter, because of its versatility. In particular, one of the most relevant applications of the DML is probably as a component to build a system called dual modulator ([1]-[10]). This scheme shouldn't be confused with the dual MZ modulator. In fact, in its general structure, the dual modulator scheme is made up of a DML and an intensity modulator one cascaded to the other, as represented in Figure 2.1. The name *dual modulator* is due to the application of an electric driving signal to both elements, which results into a double light modulation. In particular, the DML serves both as light source and as phase modulator thanks to the DML frequency chirp. The intensity modulator, instead, is devoted to improve the signal amplitude modulation with respect to the one performed by the DML and, obviously, this is done by acting on the output DML optical field. In principle, we can choose whichever intensity modulator we want, while the DML is a fixed component and it is a semiconductor laser (as discussed in Subsection 1.1.1). The dual modulator architecture proposal is extremely remarkable since this device is able to satisfy all the five "*less*" pointed out in the introduction with a pretty simple structure, that is something of the utmost importance in the metro and access network. Moreover, the dual modulator approach gives a lot of freedom and it allows to exploit many solutions proposed in Chapter 1. In fact, we use a DML in place of an EML and we can generate SSB signals with a suitable procedure, which implies that there is the possibility to use a KK receiver. Along with this, we can employ the DMT modulation to transmit the information, that means a data transmission improvement. For these reasons, this chapter is devoted first to the presentation of the main concepts related to the dual modulator and then to a deeper characterization of the approach itself. More precisely, the outline of the chapter is the following one:

- in Section 2.1 we discuss the main aspects of the DMT modulation;
- in Section 2.2 we provide a general overview of the semiconductor lasers;
- in Section 2.3 we introduce the concept of SSB signal and its generation problem;

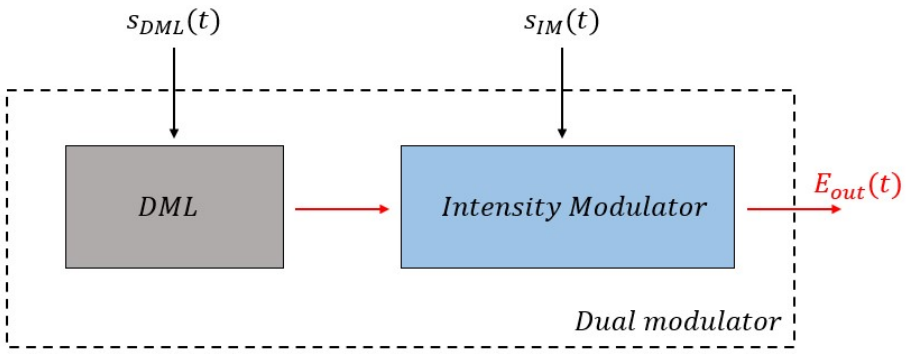

Figure 2.1: *Generic dual modulator structure.*

- in Section 2.4 we present the DML-EAM dual modulator structure and approach and we briefly discuss the results achievable with it;
- in Section 2.5 we propose the DML-MZ dual modulator, an alternative solution to the DML-EAM scheme that could be an improvement.

2.1. Discrete Multitone modulation

The Discrete Multitone (DMT) modulation is an advanced orthogonal intensity modulation format, where we exploit a space-time orthogonality to create the information signal. In particular, we divide the time axis in many time slots and, within each slot, we want to have N orthogonal sinusoids (named subcarriers) constituting N parallel channels, which do not interfere with each other, at least in principle. This leads to the generic expression of a DMT signal

$$s(t) = \sum_{l=0}^{+\infty} \sum_{k=1}^{N} a_k \, rect\left(\frac{t - T/2 - lT}{T}\right) e^{j\frac{2\pi k}{T}t} \tag{2.1}$$

where

- l is the time index;
- k is the frequency index;
- N is the total subcarriers number;
- a_k is the amplitude modulation for the $k-th$ subcarrier (typically complex and part of a M-QAM constellation);

- $rect()$ is the rectangle function;
- T is the time duration of the single DMT block/symbol.

Along with these quantities, we can introduce also the parameter $\Delta f = 1/T$, that represents the frequency gap between two consecutive subcarriers. Once we fix the time slot (so we fix the l index), the DMT symbol expression is

$$s_l(t) = \sum_{k=1}^{N} a_k \, rect\left(\frac{t - T/2}{T}\right) e^{j\frac{2\pi k}{T}t} \tag{2.2}$$

So, in the entirety we have a two-times discrete signal. It is orthogonal in time thanks to the rectangular window subdivision of the time axis. The time orthogonality and the subcarriers superposition can be seen in Figure 2.2a. On the other hand, the DMT signal is orthogonal in frequency as the subcarrier frequencies are a multiple of the fundamental Δf. This can be summarized in the expression

$$\int_0^T \phi_m(t) \cdot \phi_n^*(t)\, dt = \delta_{mn} \tag{2.3}$$

where δ_{mn} is the Kronecker's delta. A clearer idea of this concept is represented in Figure 2.2b: we can see that, where we have the peak of the cardinal sine of the $k-th$ subcarrier, the other $N-1$ cardinal sines are all equal to zero and this condition corresponds to the frequency orthogonality among the subcarriers.

These features of a DMT signal imply a lot of benefits:

- the signal bandwidth can be as large as wanted, but the various channels keep orthogonal with each other;
- the possibility of employing complex modulations, that means a higher data transmission, since both light degrees of freedom can be used to encode the information;
- it is possible to adopt the so called bit loading and power loading strategies, where the more the channel state is good for a certain subcarrier the more information and the more power one can allocate to the corresponding frequency (keeping in mind that the total power is a fixed variable). In other words, where the channel is in a bad state, we use a few power and we transmit a little information with a robust modulation (like a 4-QAM), while, where the channel is good, we use more power and we transmit the most information we can (for example, with a 64-QAM constellation). This strategy is also named Water Filling (WF) principle;

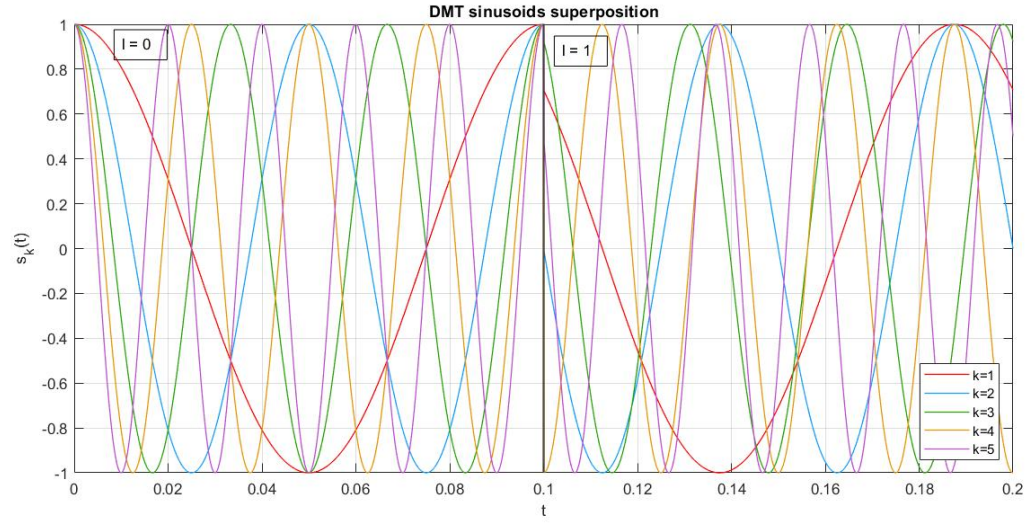

(a)

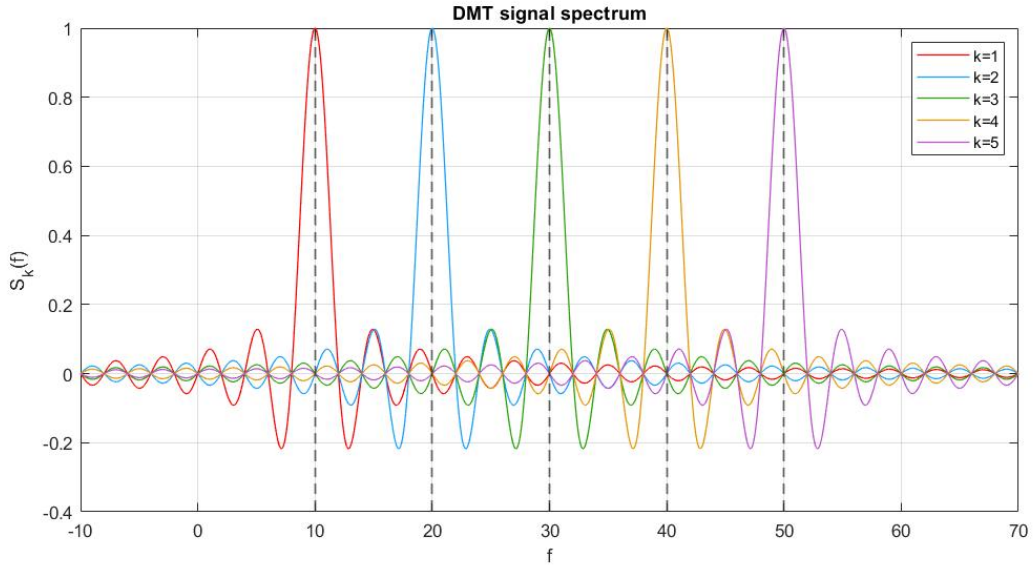

(b)

Figure 2.2: ***(a)*** *DMT time signal representation with the time slot partition for two DMT symbols;* ***(b)*** *DMT signal spectrum: the cardinal sines are due to the Fourier transform of the single block rectangle window.*

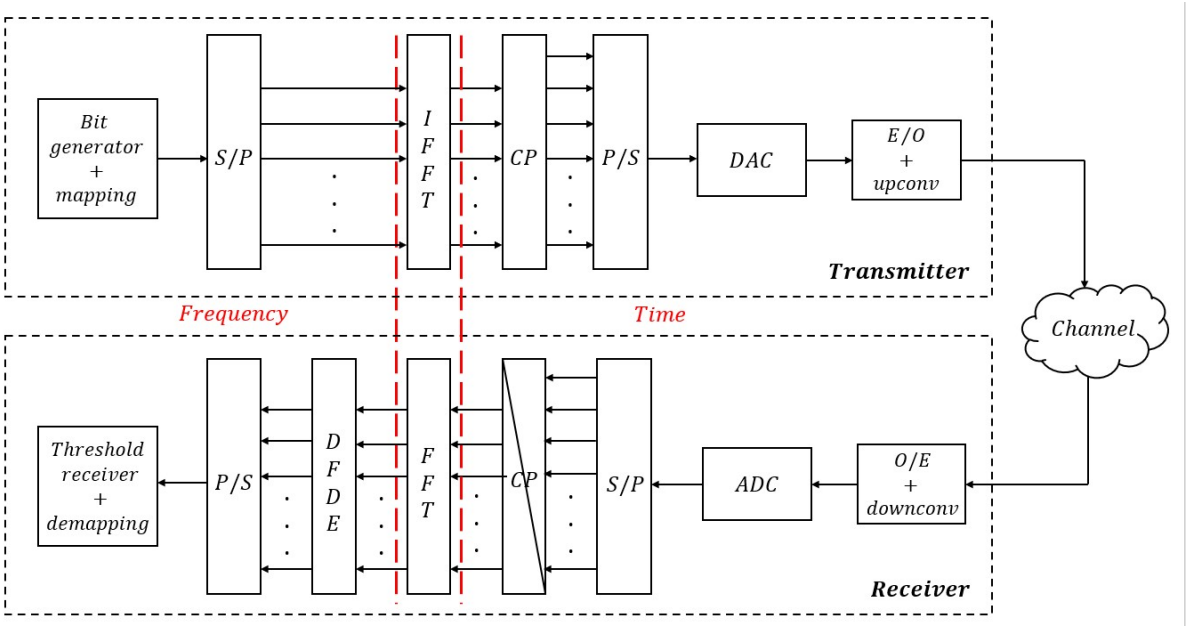

Figure 2.3: *Classical DMT system implementation for an optical communication link.*

- the digital implementation of a DMT transmitter and receiver is very simple and, as shown in Figure 2.3, it is based on an Inverse Fast Fourier Transform - Fast Fourier Transform (*IFFT-FFT*) pair at the transmitter and at receiver respectively. A huge advantage of this kind of structure is that it facilitates the channel equalization at the receiver a lot.

The second and third points allow to get a capacity that is $3-4$ (or even more times higher than the signal bandwidth, which means a very high transmission efficiency. However, the DMT modulation has also some weaknesses that must be properly taken into account. In particular, we can mention four main problems:

- the frequency orthogonality is very fragile with respect to the phase noise of the local oscillator used to generate the sinusoids, as even a little frequency deviation causes interference among the subcarriers (so high quality local oscillators are required);
- as we said in 1.2, a DMT signal PAPR can be high due to a temporary constructive interference among the subcarriers, which means that the waveform could present big and isolated power peaks at some time instants. This event is detrimental for the electrical amplifiers working regime, because they are stressed and they cannot operate in the maximum efficiency condition;
- after the channel propagation, a DMT signal suffers of the so called Inter-Symbol Interference (*ISI*) and Inter-Carrier Interference (*ICI*), that respectively consist of a time orthogonality loss among the DMT symbols and of a frequency orthogonality

loss among the subcarriers within a DMT symbol. These two problems are caused by the non-ideal channel response, which may generate undesired signal replicas with a certain delay;

- an incorrect signal synchronization and sampling at the receiver introduce in turn ICI, since in the DMT spectrum the sampling does not occur in correspondence of the peaks of the cardinal sines, but in other locations where there is a contribution by more than one cardinal sine (obviously there can be a dominant component, but it is tarnished anyway).

In order to combat these issues, people have proposed a lot of solutions. For what concerns the PAPR problem, we have already spoken about the signal pre-coding technique in Section 1.2 and we will present another solution (the so called *clipping*) in Section 3.2. Regarding ISI and ICI, the most exploited technique is the Cyclic Prefix (*CP*), where the final part of the time domain DMT symbol is repeated at the beginning of the block itself. This technique is very simple and clever, but one has to be careful in its application, because it reduces both the spectral efficiency and the energy efficiency of the DMT signal. Moreover, the CP does not prevent from the ICI generation due to an incorrect sampling and processing at the receiver.

2.2. Semiconductor lasers

When we speak about optical communications, we obviously need something able to generate the light that is then employed in the information transmission. Nowadays, all the sources used in this operation are the lasers and, in particular, the semiconductor lasers. This is because they are tiny and, as a consequence, they can be easily integrated on a chip. Moreover, as every other laser source, they produce a high quality light, that is a coherent light with both high spatial coherence and high temporal coherence. Finally, they allow to adopt several approaches for the information encoding. The two types of semiconductor lasers mainly used in the optical communications are the Distributed Feedback (*DFB*) lasers and the Vertical Cavity Surface Emitting Lasers (*VCSELs*), in particular the first ones. On a conceptual level, there is no difference between a DFB laser and a VCSEL, both in terms of working principle and in terms of parameters and description, but some characteristics are different. The operation of a semiconductor laser is the same of every other laser source, as to say that it is necessary a pumping process that creates a population inversion, from which we are able to extract the photons. In the basic form, a semiconductor laser is constituted by a pn junction made by a

direct gap semiconductor (like GaAs). This junction has a big built-in potential (so the semiconductor bands are highly bent in the depleted region) and it is pumped by the bias current. The transitions that generate the coherent light happen exactly in the depleted region (named also active region) and are electronic transitions between the conduction band and the valence band. Together with the pumping process and the population inversion, we need a cavity to start the avalanche photon generation process, as in every other laser. It is precisely here that lies the main difference between DFB lasers and VCSELs. In fact, in a DFB laser the cavity is long (in the order of $100 - 300\ \mu m$), horizontal and transverse with respect to the pumping current. In a VCSEL, instead, the cavity is short (in the order of $5 - 10\ \mu m$), vertical and in the same direction of the pumping current. Figure 2.4a and Figure 2.4b represent the two kinds of structures that we have just described. The two types of semiconductor lasers have their pros and their cons. VCSELs are very interesting because

- being very tiny, they can be really used everywhere without basically any bulk;
- the short cavity guarantees the presence of just one laser mode, which means that the laser emits naturally light just at one single wavelength (neglecting the linewidth broadening);
- they have a circular symmetry, so their emission mode resembles the gaussian mode of an optical fiber and we could have directly a good coupling between the two elements.

On the other hand, DFB lasers

- have a lower linewidth broadening, so they are characterized by a lower phase noise;
- are more stable once the desired working regime is fixed (for example, the temperature has a minor effect on the emission wavelength);
- don't need any reflection coating on the cavity terminal facets.

However, both DFB lasers and VCSELs can be used in a lot of contexts and in a lot of applications, among which we have also the DML solution presented in Subsection 1.1.1. Nevertheless, it is fundamental to discuss a couple of concepts related to this topic, so in the next subsections we are going to analyze the chirp in the direct modulation regime and the laser frequency response.

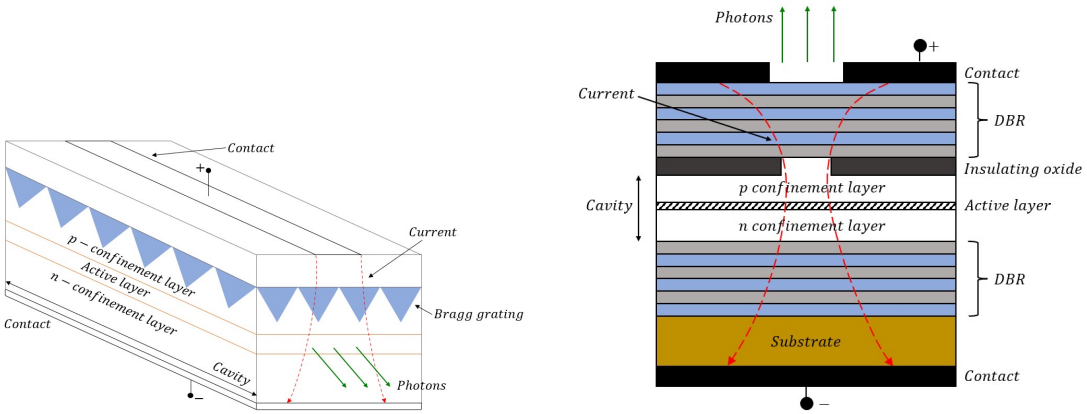

Figure 2.4: *Device structure for* ***(a)*** *a DFB laser and* ***(b)*** *a VCSEL laser (DBR = Distributed Bragg Reflector: it is a dielectric mirror made of many* $\lambda/4$ *layers).*

2.2.1. Frequency chirp in laser direct modulation

When we employ a semiconductor laser in a transmitter, we have the possibility to choose between a light external modulation and a light direct modulation. In the external modulation approach, the laser is pumped with a bias current constant in time, so that the laser behaves like a pure light source with constant power (apart for the fluctuations due to the quantum noise). Then, the light amplitude and/or phase is modulated by an external device. This is exactly what we described in the introduction of Section 1.1 and, indeed, a visual explanation of this description is reported in Figure 1.3. The direct modulation, instead, is based on the driving of the laser output power through the bias current, that, this time, is characterized by a time variation. Therefore, we directly perform the Electro-Optical (E/O) signal conversion with the laser. In particular, the output power and the bias current are related by the expression

$$P_{out}(t) = \eta \cdot [I(t) - I_{th}] \tag{2.4}$$

where η is the laser slope efficiency and I_{th} is the laser threshold current (that is the current value that, approximately, separates the on and off conditions for the device). It is evident that there is a linear correlation between the laser bias current and its output power and this allows to realize an amplitude modulation very easily. To be completely honest, we must precise that (2.4) is true when $I(t) >> I_{th}$, otherwise the relation between the two quantities becomes non-linear and, as a consequence, more complicated (so much that one wants to keep away from the transition region, where there would be distortion).

As we said, this modulation option is very interesting because it allows to reduce the bulk, the complexity, the energy consumption and the costs on the transmitter side. Together with these pros, we can add another big advantage. In fact, with a direct modulation we can realize both an amplitude modulation and a phase modulation. This latter one has to be ascribed to the so called *chirp* of a DML ([28], [29]). This phenomenon appears in the all semiconductor optoelectronic devices because of the plasma effect associated to the charge carriers and related to the electro-refraction effect. In fact, the carriers concentration impacts on the semiconductor refractive index (both real and imaginary part) and, more in general, on the characteristics of the device itself. The laws that describe the plasma effect are the so called Soref relations and, in the general form, they are

$$\Delta n^{'} = c_1(\lambda) \cdot \Delta n + c_2(\lambda) \cdot \Delta p \tag{2.5}$$

$$\Delta n^{''} = c_3(\lambda) \cdot \Delta n + c_4(\lambda) \cdot \Delta p \tag{2.6}$$

where

- $n^{'}$ is the refractive index real part;
- $n^{''}$ is the refractive index imaginary part;
- n is the electron concentration in [cm^{-3}];
- p is the holes concentration in [cm^{-3}];
- $c_1(\lambda)$, $c_2(\lambda)$, $c_3(\lambda)$ and $c_4(\lambda)$ are wavelength depending coefficients (measured in [cm^3]), characteristic of the considered semiconductor.

In order to better understand what the chirp is, let's consider a DML. As we said, we have a pn junction where we change the electron and hole concentration in time to adjust the output power. This implies a semiconductor refractive index variation described by the Soref relations. On the other hand, a refractive index variation means an optical length variation for the cavity, which in turn leads to a change of the wavelength of the mode supported by the laser cavity itself. Therefore, we obtain an emission frequency variation for the laser, that can be seen as a frequency modulation around the main carrier frequency. Going back to more general terms, this frequency shift induced by the chirp is always present for every optoelectronic device, so it must be properly taken into account. It can be demonstrated that the chirp frequency shift is a function of the power variation in time and is given by

$$\Delta f(t) = \frac{\alpha}{4\pi} \cdot \left\{ \frac{1}{P(t)} \frac{dP(t)}{dt} + \kappa P(t) \right\} \tag{2.7}$$

where α is the linewidth enhancement factor and κ is the adiabatic chirp parameter. Note that (2.7) contains two chirp contributions. The first one, depending on α and, above all, on the power derivative, is the so called *transient chirp*. The second one, depending on α, κ and, especially, linearly on the power evolution, is named *adiabatic chirp*. Usually, the chirp is a spurious and undesired effect that accompanies the amplitude modulation, but we can try to take advantage of it in order to have a laser that acts both as a light source and as a phase modulator.

2.2.2. Semiconductor laser frequency response

Ideally a semiconductor laser is a pure E/O conversion device, that behaves in the same way whichever is the frequency used in the direct modulation. This means that its transfer function should be constant both in amplitude and in phase. However, a real laser shows a certain frequency response, which must be absolutely considered in the applications, otherwise the results would be very poor. This frequency response depends on three fundamental parameters of the device:

- the intrinsic frequency f_i (also named relaxation frequency or resonance frequency);
- the parasitic frequency f_p;
- the oscillation damping parameter γ (also named simply damping parameter).

The intrinsic frequency and the damping parameter are characteristic parameters of the laser and they depend on a multitude of factors of the element itself (the threshold current, the photon lifetime in the cavity, etc...). It can be demonstrated that these two quantities are related one to the other, as the damping parameter depends quadratically on the intrinsic frequency. The parasitic frequency, instead, derives from the pad and chip parasitic effects analysis. In particular, it is linked with the laser conductance, given by the amount of current that flows in the active region with respect to the voltage drop over the whole device. Anyway, it can be demonstrated that the frequency response of a semiconductor laser can be computed as the product between a filter depending on f_i and γ and a filter depending only on f_p:

$$G_{el,DML}(f) = G_{f_i,\gamma}(f) \cdot G_{f_p}(f) = \frac{f_i^2}{f_i^2 + j\frac{\gamma}{2\pi}f - f^2} \cdot \frac{1}{1 + j\frac{f}{f_p}} \tag{2.8}$$

apart for a constant. An example of this response is reported in Figure 3.5a. Note that this frequency response is limited for every frequency and it shows a hermitian symmetry. Moreover, with some simple calculations, we can find that this function is never exactly equal to zero and this feature turns to be very important, as we will discuss in Section 3.2.

2.3. Single Side Band signals

In principle, an IM-DD system is intrinsically based on Double Sideband (*DSB*) signals, as to say signals having a spectrum with hermitian symmetry (so there are the two signal bands around the zero frequency). A DSB signal is very easy to be generated, but, at the same, it is a major limiting factor of the system. In fact, the employment of DSB signals acts so that an IM-DD system is subjected to a frequency selective power fading caused by the chromatic dispersion of the optical fiber and the photodetector square law. Basically, the propagation channel can be described with a transfer function with actual "holes" (dips), as represented in Figure 2.5. This phenomenon is due to the superposition of two signal components that undergo a different phase shift during the propagation along the optical fiber, where we have the effect of the chromatic dispersion. This superposition is caused by the photodetector square law, so it cannot be avoided in a direct receiver. In the lucky case, the two contributions are in phase, we get a constructive interference that maximizes the signal power; in the unlucky case, instead, the superposition is destructive and this originates a dip in the frequency response,. Obviously, this is detrimental for the signal and the system performance, because we cannot exploit the whole signal bandwidth and we are wasting resources. Moreover, it's not so easy to predict the effect of the frequency selective power fading, because it depends strongly on the transmission distance. The solution of this problem is a simple change of signal kind, moving to exploit the Single Sideband (*SSB*) signals. From a purely mathematical point of view, a baseband SSB signal can be expressed in the form

$$s_{SSB}(t) = s(t) + j\tilde{s}(t) \tag{2.9}$$

where $\tilde{s}(t)$ is the Hilbert transform of the signal $s(t)$. This operation is defined as

$$\tilde{s}(t) = \mathbf{H}\{s(t)\} = \frac{1}{\pi} \cdot p.v. \int_{-\infty}^{+\infty} \frac{s(\tau)}{t-\tau}\, d\tau \tag{2.10}$$

where $p.v.$ is the principal value integral. Therefore, a SSB signal is made of a certain

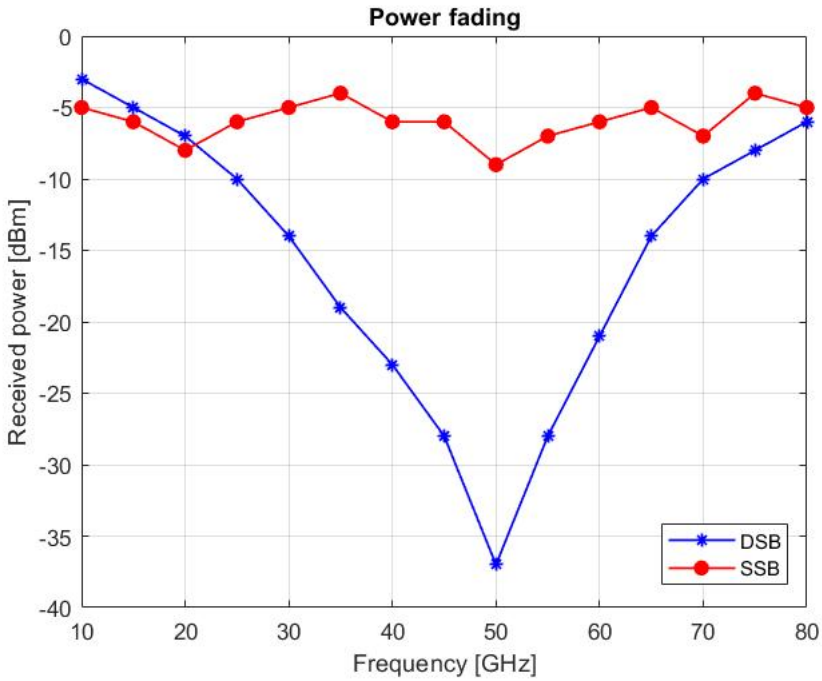

Figure 2.5: *Frequency selective power fading. We represent the received power because it is determined by the channel transfer function. In this picture we fix the propagation length and change the frequency, but the viceversa returns the same result.*

signal and its Hilbert transform in quadrature. It can be demonstrated that a fundamental property of the Fourier transform of such signal is that it is not zero just either for $f > 0$ or for $f < 0$. This implies that, after the upconversion to the passband with a carrier, we just generate either the Upper Sideband (USB) or the Lower Sideband (LSB) respectively. Physically speaking, instead, a SSB signal is essentially a DSB signal where we eliminate either the USB or the LSB with a proper technique. Figure 2.6a and Figure 2.6b represent the power spectrum of a DSB signal and a SSB signal respectively. To tell completely the truth, the conditions on the SSB signal definition can be a little relaxed, because usually a signal can be considered a SSB signal starting with a suppression value equal to $12 - 15\,,\ dB$ of one of the bands. However, SSB signals have five big advantages with respect to DSB signals:

- in the SSB case we double the signal spectral efficiency, since we transmit the same amount of information with the same rate but occupying more or less half of the bandwidth with respect to the DSB case;
- we considerably solve the power fading problem, since now every signal component is superimposed with its corresponding that is much smaller and this limits the destructive interference events a lot;

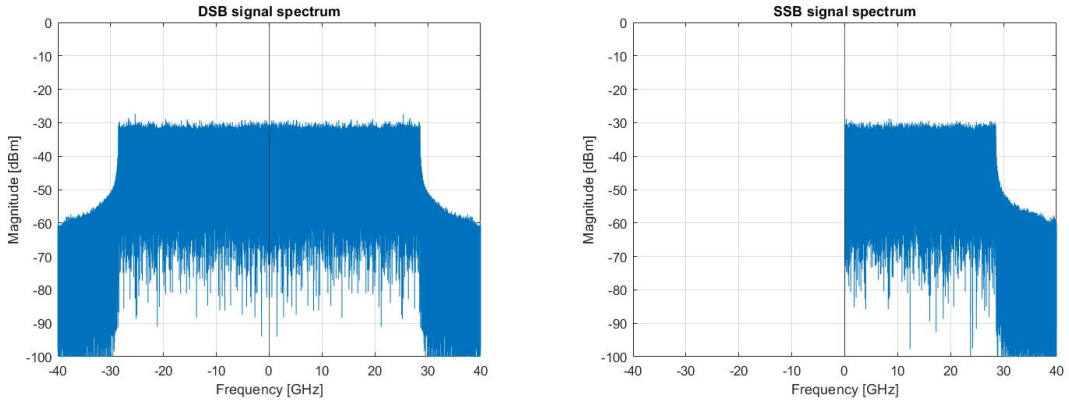

(a) (b)

Figure 2.6: *Power spectrum for* ***(a)*** *a DSB signal and* ***(b)*** *a SSB signal.*

- because of the previous consideration, SSB signals are very attractive for amplified and dispersion uncompensated networks ([7]-[9]);
- SSB signals can be exploited with high level receivers that implement the KK algorithm to improve the detection process;
- since we have a suppression of one of the two sidebands, there is the possibility (at least potentially) to move the adjacent channel closer without suffering a huge cross-talk, that is remarkable if we think about a WDM context.

2.3.1. SSB signal generation approaches

The problem that has to be tackled now is the generation of SSB signals. In fact, they are very attractive, but they are more complicated to be realized with respect to DSB signals. Speaking about the state of the art, there are two simple generation methods that apply exactly the mathematical and physical definitions of SSB signal, but they have some drawbacks that don't make them ideal to be used in an IM-DD system.
The first technique employs an EML constituted by a CW laser and a cascaded IQ MZ modulator, which can be used in two different working conditions (Null Power working point or Half-Fringe working point, we change just the bias point). This kind of structure has been already shown in Figure 1.3. However, in this scheme we just apply the SSB mathematical definition contained in expression (2.9), because we simply drive the In-Phase MZ modulator with the desired signal, we drive the Quadrature MZ modulator with the Hilbert transform of the signal itself and, finally, we sum the two contributions up to generate the final signal to be transmitted. The structure described is the basic one, but it can be complicated in order to obtain a better performance. Despite this scheme

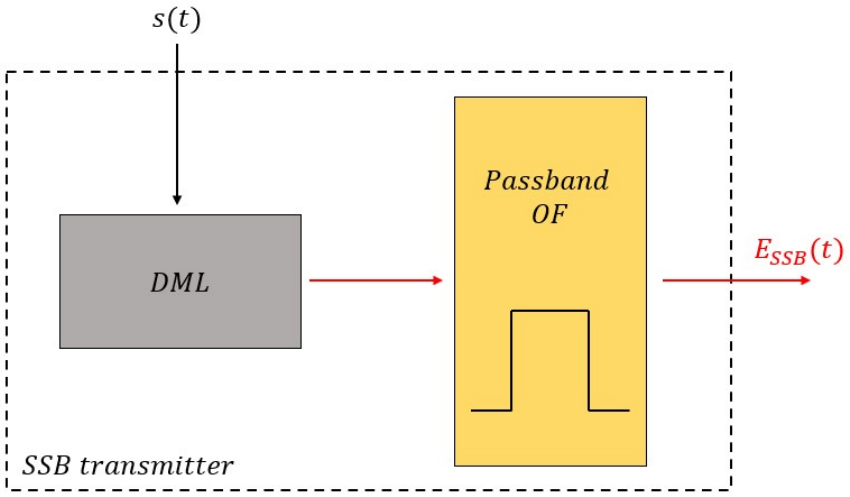

Figure 2.7: *SSB transmitter implementation with a DML and an optical filter.*

is very simple and the concepts behind its functioning are very intuitive, it is costly and quite bulky, which is the opposite of the objectives that have to be pursued in an IM-DD system. Moreover, this solution requires a strong optical carrier, but this can produce detrimental effects for the system performance, especially during the signal propagation along the optical fiber.

The second approach exploits the physical definition of SSB signal and it is based on the use of a very narrow passband Optical Filter (OF), like a super-gaussian filter ([30], [31]). The block diagram of this scheme is represented in Figure 2.7. In practice, we start from a DSB signal generated by a DML and then we remove either the USB or the LSB of the optical signal with a filtering operation. This solution is even easier than the IQ MZ one in terms of implementation, but it has its problems too. The main critical point is the correct filter alignment in the frequency domain. In fact, its transfer function is not a perfect rectangle (such filter is not realizable or, at least, not convenient), but it shows an approximately constant region followed by a transition zone (or decay zone). Therefore, if one does not care about the filter alignment, this can make the system performance a lot worse, as we can have two possible effects. On one hand, there is the risk of an excessive optical carrier attenuation, which can be detrimental at the detection stage (in particular if a KK receiver is employed). On the other hand, there is the risk of a low attenuation of the undesired band, that turns the SSB signal into a VSB signal. This latter signal kind is similar to a SSB one but with a lower suppression between the sidebands. Obviously this is something unwanted, since the power fading becomes an issue again. Together with this criticality, we have also bulk, cost, integration and stability issues.

These numerous problems related to these solutions have driven the research to find other

possible approaches to accomplish the SSB signal generation goal. The most interesting proposal in this sense is the dual modulator scheme one.

2.4. DML-EAM dual modulator

As we have said, the dual modulator is a system made by a DML and a cascaded intensity modulator, as shown in Figure 2.1. The idea behind this device is a double modulation of the light or, in other words, a separation of the amplitude and phase modulation operations, assigning them to two different elements driven with different electrical signals. In particular, the DML is typically a DFB laser and it operates both as light source and as phase modulator thanks to the chirp phenomenon. So, what we are doing here is basically try to exploit the chirp induced by the direct modulation in a smart way. Then, the output of the DML is in turn modulated by an intensity modulator. The most employed one during the studies is an EAM, because it is little and can be easily integrated on a chip. These two components constitute the so called DFB-EAM dual modulator, whose scheme is shown in Figure 2.8. This second modulation performed by the EAM has a double aim. The first one is to improve the amplitude modulation quality, as the DML one is not particularly good. The second one is related to the SSB signals generation. This is because the dual modulator architecture is very versatile and we can even use it to generate SSB signals. The EAM introduction plays a key role in this task, as it allows to reach the goal quite easily by satisfying the proper conditions. These requirements have been inferred in plenty of works during the last decade. However, in most of the cases the performance was not particularly impressive, both in terms of sideband suppression and in terms of transmitted capacity ([2], [3], [7]-[10]). This was due to a lack of general theory

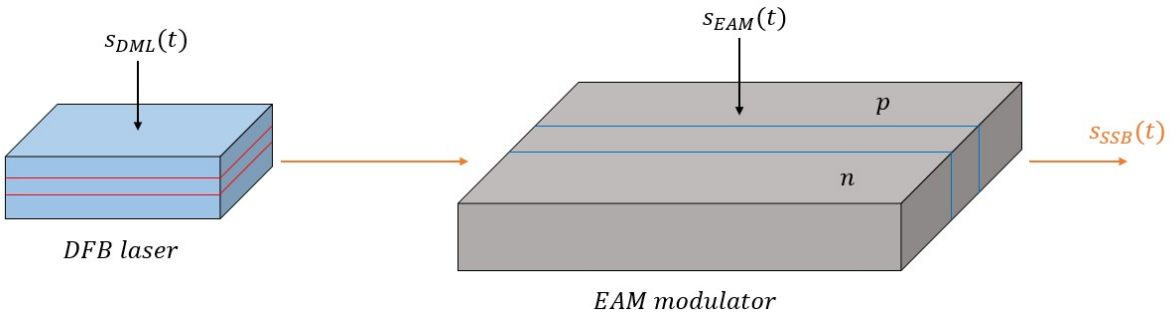

Figure 2.8: *DML-EAM modulator structure and driving strategy. In this picture we can see also the concept at the basis of the EAM modulator: it is a pn junction where the charge carriers concentrations are modified in time with a proper voltage signal.*

and non realistic approximations, among which we even have the absence of the chirp for the EAM and, considering that the EAM is an optoelectronic device, this assumption is for sure not correct at all. Nevertheless, starting from the simple case of a single sinusoid signal, the complete modulation theory for the DML-EAM dual modulator was recently developed ([4]), taking every aspect into account (the chirp of the EAM too). From this analysis, it was possible to extract the fundamental conditions needed for the generation of a SSB signal. One of the key points of the discussion is the small signal approximation, because it makes some simplifications in the formulas and, especially, an analysis limited to the first order terms possible. These factors allow to get approximately linear relations, that are much easier to treat with respect to the actual non linear ones. We are not going to repeat all the performed procedure (also because in Chapter 3 we will present a similar one), but an example of output signal spectrum applying the theory in [4] is shown in Figure 2.9a.

After the successful study of the simplified case with just one harmonic, it was immediately developed a generalized model that can be applied in the more complicated case of a DMT signal ([5], [6]). In fact, as we saw in Section 2.1, a DMT signal is basically a superposition of sinusoids, so the model generalization is quite natural. Conceptually speaking, the steps are exactly the same, but, obviously, there are some differences in the realization. Also in this case, we don't go through all the theory, since we will develop a similar one again in Chapter 3. However, an example of output spectrum for this device in the DMT case is reported in Figure 2.9b.

Apart for these theoretical and specific aspects, the DML-EAM dual modulator in extremely interesting because it satisfies all the requirements regarding a lower power consumption, a lower complexity and a lower bulk thanks to the small footprint. Along with this, we have an increased device simplicity, a higher output power due to the DML employment and the possibility of an easy integration and mass production.

2.5. DML-MZ dual modulator

The DML-EAM modulator has some little drawbacks that could be problematic. In particular, we can mention the fact that, nowadays, the EAM production is quite limited. Moreover, as we said in the previous section, an EAM is an optoelectronic device and, as a consequence, it is characterized by its own chirp, which means a further complication in the system analysis. For these reasons, it could be interesting to propose and analyze a possible alternative solution still based on the same dual modulator concept. This leads to the introduction of the DML-MZ dual modulator approach, whose structure is shown

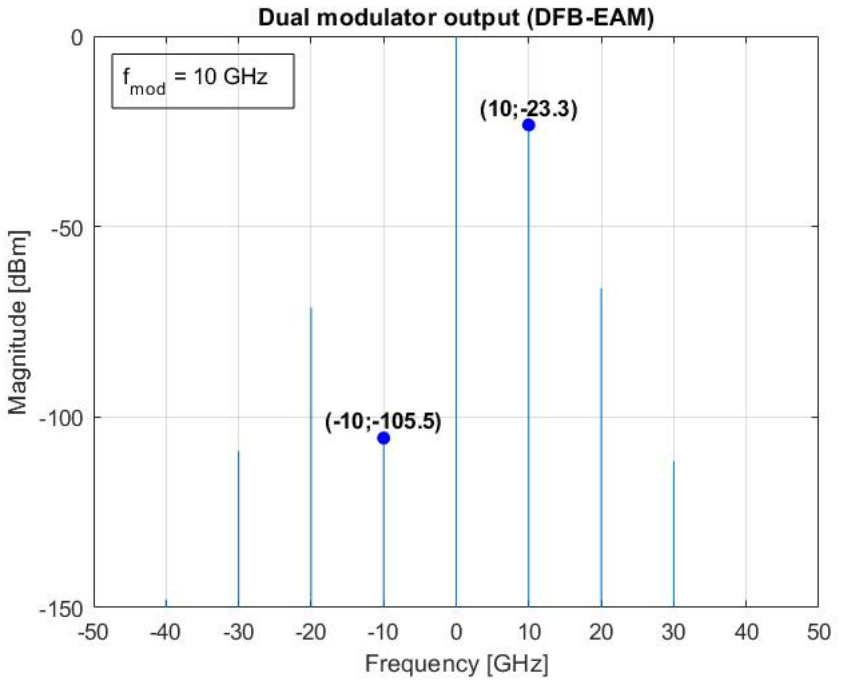

(a)

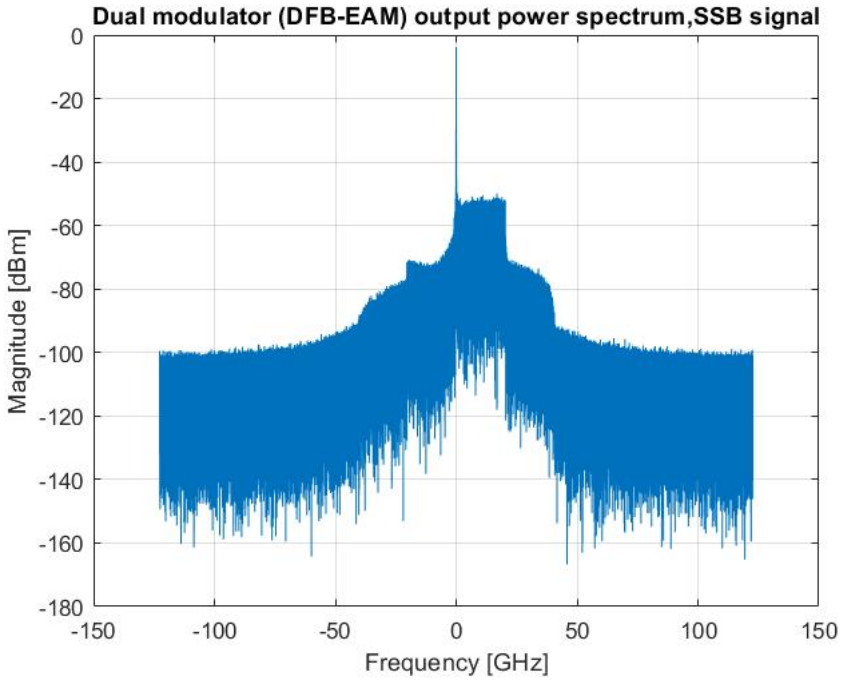

(b)

Figure 2.9: ***(a)*** *Single sinusoid output spectrum for the DML-EAM dual modulator with a modulation frequency f_{mod} = 10 GHz;* ***(b)*** *DMT SSB signal output spectrum produced by a DFB-EAM dual modulator.*

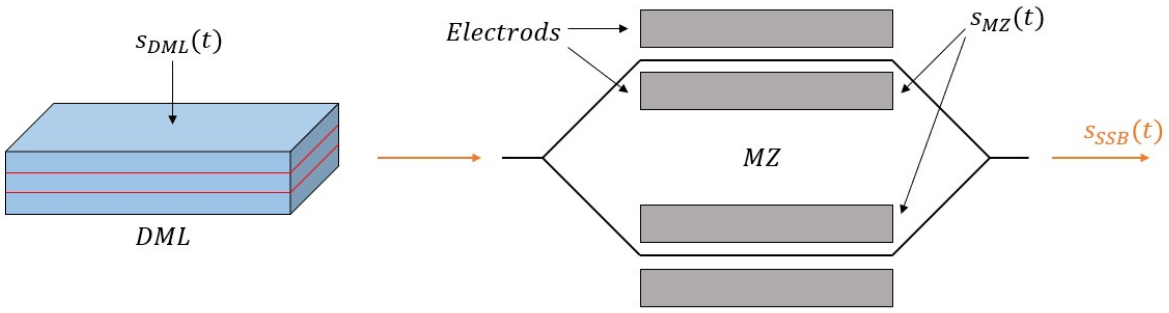

Figure 2.10: *DML-MZ dual modulator structure and driving strategy. It's not possible to represent the operating principle of the MZ modulator for a sake of clarity, but, similarly to the EAM, it is still a pn junction controlled with a voltage signal.*

in Figure 2.10. The DML in this new device can be either a DFB laser or a VCSEL, since both have their advantages and their drawbacks. The intensity modulator, instead, becomes a MZ modulator. This choice too has its pros and cons. The main drawback is that a MZ is bulkier than an EAM. This is generally true, but, to be completely fair, we must precise that we are not referring to the Lithium Niobate MZ modulators (which are even $2-3\ cm$ long), but we are speaking about MZ modulators realized in the semiconductor technology ([32]-[37]), like the silicon or the InP technology. During last decades, the intensive studies in the semiconductor field for the photonic have led to have MZ modulators typically $200-500\,\mu m$ long, that is an extension comparable to a usual EAM one ($100-200\,\mu m$). The operating principle of these semiconductor MZ modulators is based on the electro-refraction phenomenon due to the carrier plasma effect. In particular, we drive the device with a certain electrical signal in order to act on the refractive index real part (responsible for the field phase shift) thanks to (2.5). By doing so for both MZ branches, we are able to modulate the output light intensity through a semiconductor refractive index modulation. However, the semiconductor technology is able to limit the bulk of a MZ modulator with respect to an EAM. On the other side, if it works in proper conditions that will be presented in Section 3.1, the big advantage of a MZ is that this device does not introduce any chirp contribution. This is a nice point because it means that the amplitude modulation performed with a MZ is possibly better than the one obtained with an EAM.

Moving from a structure point of view to a more operating one, we can say that the SSB generation process for this dual modulator alternative does not change at all. In fact, we still need a driving signal for the DML and a driving signal for the intensity modulator, but this latter one is built in a different way with respect to the EAM case. Moreover, the small signal regime has to be respected in this new system too, so that we

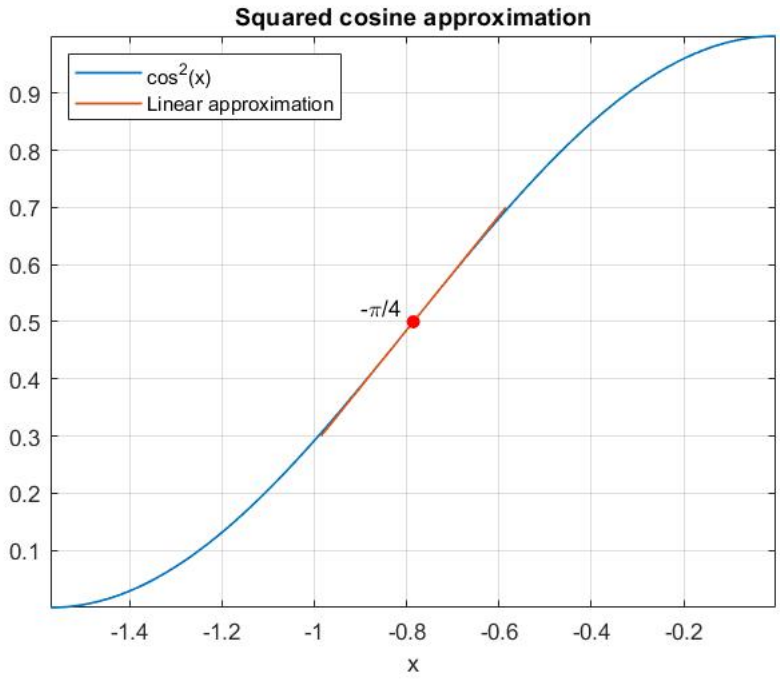

Figure 2.11: *Squared cosine linear approximation, needed in the following discussion.*

are still able to work with linear expressions. This implies to have a correct bias both for the DML and for the MZ. For what concerns the DML, the requirement is the same made explicit in Section 2.2.1. For the MZ, instead, we must clarify an important point. As we will say in Section 3.1, the field transfer function of a MZ modulator is a cosine. Therefore, the linear region changes whether we reason in the field domain or in the intensity domain, which means that we have to choose the kind of wanted linearity. This selection reflects directly on the bias of the device itself. Between the two possibilities, the desired linearity is the intensity one, so that we can move in a region with a constant sign transfer function. Otherwise, we would create a huge signal distortion due to the incessant sign change of the MZ transfer function. However, considering that the intensity transfer function is given by the absolute squared value of the field transfer function (so it is a squared cosine), the linearity in the intensity domain is achieved by fixing the working point around $\pi/4$, as Figure 2.11 shows. Actually, the working point should be fixed around $-\pi/4$, so that the rising part of the cosine is exploited. Once this point is selected, we move in the neighborhood of it with the MZ small modulation signal. If we satisfy the proper conditions, we should find a SSB signal at the output of this dual modulator scheme as much as we obtain it with the DML-EAM one. The next step that must be done is find these requirements.

3 | Simulator implementation

In order to evaluate the DML-MZ dual modulator scheme performance, we have simulated its behaviour with Matlab®. In this chapter we are going to present and discuss the simulator implementation, touching upon the various theoretical aspects. The results are reported in Chapter 4 and Chapter 5, where we also make some comparisons between the DML-EAM dual modulator and our DML-MZ solution. During the realization, we have tried to develop a simulator as general as possible by introducing many flags, which give the chance to

- generate a SSB signal or a DSB signal;
- choose a DFB laser or a VCSEL;
- choose an EAM modulator or a MZ modulator;
- propagate the signal on a certain distance or not;
- perform the bit and power loading or not;
- perform the clipping operation or not.

All these options will be important in the following discussions. The outline of this chapter is the following one:

- in Section 3.1 we analyze the SSB generations problem for the DML-MZ dual modulator scheme using just a sinusoidal signal;
- in Section 3.2 we make a similar discussion but using a DMT signal;
- in Section 3.3 we show the DMT detection procedure when direct detection is employed.

3.1. Single sinusoid model

Considering that we are substituting the EAM with a MZ, it is quite likely that the modulation conditions for the SSB signal generation change as well. For this reason, it is fundamental to retrieve them before any other discussion. With this aim, we start from the very simple case of a single harmonic having frequency f_{mod} as modulation signal. This study on the single sinusoid case will be the base for Section 3.2. The single sinusoid signal can be written as

$$s(t) = \cos(\omega t) \tag{3.1}$$

where $\omega = 2\pi f_{mod}$ is the cosinusoid angular frequency. As in the DFB-EAM dual modulator case, we have to operate in the small signal regime. For this reason, we associate an amplitude modulation index $m << 1$ to this sinusoid. So, the modulation signal for the DML driving is

$$s(t) = m_{DML} \cos(\omega t) \tag{3.2}$$

with m_{DML} amplitude modulation index for the DML. Considering that, as we said in 2.2, the DML must work in the linear region as far from the threshold as possible, from (3.2) it is straightforward to say that the power signal coming out from the DML is

$$\begin{aligned} P(t) &= \eta I_B \cdot [1 + s(t)] = \\ &= P_0 \cdot [1 + m_{DML} \cos(\omega t)] \end{aligned} \tag{3.3}$$

where η is the laser slope efficiency, I_B is the laser bias current and $P_0 = \eta I_B$ is the laser average output power, that is the power that it would emit if it worked in the CW regime. Keeping in mind that the electric field is proportional to the square root of the optical power and that the DML introduces a certain phase contribution, we can affirm that the signal electric field at the DML output is

$$E_{DML}(t) = \sqrt{P_0 \cdot [1 + m_{DML} \cos(\omega t)]} \cdot e^{j\phi(t)} \tag{3.4}$$

where the phase $\phi(t)$ is given by

$$\phi(t) = 2\pi \cdot \int_0^t \Delta f(t)\, dt \tag{3.5}$$

As we said in Section 2.2, and in particular in 2.2.1, the frequency modulation $\Delta f(t)$ that determines the phase term in (3.4) is due to the DML chirp. This frequency shift with respect to the central emission frequency for the DML is given by

$$\begin{aligned} \Delta f(t) &= \frac{\alpha_{DML}}{4\pi} \cdot \left\{ \frac{d}{dt} \left\{ ln[P(t))] \right\} + \kappa P(t)) \right\} = \\ &= \frac{\alpha_{DML}}{4\pi} \cdot \left\{ \frac{1}{P(t)} \frac{dP(t))}{dt} + \kappa P(t)) \right\} \end{aligned} \tag{3.6}$$

where α_{DML} is the DML linewidth enhancement factor and κ is the DML adiabatic chirp parameter. By substituting (3.6) in (3.5) and using the small approximation signal, we can perform a first order approximation and demonstrate (Appendix A) that the electric field phase is more or less

$$\phi(t) \simeq m_{PM} \sin(\omega t + \phi_{PM}) + \omega_c t + \frac{\alpha_{DML}}{2} ln(P_0) \tag{3.7}$$

where we have introduced the DML phase modulation index m_{PM}, the quadrature phase shift ϕ_{PM} and the central angular frequency ω_c, defined respectively as

$$m_{PM} = \frac{\alpha_{DML} m_{DML}}{2} \cdot \sqrt{1 + \left(\frac{\kappa P_0}{\omega} \right)^2} \tag{3.8}$$

$$\phi_{PM} = \frac{\pi}{2} - \arctan\left(\frac{\kappa P_0}{\omega} \right) \tag{3.9}$$

$$\omega_c = \frac{\alpha_{DML} \kappa P_0}{2} \tag{3.10}$$

Note that (3.8) shows that the two DML modulation indices depend one on the other. In (3.7) we can neglect the second and the third term:

- the second contribution can be shown that is associated to the DC component of the laser power, so it is irrelevant in the further discussion;
- the third contribution is just a constant phase term.

Therefore, by introducing the relevant terms of (3.7) in (3.4), we obtain the approximated

DML electric field

$$E_{DML}(t) = \sqrt{P_0} \cdot \left[1 + \frac{m_{DML}}{2}\cos(\omega t) + j m_{PM}\sin(\omega t + \phi_{PM})\right] \tag{3.11}$$

In principle, we could already impose the SSB generation requirements on this optical field and find the related conditions. In the case of a single sinusoid this conclusion can even work. However, if we move to a multiple harmonic context (as we have in a DMT signal), the generation of an optical SSB signal becomes a tougher task because of the laser parameters α_{DML} and κ dependence on the modulation frequency. Moreover, being the laser used mainly as phase modulator, the quality of the amplitude modulation (necessary in order to have the chirp for the phase modulation) is not particularly good. For these reasons, we introduce an intensity modulator cascaded to the DML, so that we can improve the amplitude modulation and we can try to obtain new SSB conditions easier to be fulfilled. As we said, in [4] an EAM plays the role of the IM modulator, while we employ a MZ modulator. The following discussion is completely general about this latter device, so it can be applied with a MZ realized in any technology. In the most general working condition possible, the field transfer function for a MZ modulator is

$$h_{MZ}(t) = \cos\left[\frac{\pi}{2} \cdot \frac{V_1(t) - V_2(t)}{V_\pi}\right] \cdot e^{j\frac{\pi}{2} \cdot \frac{V_1(t)+V_2(t)}{V_\pi}} \tag{3.12}$$

with $V_1(t)$ and $V_2(t)$ voltage modulation signals supplied to the two branches of the MZ and V_π device parameter that represents the voltage to be applied in order to move from a maximum to minimum of the intensity transfer function (reported ahead in (3.15)) and viceversa. It is evident that there is an amplitude contribution and a phase contribution in this case too, the latter one corresponding again to a chirp. Since we want a pure amplitude/ intensity modulator, the chirp is something really undesired. In order to eliminate the presence of this element, it is possible to operate in the so called Push-Pull (PP) configuration, in which we impose that $V_2(t) = -V_1(t)$. Introducing this choice in (3.12), the MZ field transfer function becomes

$$h_{MZ}(t) = \cos\left[\frac{\pi}{2} \cdot \frac{2V_1(t)}{V_\pi}\right] \tag{3.13}$$

and, indeed, the phase term has disappeared. Along with the PP configuration, we can also introduce a certain bias voltage V_B between the two MZ branches. This possibility is very important for reasons that will be clear in a moment. With the bias voltage

addition, the second driving signal becomes $V_2(t) = V_B - V_1(t)$ and the substitution of this expression into (3.12) leads to the field transfer function

$$h_{MZ}(t) = \cos\left[\frac{\pi}{2} \cdot \frac{2V_1(t) - V_B}{V_\pi}\right] \cdot e^{j\frac{\pi}{2}\cdot\frac{V_B}{V_\pi}} \tag{3.14}$$

Even if in (3.14) appears a phase term, it is constant and, as a consequence, negligible. Now, as done for the DML, we temporarily move to the intensity domain and then we come back to the field approach. Therefore, we consider the MZ intensity transfer function

$$h'_{MZ}(t) = |h_{MZ}(t)|^2 = \cos^2\left[\frac{\pi}{2} \cdot \frac{2V_1(t) - V_B}{V_\pi}\right] \tag{3.15}$$

As we said before, we want to employ the IM modulator where its transfer function is approximately linear, so that we have an amplitude/intensity modulator linear at first order. In Section 2.5 and in particular in Figure 2.11, we have seen that, for a MZ modulator, this happens when the cosine argument is (in absolute value) equal to $\pi/4$. Therefore, we impose that $V_B = V_{\pi/4} = V_\pi/2$. In this way, we fix the working point where the cosine intensity transfer function is as most linear as possible and then we move in a neighborhood of this point with the small modulation signal. The introduction of this bias in (3.15) makes the transfer function equal to

$$h'_{MZ}(t) = \cos^2\left[\pi\frac{V_1(t)}{V_\pi} - \frac{\pi}{4}\right] \tag{3.16}$$

Then, we can consider that, typically, the modulation signal when we use a MZ modulator is built such that $V_1(t) = m_{MZ}V_\pi s(t)$ with m_{MZ} amplitude modulation index of the MZ and $s(t)$ data signal. Therefore, thanks to this driving signal we can develop (3.16) in the form

$$h'_{MZ}(t) = \cos^2\left[\pi m_{MZ} s(t) - \frac{\pi}{4}\right] \tag{3.17}$$

As we have done for the DML, we assume to be in the small signal regime, so that we perform a first order approximation of (3.17) for the transfer function. This leads to the expression

$$h'_{MZ}(t) = \frac{1}{2}[1 + 2\pi m_{MZ} s(t)] \tag{3.18}$$

which, going back to the field domain, becomes

$$h_{MZ}(t) = \sqrt{\frac{1}{2}[1 + 2\pi m_{MZ} s(t)]} = \frac{1}{\sqrt{2}}[1 + \pi m_{MZ} s(t)] \tag{3.19}$$

It is evident that we have reached an expression approximately linear with respect to the signal $s(t)$, that is the result we initially wanted. This waveform is absolutely arbitrary: the only restriction is the small signal condition. For this reason, we can choose to impose

$$s(t) = \cos(\omega t + \phi_{PM} + \Delta) - K \cdot \cos(\omega t) \tag{3.20}$$

where Δ is the differential phase shift between the DML and the MZ signals and K is a parameter. The reason behind this selection is that it allows to have a first order suppression of the DML undesired modulation amplitude (second term) and, consequently, to have a high quality amplitude modulation realized just by the MZ modulator (first term), without changing anything of the phase modulation performed by the DML. Clearly, the expression of the parameter K has to be set to reach this goal. This can be done just by determining the electric field at the output of the dual modulator, as to say at the output of the MZ. Combining (3.11), (3.19) and (3.20), at first order we get to the approximated optical field

$$\begin{gathered} E_{out} = E_{DML}(t) \cdot h_{MZ}(t) \simeq \\ \simeq \sqrt{\frac{P_0}{2}} \cdot \Big[1 + \pi m_{MZ} \cos(\omega t + \phi_{PM} + \Delta) + j m_{PM} \sin(\omega t + \phi_{PM}) + \\ + \left(\frac{m_{DML}}{2} + \pi m_{MZ} K\right) \cos(\omega t)\Big] \end{gathered} \tag{3.21}$$

At this point, we must impose the various needed conditions. First of all, we fix the coefficient of the last term equal to zero, so that we suppress the amplitude modulation of the DML. This leads to the expression

$$K = \frac{1}{2\pi} \frac{m_{DML}}{m_{MZ}} \tag{3.22}$$

Note that the index m_{MZ} is still to be determined. To get this result, we must assume to eliminate the spurious amplitude modulation and then we have to study the conditions for the generation of an optical SSB signal. In particular, as we pointed out in (2.9), in order to obtain such kind of signal the real and the imaginary part of the electric field

must be linked through the relation

$$Im\{E_{out}(t)\} = \boldsymbol{H}\{Re\{E_{out}(t)\}\} \tag{3.23}$$

where $\boldsymbol{H}$ is the Hilbert transform. Using the fundamental transforms, we get the expressions

$$m_{PM} = \pi m_{MZ} \quad \left(\Longrightarrow \; m_{MZ} = \frac{m_{PM}}{\pi} \right) \tag{3.24}$$

$$\Delta = 2n\pi \quad (\Longrightarrow \; \Delta = 0) \tag{3.25}$$

which are exactly the SSB generation conditions. Introducing (3.22), (3.24) and (3.25) in (3.21), the output optical field is

$$E_{out}(t) = \sqrt{\frac{P_0}{2}} \cdot [1 + \pi m_{MZ} \cos(\omega t + \phi_{PM}) + j\pi m_{MZ} \sin(\omega t + \phi_{PM})] \tag{3.26}$$

and this is a SSB signal, as we wanted.

3.2. DMT signal generation

The simplified discussion of the previous section is preparatory to the analysis of the more complicated case of a DMT signal. In particular, in this section we focus on the generation of a SSB DMT signal in the optical domain. As we have done in Section 3.1, we consider the DML-MZ dual modulator to establish the procedure be followed to reach this goal, that is inspired by [5].
In Section 2.1 and, in particular, in (2.2), we observed that a DMT signal can be basically written as a superposition of sinusoids and cosinusoids, orthogonal one to the other because of (2.3). As a consequence, it comes naturally to try to extend the results in the single harmonic case to this new situation. Obviously, this operation requires the proper modifications, but the conceptual basis does not change. First of all, we must remark that the small signal approximation must be still valid, so the amplitude of each single subcarrier must be sufficiently low with respect to the DC component. With this said, the block diagram of the implemented generation process is shown in Figure 3.1. In particular, Figure 3.1a shows the main blocks, while Figure 3.1b represents the sub-blocks that constitute the so called Arbitrary Waveform Generator (AWG). Clearly, here we assume

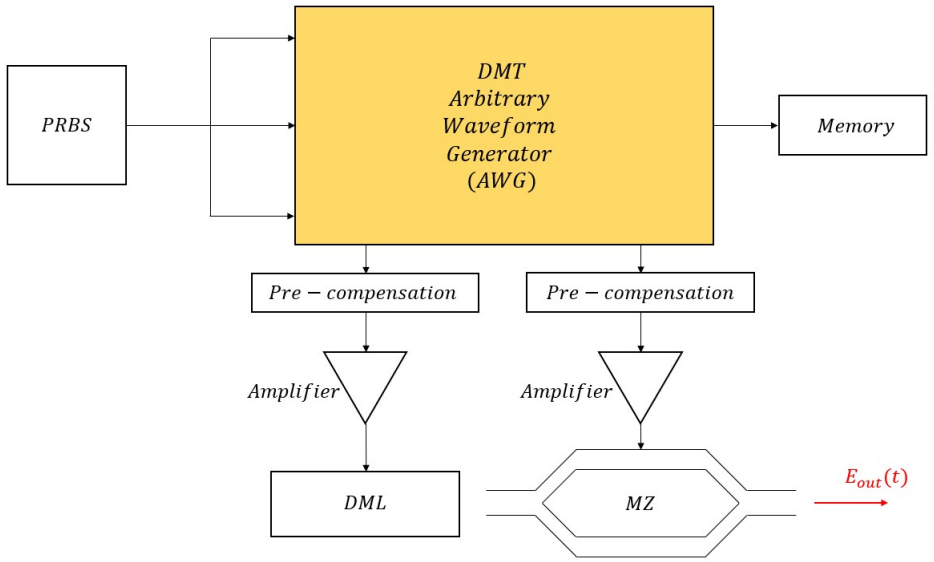

(a)

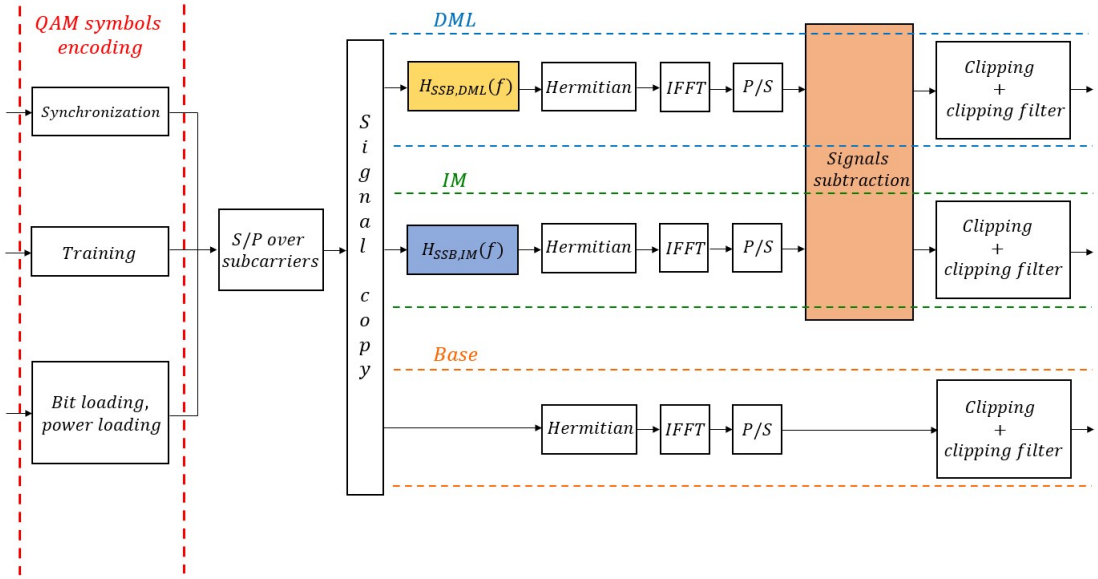

(b)

Figure 3.1: ***(a)*** *Block diagram for the DMT generation procedure;* ***(b)*** *Block diagram for the AWG implementation, the highlighted blocks are the fundamental ones.*

that all the relevant parameters of the DMT signal are properly fixed. The generation of the DMT waveform starts from the creation of a Pseudo-Random Bit Sequence ($PRBS$), which is then sent to the mapping process. In this passage, we don't generate just the bits and symbols for the actual data signal, but we do the same also for the synchronization and training symbols. These latter two categories are part of the DMT frame overhead (also named preamble) and they are fundamental upon the detection and the processing on the receiver side. The utility of these symbols will be clearer in Section 3.3. For the synchronization part, we produce symbols with a 64-QAM constellation, while for the training part we generate symbols with a 4-QAM constellation (we choose a very simple modulation in order to easily evaluate the channel frequency response). For the data part of the DMT signal, instead, we employ the bit loading and the power loading to optimize the information transmission depending on the propagation channel state at the subcarrier frequencies. Once the generation process is ended, we perform a Serial-to-Parallel (S/P) operation over the subcarriers, as to say that we create a matrix where we gather the various symbols subcarrier by subcarrier. Moreover, we have determined all the complex amplitudes associated to the sinusoids, which means that we have built the DMT signal complex spectrum. Note that this spectrum contains just the positive frequencies. Now, we realize three copies of this spectrum: one for the DML, one for the MZ and one that constitutes a reference signal (it will be subjected to the classic DMT generation procedure). The next step in the common algorithm presented in Section 2.1 (and shown in Figure 2.3) would be the application of the IFFT in order to go from the signal in the frequency domain to the signal in the time domain. Nevertheless, in our case this operation would lead to two problems:

- we would have the generation of a DMT SSB signal in the electric domain, but the dual modulator output signal in the optical domain would be a DSB signal;
- being the signal spectrum non-hermitian (we have contributions just for positive frequencies, as we said), the electrical signal obtained after the IFFT would be a complex signal, while all the discussion developed in Section 3.1 is based on the implicit hypothesis of a real modulation electrical signal.

These issues suggest that, before the IFFT, it is necessary to perform a certain signal processing. For sure, we must introduce the hermitian spectrum at negative frequencies, which makes the electrical signal a DMT DSB signal. This operation on its own is not sufficient yet, since we have seen that we need to satisfy some conditions to realize an optical SSB signal. For this reason, we have to add another passage before the spectrum hermitian symmetry imposition and it is one of the two core operations of this procedure. In particular, it is based on a digital filtering of the electrical signals associated to the

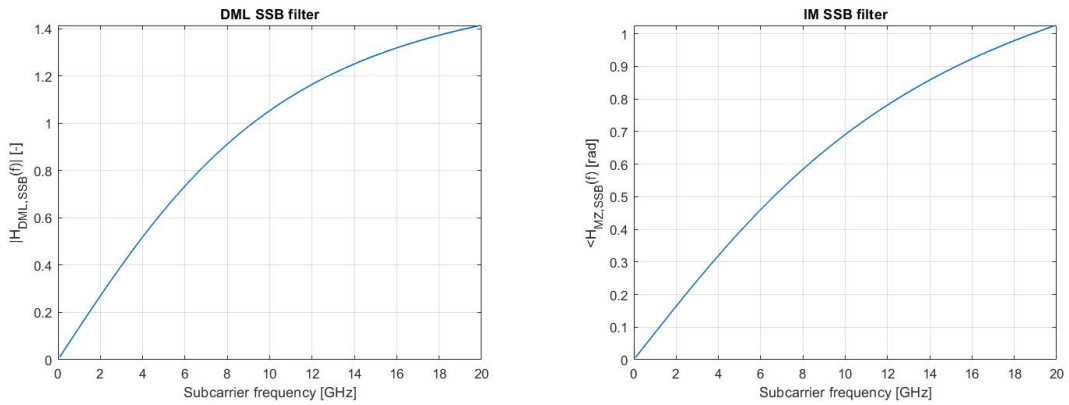

(a) (b)

Figure 3.2: *Digital SSB filter frequency response for* ***(a)*** *the DML and* ***(b)*** *the MZ.*

DML and to the MZ modulator. This task is greatly simplified by the fact that we are working in the frequency domain, so we have just to determine the filter shape at the subcarriers frequencies and then apply it to the signal. The DML SSB filter is a pure amplitude filter having frequency response

$$H_{SSB,DML}(\omega) = \frac{m_{DML}(\omega)}{m_{MZ}(\omega} = \frac{2\pi}{\alpha_{DML} \cdot \sqrt{1 + \left(\frac{\kappa P_0}{\omega}\right)^2}} \tag{3.27}$$

Its main task is the attenuation of low-frequency components and, indeed, it behaves like a high-pass filter. On the other hand, the MZ SSB filter is a pure phase filter and the frequency response is

$$H_{SSB,MZ}(\omega) = e^{j\cdot[\phi_{PM}(\omega)+\Delta(\omega)]} = e^{j\cdot\left[\frac{\pi}{2}-\arctan\left(\frac{\kappa P_0}{\omega}\right)\right]} \tag{3.28}$$

The main function of this filter is the introduction of the quadrature phase term $\phi_{PM}(\omega)$, generated by the DML modulation for all the spectrum components. The transfer functions of these two filters are shown if Figure 3.2a and Figure 3.2b respectively. Actually, the two SSB filters could be unified in an single digital filter having a frequency response slightly different with respect to the product of the two (and depending on the chosen device). However, not only the total number of operations do not change, but it is also easier to understand the meaning of the two passages. For what concerns the DML, the filtering follows what we have seen in the single sinusoid model:

- it is needed to cancel the spurious DML amplitude modulation (the ratio is exactly the one appearing in (3.20) when we apply (3.22));

- it is needed to get the same amplitude for the real and imaginary part of the output optical field (as in (3.26)).

Moreover, it is far more convenient to attenuate the DML low frequencies with respect to enhance the MZ high frequencies. For what regards the MZ, instead, intuitively we can understand that the multiplication of a complex sinusoid by a pure phase term and the subsequent introduction of the hermitian component in the spectrum allow to get a phase shift of that sinusoid exactly by the desired contribution. In this way, if the phase is the quadrature phase shift generated by the DML, we are able to obtain the same phase term for the sinusoids of the MZ signal too. Note that the definitions of the parameters m_{DML}, m_{MZ}, ϕ_{PM} and Δ used for the two filters computation are exactly the same found in Section 3.1. Once the filtering operations are done, we introduce the spectrum hermitian for $f < 0$ and then we apply the IFFT. The same two passages are valid also for the reference signal. Next, we add the CP and we apply a Parallel-to-Serial (P/S) transformation for all the signals. In this way, we obtain a DMT signal frame with the structure shown in Figure 3.3. In the typical generation algorithm, at this point we

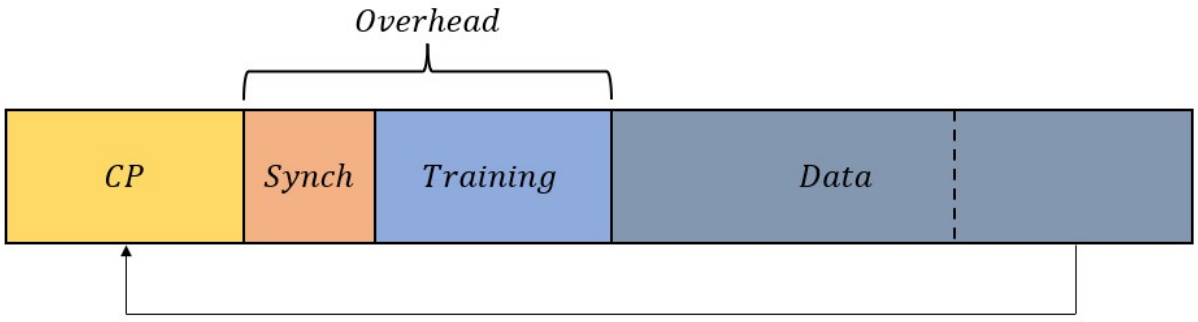

Figure 3.3: *DMT frame structure.*

have basically generated the driving signals, apart from a couple of manipulations. In our case this is not true, as the other fundamental operation of this procedure has still to be applied. In the block diagram, this passage is represented by the block "*Signals subtraction*" and it is based on its equivalent presented in (3.20): we must perform a subtraction between the MZ signal and the DML signal. However, in order to get to the correct result, we have to find the right coefficients that should be associated to the waveforms in this operation. By developing all the theory and the calculations, it can be demonstrated that the two coefficients must be respectively

$$c_{DML} = \frac{V_\pi}{2} \frac{\bar{m}_{DML}}{\bar{m}_{MZ}} \tag{3.29}$$

$$c_{MZ} = V_\pi \tag{3.30}$$

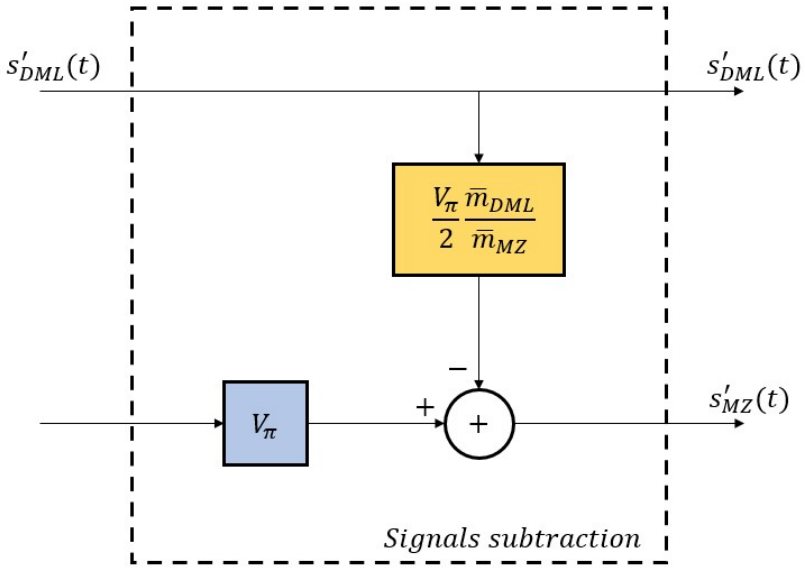

Figure 3.4: *Signals subtraction block implementation for a MZ modulator.*

where $\bar{m}_{DML}$ and $\bar{m}_{MZ}$ are the amplitude modulation Root Mean Square (RMS) indices for the DML and the MZ respectively. Therefore, we multiply the DML and MZ signals by the coefficients c_{DML} and c_{MZ} respectively and then we subtract the result, as shown in Figure 3.4. Employing (3.27), (3.28), (3.29) and (3.30), the DML and MZ electrical signals at the output of this operation are

$$s'_{DML}(t) = s(t) * h_{SSB,DML}(t) \tag{3.31}$$

$$s'_{MZ}(t) = V_\pi \cdot [s(t) * h_{SSB,MZ}(t)] - \frac{V_\pi}{2}\frac{\bar{m}_{DML}}{\bar{m}_{MZ}} s'_{DML}(t) \tag{3.32}$$

where $s(t)$ is the reference DMT signal, the symbol $*$ represents the convolution product and $h_{SSB,DML}(t)$ and $h_{SSB,MZ}(t)$ are the SSB filters impulse responses. Expressions (3.31) and (3.32) represent almost the driving signals for the two components of the dual modulator: there are just a couple of operations left. The first one is the clipping, which is applied to all three DMT signals. The clipping (and its subsequent electric filter) is able to limit possible big amplitude peaks in the signals. This is an important passage because, together with an advantage for the power amplifiers operation regime due to the PAPR reduction, it cuts those problematic samples that would make the small signal approximation not true anymore. The final passage is constituted by a frequency response pre-compensation for the DML and MZ signals, which must be taken into account, otherwise all the discussion of this section would be pointless. For what concerns

the DML, we have already stated that we can describe the device frequency response with the equivalent electrical filter reported in (2.8). For the MZ, instead, we assume to have a frequency response that can be modelled with a 5^{th}-order Bessel filter, which is just characterized by its *3 dB* bandwidth, that we name B_{MZ}. Figure 3.5a and Figure 3.5b show the two frequency responses for these filters. We can immediately observe that the two functions are always limited and they are never exactly equal to zero (the real part or the imaginary part can be zero, but never at the same time). For this reason, we can perform the frequency response pre-compensation with a very simple inverse filter in both case. If we name $G_{el,DML}(f)$ and $G_{el,MZ}(f)$ the frequency response respectively for the DML and for the MZ, we can finally say that the electric driving signals for the two devices are

$$s_{DML}(t) = \mathcal{F}^{-1}\left\{\frac{S'_{DML}(f)}{G_{el,DML}(f)}\right\} \tag{3.33}$$

$$s_{MZ}(t) = \mathcal{F}^{-1}\left\{\frac{S'_{MZ}(f)}{G_{el,MZ}(f)}\right\} \tag{3.34}$$

where $\mathcal{F}^{-1}$ is the inverse Fourier transform, $S'_{DML}(f)$ is the spectrum of the DML signal (after the clipping) and $S'_{MZ}(f)$ is the spectrum of the MZ signal (after the clipping). After a final electrical amplification, these waveforms get to the DML and the MZ modulator and they are the responsible for the light modulation. The output electric field is basically given by the same law that we have used in (3.21) (first line), but this time we add also the laser phase noise contribution to be closer to a real system. Therefore, using (3.33) and (3.34), the output optical field expression is

$$\begin{aligned} E_{out}(t) = \sqrt{P_0 \cdot \{1 + \mathcal{F}^{-1}[\mathcal{F}\{s_{DML}(t)\} \cdot G_{el,DML}(f)]\}} \cdot e^{j\phi(t)} \cdot e^{j\phi_n(t)} \cdot \\ \cdot \cos\left\{\frac{\pi}{2}\frac{2 \cdot \mathcal{F}^{-1}[\mathcal{F}\{s_{MZ}(t)\} \cdot G_{el,MZ}(f)] - V_\pi/2}{V_\pi}\right\} \end{aligned} \tag{3.35}$$

where $\mathcal{F}$ is the Fourier transform, $\phi_n(t)$ is the laser phase noise (related to the laser linewidth broadening) and $\phi(t)$ field phase due to the DML chirp and given by

$$\phi(t) = \frac{\alpha_{DML}}{2} \cdot s'_{DML}(t) + \frac{\alpha_{DML}\kappa P_0}{2} \cdot \int_0^t s'_{DML}(\tau)\, d\tau \tag{3.36}$$

Note that in the phase calculation we use $s'_{DML}(t)$ and not $s_{DML}(t)$ because the driving

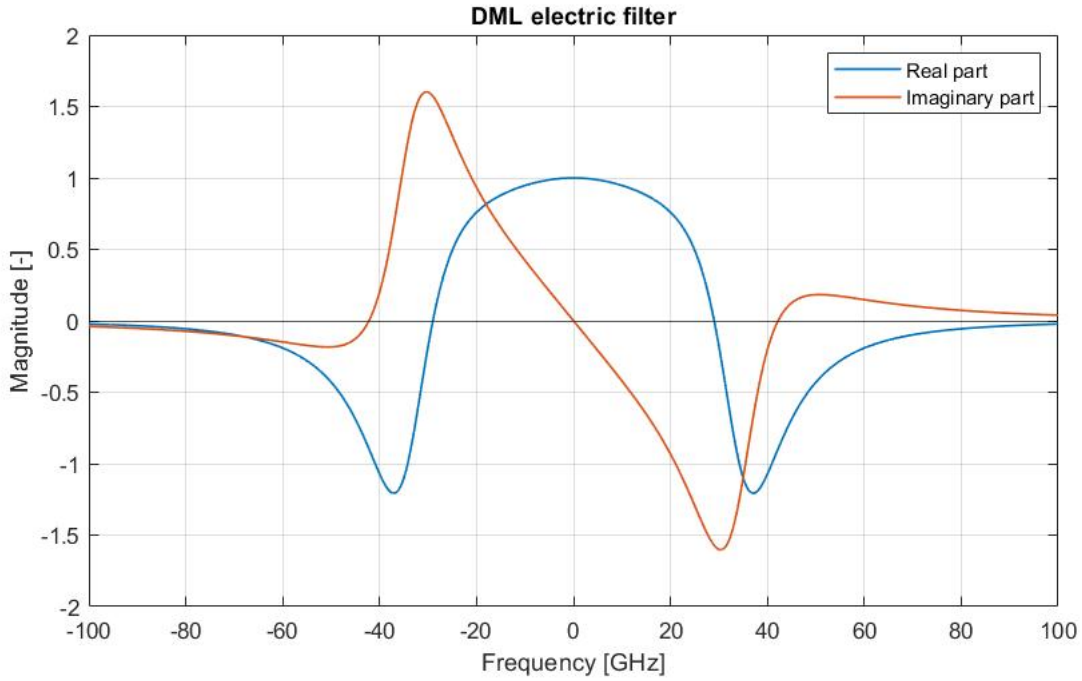

(a)

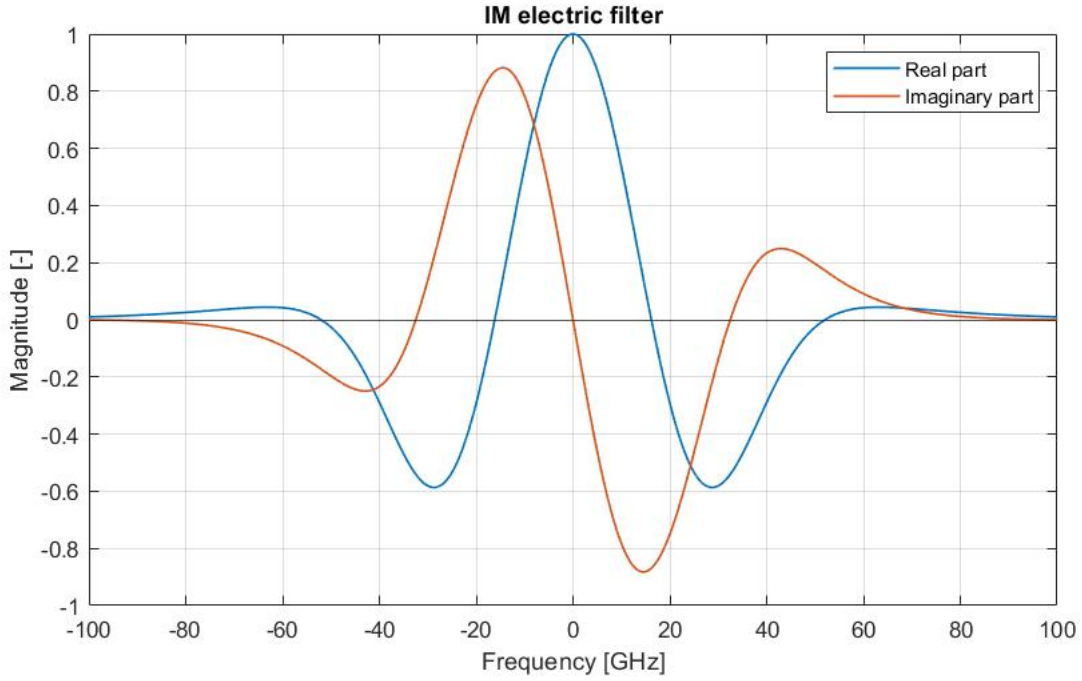

(b)

Figure 3.5: *Frequency response of the equivalent electrical filter associated to* ***(a)*** *the DML (f_i = 35 GHz, f_p = 35 GHz, γ = 100 GHz) and* ***(b)*** *the MZ modulator (B_{MZ} = 25 GHz)*

signal is first subjected to the DML frequency response and the output of this operation is what determines the laser chirp. In other words, it's like we had the DML frequency filter cascaded with an ideal DML. Moreover, note that the optical field phase depends not only on the DMT signal at a certain time instant t_0 but also on the signal itself at all the previous time instants by means of the integral. This is interesting because it's like the system had a memory. However, by substituting (3.33), (3.34) and (3.36) into (3.2) and by applying the small signal approximation, the output electric field becomes

$$E_{out}(t) = \sqrt{\frac{P_0}{2}} \cdot [1 + \pi \bar{m}_{MZ} s(t) + \pi \bar{m}_{MZ} \tilde{s}(t)] \cdot e^{j\phi_n(t)} \tag{3.37}$$

that, apart for the laser phase noise, corresponds to a SSB signal.
This discussion is basically valid also in the DML-EAM case ([5]): the differences in the procedure are represented by the two SSB filters frequency responses and the coefficients applied in the signals subtraction passage, which are due to the EAM chirp and EAM transfer function respectively. In our simulator we have implemented this generation case as well, so that we can compare the two solutions.

3.3. DMT signal detection

After the discussion of the SSB generation algorithm for the dual modulator scheme, we must also take into account the signal detection. In fact, considering just the electric field and the signal spectrum, we are not able to understand whether the produced waveform is a good signal for the data transmission or not. Moreover, as we said in Section 2.3, SSB signals are a very interesting and promising solution for amplified and un-compensated networks, so we must check if, under the hypothesis of a correct generation, the detection of the signal after a certain distance returns a good performance. For these reasons, we need to simulate the optical field detection. With respect to the previous sections in this chapter, the discussion that we are going to deal with is completely general, so it's applicable both to the DML-EAM architecture and to the DML-MZ scheme. Moreover, it's applicable both in case of Back-to-Back (*B2B*) transmission and in case of signal propagation along the optical fiber.
Considering that we are working in an IM-DD context, we have to implement the direct detection approach for the signal. This makes life easier, since, with this kind of detection, it's enough to characterize the receiver just with three parameters, which are

- the photodiode responsivity;

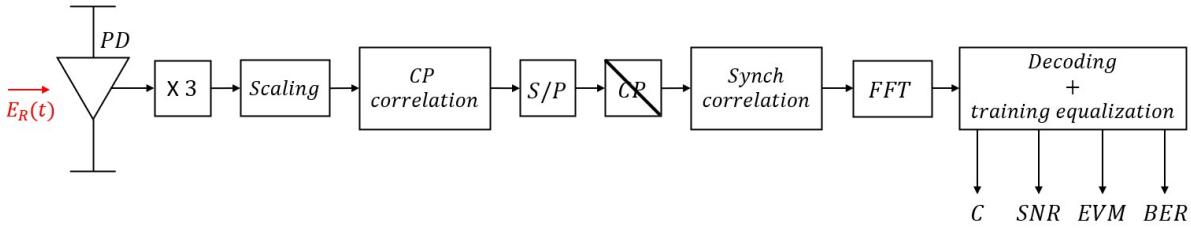

Figure 3.6: *Block diagram of the DMT detection algorithm for direct revelation.*

- the photodiode equivalent filter *3 dB* bandwidth;
- the receiver electrical noise power.

The photodiode responsivity ρ is the parameter that describes the opto-electrical (O/E) conversion. In particular, it is the proportionality constant that links the generated photocurrent I_{ph} and the optical field power at the receiver P_R in the relation

$$I_{ph}(t) = \rho P_R(t) \tag{3.38}$$

The photodiode bandwidth B_{ph} takes into account the photodetector frequency response, which can modelled with an electrical filter acting on the photocurrent. In our simulator, this frequency response in modelled with a 5^{th}-order Bessel filter, which has been already shown in Figure 3.5b. Finally, we must introduce something to consider the receiver electrical noise associated to the photocurrent. The designated parameter is the Noise Equivalent Current (NEC), that contains a contribution for all the noise sources (shot noise, Johnson noise, etc...). This quantity is related to the photocurrent variance through the expression

$$(\Delta I_{ph})^2 = NEC^2 \cdot \frac{f_c}{2} \tag{3.39}$$

where f_c is the signal sampling frequency. This variance corresponds exactly to the receiver electrical power noise.

Once we have understood which the fundamental parameters are, we can move to the analysis of the real detection algorithm implementation. The block diagram of the procedure is reported in Figure 3.6. The first step is the O/E conversion from the optical domain to the electrical domain performed by the photodiode. Equations (3.38) and (3.39) are the two contributions that constitute the whole photocurrent:

$$I_{ph}(t) = \rho \cdot |E_R(t)|^2 + (\Delta I_{ph})^2 \cdot N(\mu = 0, \sigma = 1, t) \tag{3.40}$$

where we have considered that the optical power is proportional to the absolute squared value of the optical field E_R. The term $N(\mu = 0, \sigma = 1, t)$ in (3.40) that multiplies the electrical noise power represents a standard gaussian distribution, that is a bell-shaped distribution having zero average and standard deviation equal to 1. This basically means that we are assuming to have a gaussian electrical noise with a mean value equal to zero. This current is filtered by the electrical filter associated to the photodiode and then the DC component is removed, as it does not contain any information. At this point, we build two replicas of the current signal and we tailor them the the original waveform. This operation is necessary for the following DSP. From now on, we present the DSP part of the DMT detection algorithm. After a signal scaling useful to have a clearer definition of the signal itself, it is subjected to a first correlation, based on the CP. This operation's aim is to obtain the correct alignment for the DMT frame. An example of the correlation output is represented if Figure 3.7. We can observe that it is a function

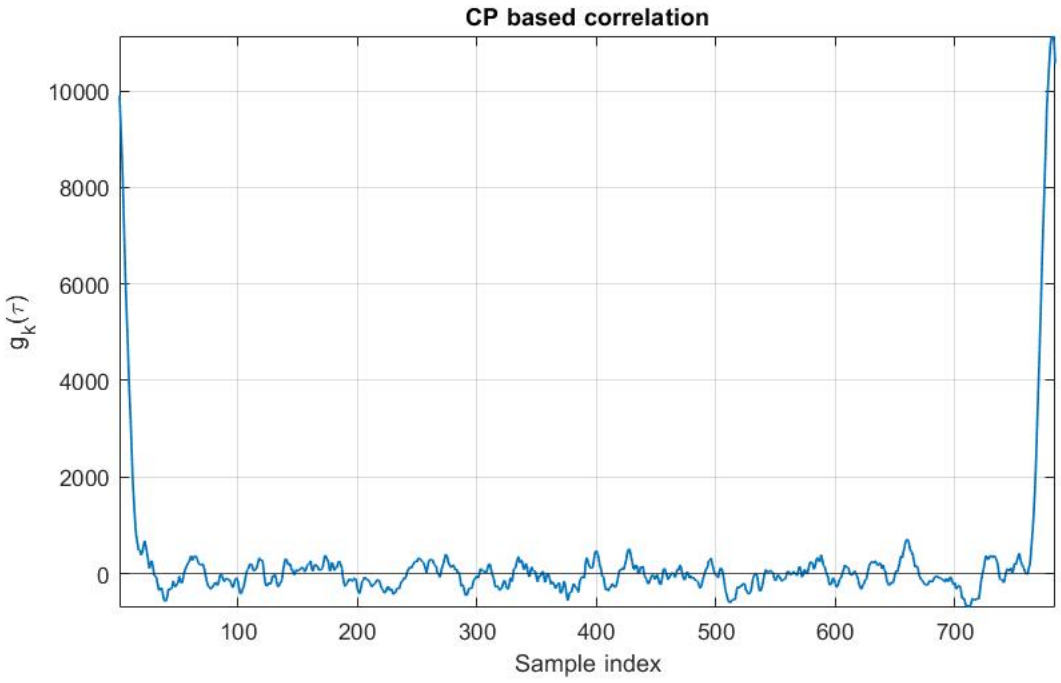

Figure 3.7: *CP based correlation for the DMT signal detection.*

where there are huge peaks separated by a random oscillation around zero. The spikes are situated in correspondence of those points where the CP is perfectly superimposed to one of its replicas, while the random oscillation is justified by the superimposition of totally uncorrelated signal sections. In this way, we get the correct alignment of the

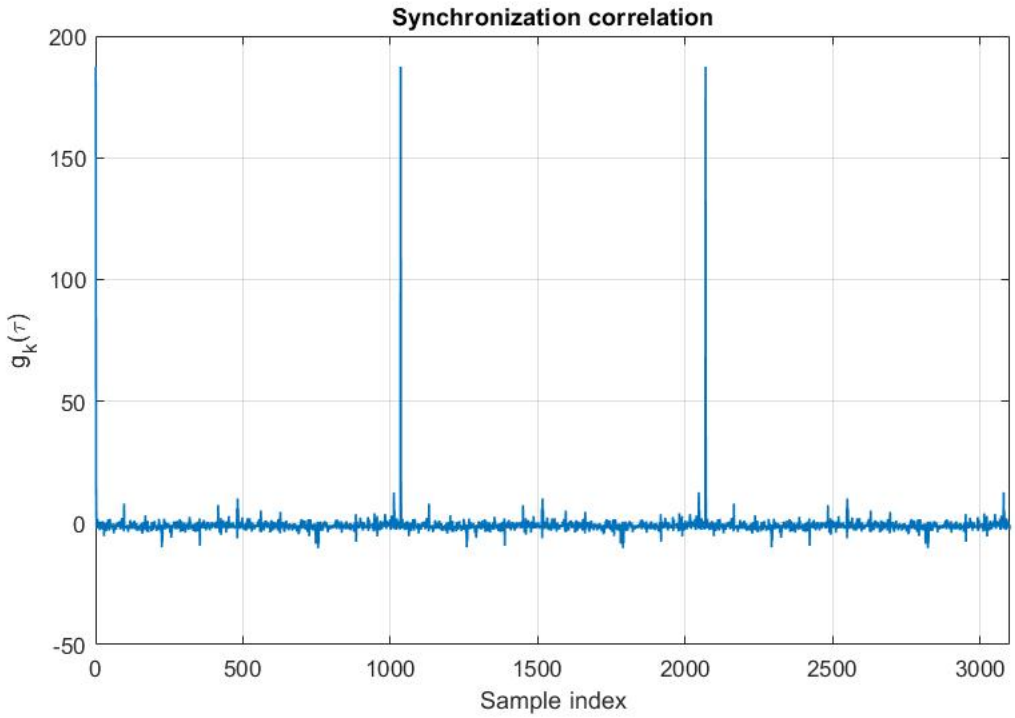

Figure 3.8: *Synchronization based correlation for the DMT signal detection.*

symbols and we determine the desired frame position. From this result, we perform a S/P operation and we remove the CP, leaving just the synchronization, training and data symbols. The next passage is constituted by a second correlation, based, this time, on the synchronization symbols. This operation is needed for the correct frame synchronization and it is as fundamental as the previous one. In fact, as we discussed in Section 2.1, an error in the signal sampling process causes the generation of ICI, which is detrimental for the system performance. The output of this correlation is reported in Figure 3.8. In this case too, the autocorrelation peaks are clearly evident with respect to the random oscillation around the zero value. These peaks are located where the synchronization symbols of the signal replicas are superimposed, so they allow to find the beginning and the end of the DMT frame and to correctly set the sampling time instants. Once the frame is properly aligned and synchronized, we apply a FFT and we select the data symbols associated to the various subcarriers. The final operation left is the actual decoding of the QAM symbols subcarrier by subcarrier. First, all the synchronization symbols are removed. Then, for each subcarrier we apply the channel equalization based on the training symbols and, at last, we retrieve the information contained in the data symbols. After this process, we are able to evaluate the system performance by computing

- the capacity (C) in $Gbit/s$;

- the Signal-to-Noise Ratio (SNR) for each subcarrier;
- the Error Vector Magnitude (EVM) for each subcarrier;
- the Bit Error Rate (BER) both for each subcarrier (starting from the EVM) and the real one (derived by a bit-to-bit comparison between the detection output and the starting PRBS).

4 | Simulation design results

In Chapter 3 we have presented and discussed in detail all the theory needed for the SSB signal generation, both in the single harmonic case and in the more advanced DMT signal case. Now, we have to run the simulations and evaluate the results, obviously assuming that the developed models are correct. In particular, not only we have to analyze the SSB generation performance for the DML-MZ dual modulator scheme, but we must also perform a first comparison with the results achievable with a DML-EAM dual modulator architecture. This is something that will be done considering various aspects and it will possibly help us begin to understand the system performance with the new dual modulator scheme proposal. The chapter is organized as follows;

- in Section 4.1 we discuss the results with a single sinusoid as modulation signal;
- in Section 4.2 we show the effect of possible errors on the model in the single harmonic case;
- in Section 4.3 we analyze the generation outcomes in the DMT signal case.

4.1. Single sinusoid model validation

The starting point has inevitably to be the validation of the single sinusoid theory that we have developed in Section 3.1, because this can helps us to understand, in case the model is valid, whether the performance are comparable with the DML-EAM dual modulator ones or not.
In order to perform this analysis, we have to fix some parameters. In particular, we have to set

- the modulation frequency;
- the laser parameters;
- the intensity modulator parameters.

Parameter	**DFB**	**VCSEL**
α_{DML} [-]	2.7	3.8
κ_{DML} [GHz/mW]	10	15.2
CW power [mW]	10	10
$\Delta\nu_L$ [MHz]	1	5
m_{DML} [-]	0.01	0.01

Table 4.1: *DFB laser and VCSEL parameters used in the simulations.*

As we want to compare the results with an EAM and with a MZ modulator, we have to define the parameters for both of them. For what concerns the EAM, we can fix the linewidth enhancement factor $\alpha_{EAM} = 0.5$ in order to take its chirp into account ([4]). For the MZ, instead, we have $\alpha_{MZ} = 0$ as it does not introduce any chirp contribution in the PP configuration and then we can select a π-voltage $V_\pi = 5\ V$, which implies a bias voltage $V_B = 2.5\ V$ (values deduced from [32]-[37]). Regarding the lasers, we said that both DFB lasers and VCSELs can be good solutions, so we can fix the necessary parameters for both devices in order to perform a comparison between the two possibilities. The values are reported in Table 4.1. Finally, we have to choose the frequency modulation. Since the scope is the development of an analysis as much complete as possible, we can perform the simulations with four modulation frequencies, respectively equal to 1 GHz, 5 GHz, 10 GHz and 20 GHz. Obviously, all the values are realistic, otherwise the simulation would be pointless. Before proceeding, note that the laser emission central wavelength has not been mentioned in the simulation parameters. This is because the laser wavelength becomes relevant when one thinks in passband terms and lets the signal propagate along the optical fiber. However, once all the needed quantities are fixed, we run the simulations: the results are represented in Figure 4.1 and in Figure 4.2 (in both cases the 20 GHz spectrum is not shown for a sake of clarity of the images, but, in the following, we still report the various parameters for this frequency too). Moreover, in Table 4.2 and in Table 4.3 we report all the model parameters derived from the fundamental ones (as to say the fixed ones), so that we can make some comments about them. Finally, in Table 4.4 we compute and report the Optical Sideband Suppression Ratio ($OSSR$) values expressed in dB for each one of the four modulation frequencies chosen for the four dual modulators schemes that can be built with a DFB laser, a VCSEL, a EAM modulator and a MZ modulator.

First of all, note that all the simulations do not include the laser phase noise, as evidenced by the presence of Dirac deltas in the power spectra. We can make this choice

	DFB				VCSEL			
f_{mod} [GHz]	m_{PM} [-]	ϕ_{PM} [rad]	m_{IM} [-]	Δ [rad]	m_{PM} [-]	ϕ_{PM} [rad]	m_{IM} [-]	Δ [rad]
1	0.2153	0.0627	0.0685	0	0.4600	0.0413	0.1464	0
5	0.0450	0.3044	0.0143	0	0.0939	0.2038	0.0299	0
10	0.0254	0.5610	0.0081	0	0.0497	0.3920	0.0158	0
20	0.0173	0.8986	0.0055	0	0.0298	0.6908	0.0095	0

Table 4.2: *Values of the model parameters derived from the laser and IM modulator fundamental ones in the case of a* ***MZ modulator****.*

	DFB				VCSEL			
f_{mod} [GHz]	m_{PM} [-]	ϕ_{PM} [rad]	m_{IM} [-]	Δ [rad]	m_{PM} [-]	ϕ_{PM} [rad]	m_{IM} [-]	Δ [rad]
1	0.2153	0.0627	0.3849	0.4520	0.4600	0.0413	0.8228	0.4582
5	0.0450	0.3044	0.0793	0.4099	0.0939	0.2038	0.1671	0.4374
10	0.0254	0.5610	0.0432	0.3758	0.0497	0.3920	0.0874	0.4163
20	0.0173	0.8986	0.0275	0.3622	0.0298	0.6908	0.0506	0.3955

Table 4.3: *Values of the model parameters derived from the laser and IM modulator fundamental ones in the case of an* ***EAM modulator****.*

	OSSR [dB]			
f_{mod} [GHz]	*DFB-EAM*	*DFB-MZ*	*VCSEL-EAM*	*VCSEL-MZ*
1	41.1	71.6	25.6	64.8
5	71.4	86.5	56.8	79.2
10	82.2	94.0	69.1	85.6
20	85.8	97.7	78.0	92.2

Table 4.4: *OSSR values obtained from the simulations for the four type of dual modulator schemes at the selected modulation frequencies*

because the main phase noise contribution is a broadening of the harmonics peaks, while it does not have a relevant effect on the amplitudes. For this reason, in this analysis the laser phase noise can be neglected for simplicity.
Secondly, we can clearly observe that the intensity modulator choice has the biggest impact on the output spectrum quality, but the laser selection affects the output too. In particular, by looking at Table 4.4, the OSSR values obtained with the MZ modulator are better (in certain circumstances even much better) than the one obtained with the EAM modulator. At the same time, once the intensity modulator is fixed, it is evident that the results obtained using the DFB laser are slightly better than the outcomes recovered with the VCSEL. This last improvement is marginal but not negligible. We can also notice that these statements are less and less true as the modulation frequency increases. The reason behind these behaviours is easily explainable by looking at Table 4.2 and Table 4.3. The relevant parameter in this analysis is the amplitude modulation index m_{IM}, because it is the responsible for the output signal amplitude and, in the end, for the small signal approximation correctness (see (3.26)). Due to the different definition in the two models, it stands immediately out that the parameter values with an EAM are much higher than with a MZ. This is a big issue especially when the modulation frequency is low, as the modulation index can become so high that the small signal regime is not verified anymore. Indeed, this is exactly what happens when the modulation frequency is 1 GHz and, as a consequence, leads to the worst results. For the other three modulation frequencies, this effect is less evident and we can also observe that the situation improves as the index value decreases with an increase of the modulation frequency. When we use a MZ, instead, this problem does not appear and we are able to obtain a very good OSSR even with the modulation frequency of 1 GHz. Therefore, standing on this analysis, the MZ modulator prevails over the EAM modulator.
Then, for what regards the laser, the discussion is very simple too. In fact, looking at Table 4.1, we can conclude that a DFB laser is more stable than a VCSEL, since its chirp

parameters (and linewidth broadening) are lower. This implies that all the derived parameters m_{PM}, ϕ_{PM}, m_{IM} and Δ (if not zero) assume a lower value in the DFB case with respect to the VCSEL one, which means that model assumptions work better in the first case than in the second one. Again, this affirmation is more important for the parameter m_{IM}, because it is directly related to the small signal regime validity. However, in this analysis too, the difference between the results achievable with the two DMLs decreases as the frequency modulation increases, as the small signal condition is more and more satisfied. Moreover, even if we consider the worst case at 1 GHz, the difference between the OSSR values is not so relevant to allow us to say that a laser choice is better than the other one, especially when a MZ modulator is employed as intensity modulator.

Finally, a possible doubt that can arise is why in all the spectra there is still a contribution of LSB. In fact, the moment we perfectly satisfy the SSB conditions for both dual modulator architectures, we would expect to have a total suppression for the Dirac delta at frequency $f = -f_{mod}$, but that is not the case. The explanation of this event is simply that DML, EAM and MZ are devices characterized by non-linear transfer functions, which implies a generation of higher order harmonics. Indeed, in all the power spectra some Dirac deltas at frequencies multiple of the modulation frequency are visible. Among these higher order terms, the odd order harmonics (3^{rd}, 5^{th}, etc...) originate spurious contributions exactly at the modulation frequency. Nevertheless, being the small signal condition valid, the amplitude of these terms greatly drops when the harmonic order increases. For this reason, the impact of these contributions is not as much visible for the USB as much it is for the LSB. This is exactly what creates the LSB Dirac delta, but it's amplitude is so small that it is negligible for sure, so it is not a problem at all.
However, we can see how the USB harmonic at frequency $f = f_{mod}$ is greatly enhanced with respect to its corresponding LSB one with huge OSSR values (reported in Table 4.4). It is interesting two note that the OSSR tends to reduce when the modulation frequency lowers. This is due to two main factors:

- the parameters m_{PM}, ϕ_{PM} and m_{MZ} depend on the modulation frequency (as we have said, they increase when the modulation frequency decreases, potentially undermining the small signal approximation);
- the beating between the DC component and the harmonic becomes more and more effective and relevant as the modulation frequency lowers.

Apart for this detail, the obtained OSSR values in both cases are very good, so we can affirm that the SSB signal generation is absolutely effective and satisfying and the performance obtained in the MZ case is even better than what we have with an EAM. This certifies the correctness of the developed single sinusoid model and the potential

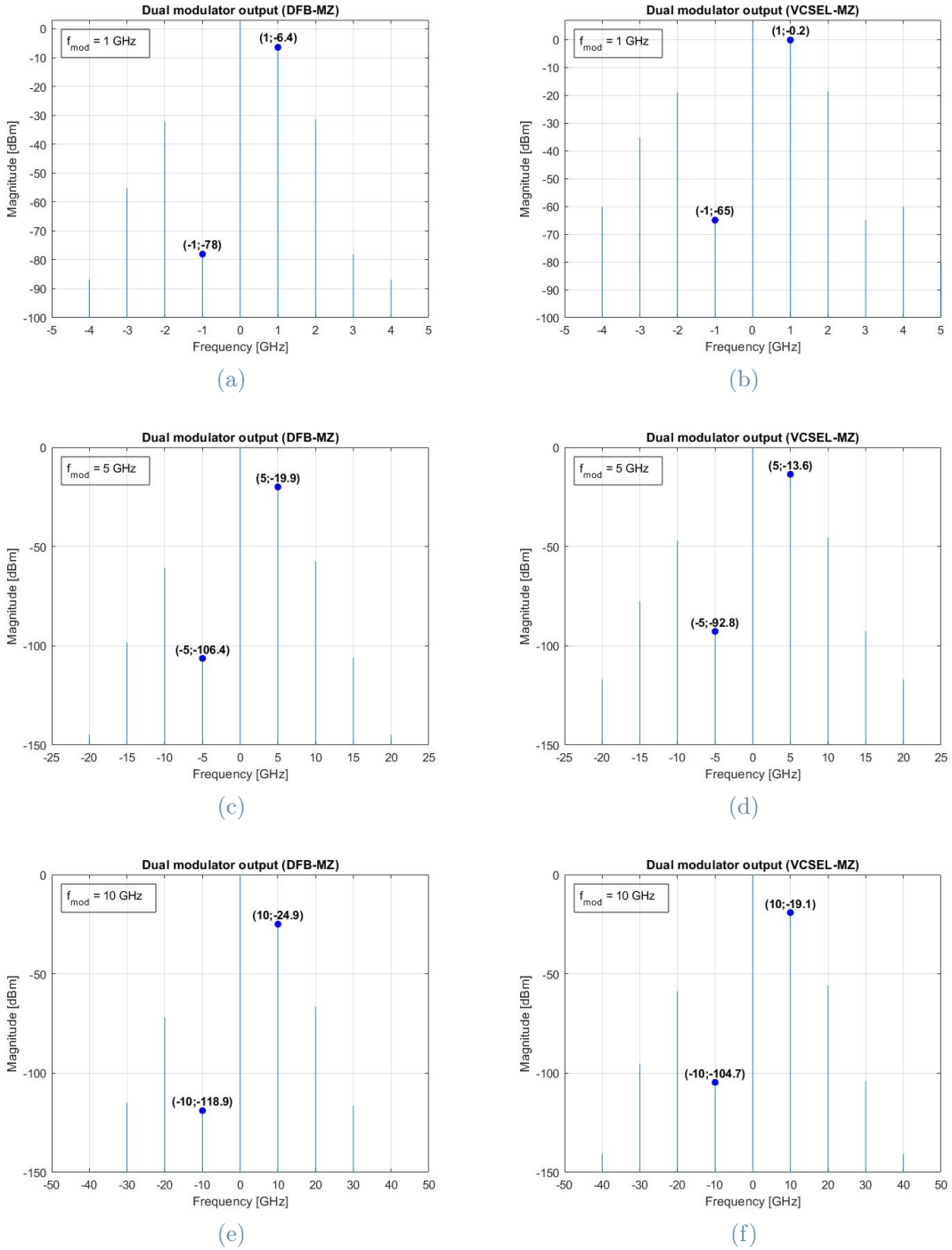

Figure 4.1: *Optical output spectra for the DML-MZ dual modulator scheme. For figures* ***(a)***, ***(c)***, ***(e)*** *was used a DFB laser; for figures* ***(b)***, ***(d)***, ***(f)*** *was used a VCSEL.*

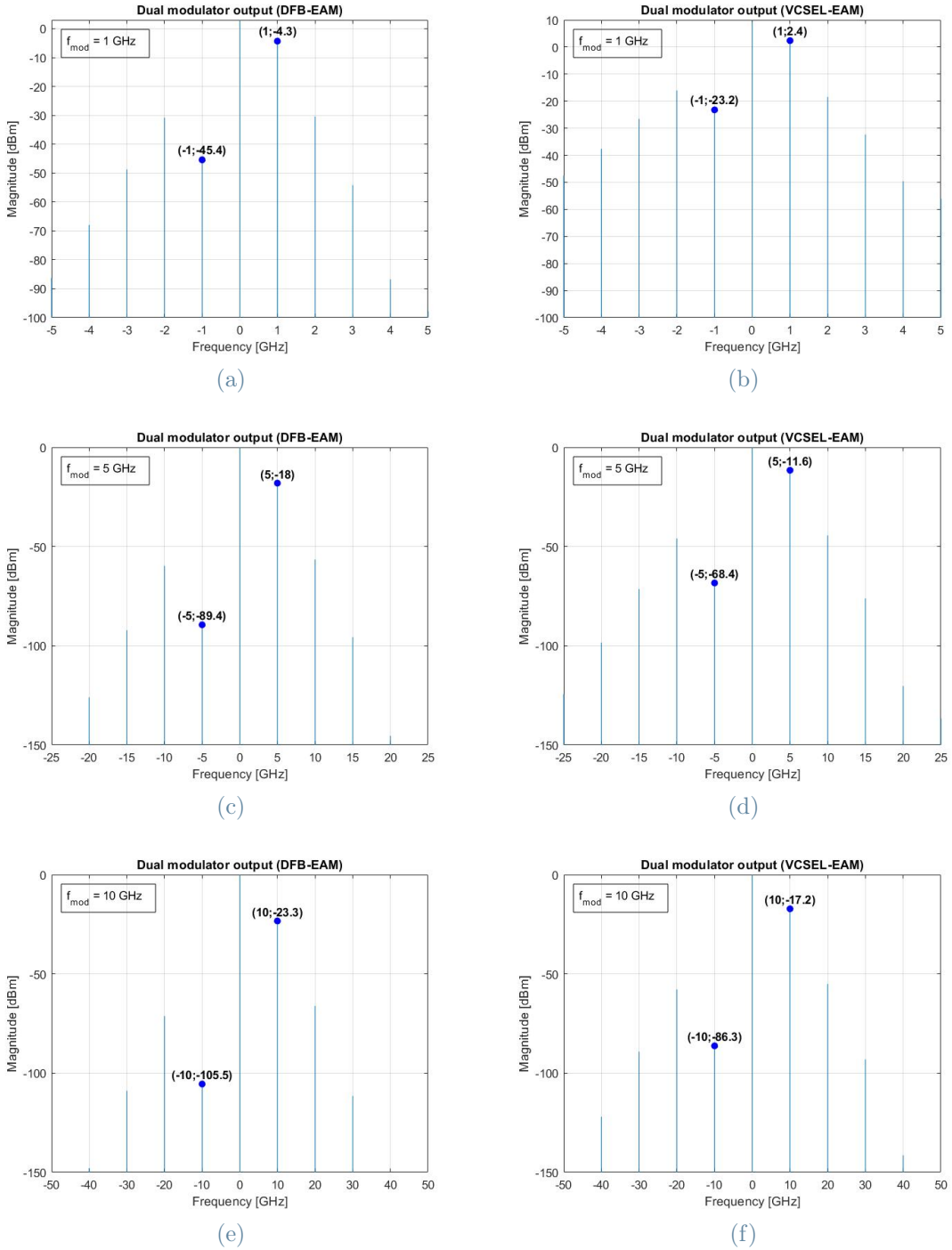

Figure 4.2: *Optical output spectra for the DML-EAM dual modulator scheme. For figures* ***(a)***, ***(c)***, ***(e)*** *was used a DFB laser; for figures* ***(b)***, ***(d)***, ***(f)*** *was used a VCSEL.*

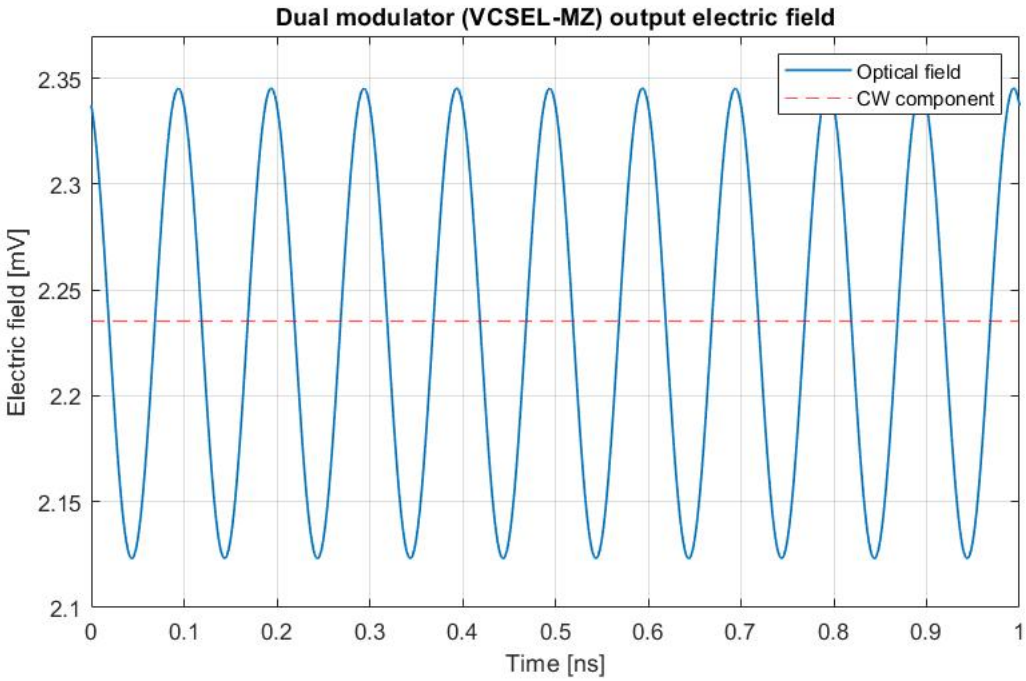

Figure 4.3: *Output optical field for the VCSEL-MZ dual modulator with the modulation frequency* $f_{mod} = 10\ GHz$.

quality of the DML-MZ dual modulator architecture. Passing from the frequency domain to the time domain, the output electric field consist of a sinusoid at the used modulation frequency that oscillates around a DC value. Figure 4.3 shows this behaviour for a DFB-MZ dual modulator driven with a cosinusoid at frequency $f_{mod} = 10\ GHz$. So, we have obtained an optical field that goes exactly as the modulation signal, apart for a phase shift induced by the DML direct modulation (this is evident especially for $t = 0$. The same result can be found with the VCSEL-MZ modulator and for all the other modulation frequencies with both dual modulator schemes.

4.2. Errors impact on the model performance

Together with the theoretical model, it is very important also to go through an analysis focused on the performance evaluation in a non-ideal condition. For this reason, now the scope is to evaluate the single sinusoid model limitations in presence of errors in the signal generation process. This study about the model stability is fundamental to understand the margin that we have before the model performance dramatically drops. In our case, this implies a discussion about the OSSR variation when we introduce an amplitude error

and/or a phase error. We perform this kind of investigation in the single sinusoid case and not with a DMT signal mainly for two reasons:

- the single harmonic is a simplified case, so all the evaluation process and the results explanation is much easier;
- if an error has a huge impact on the system performance with one sinusoid, the effect can just worsen for a DMT signal.

Therefore, in order to develop this topic, we choose to use a DFB laser with the parameters reported in Table 4.1 (we still neglect the phase noise for simplicity) and, in addition, we fix also a modulation frequency $f_{mod} = 10\ GHz$. Then, we can consider different situations where the error can be either in amplitude or in phase or it can be both in amplitude and phase. Before showing the results, we have to clarify what we mean with phase error and amplitude error. The first one is related to the differential phase shift Δ between the two devices, while the latter one is referred to the ratio m_{MZ}/m_{DML}, both defined in (3.20). These two quantities, as demonstrated in Sections 3.1 and 4.1, are essential to obtain a good SSB signal at the output of the dual modulator. Therefore, what we do now in this simulation is to use the wrong parameter pair $\{(m_{MZ} + \varepsilon_{am})/m_{DML}\ ;\ \Delta + \varepsilon_{ph}\}$ instead of the right one $\{m_{MZ}/m_{DML}\ ;\ \Delta\}$, where ε_{am} and ε_{ph} represent the error in amplitude and phase respectively. With this said, we run the simulation and we obtain the results shown in the following figures. In particular, Figure 4.4 represents the OSSR surface obtained by using different error pairs, while Figure 4.5a and Figure 4.5b are two surface sections where one of the two errors is fixed and we study the effect of the other one. Obviously,the best realization condition for the SSB signal corresponds to the ideal one, where there are no errors at all: the recovered OSSR is equal to 85.6 dB. However, as soon as we move away from this situation, there is a very fast and dramatic drop of the OSSR, so it is utmost important to have a high precision degree available working with this system and this kind of signals. In fact, note that the plots are made with relatively small errors: for what concerns the phase, the maximum error (in absolute value) is 0.2 rad; the maximum error for the amplitude, instead, is equal to 0.02, chosen in order to have a maximum deviation (in absolute value) equal to 2 with respect to the correct indices ratio. Nevertheless, even such small errors are enough to cause a fast deterioration of the OSSR from its peak value to definitely lower values ($20 - 25\ dB$). For the phase error, in Figure 4.5a we can observe that an amplitude error introduces a slight asymmetry in the OSSR trend (something not happening in the ideal case $\varepsilon_{am} = 0$), which means that the two error terms are somehow related. In Figure 4.5b, instead, we notice that the OSSR function is extremely asymmetric and it shows an asymptotic tendency as the amplitude error increases. This behaviour can be explained quite easily. For this analysis, we need

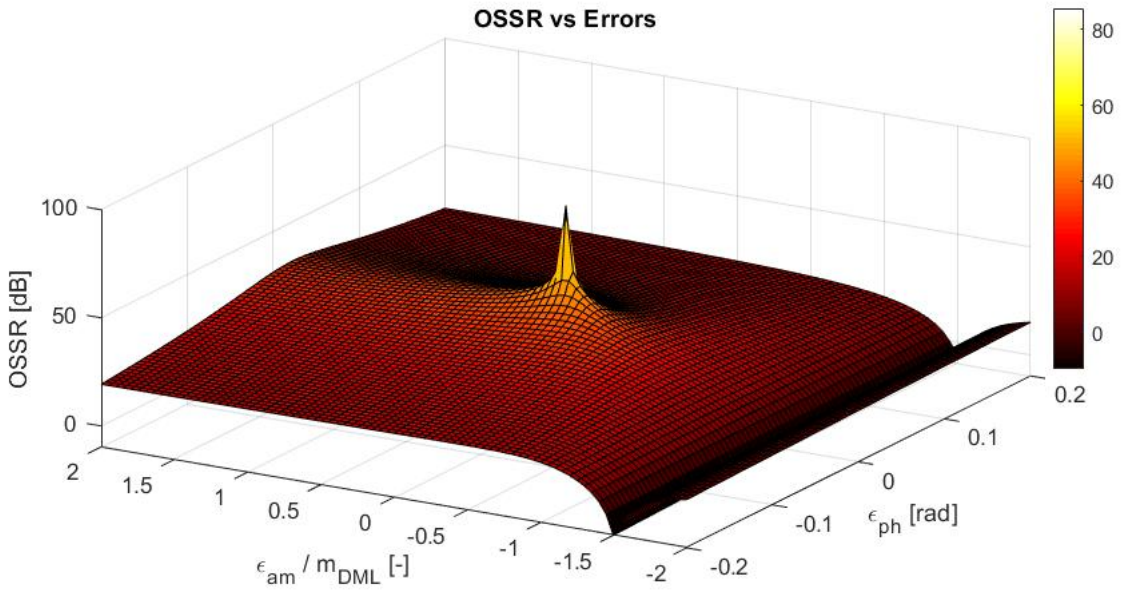

Figure 4.4: *Single harmonic model performance in the presence of amplitude and phase errors.*

to keep in mind that the LSB suppression is entrusted to a cancellation of the DML amplitude modulation with the MZ driving signal and this happens by means of the the arithmetic sum

$$x(\varepsilon_{am}) = \frac{m_{DML}}{2}\cos(\omega t) - \frac{m_{DML}}{m_{MZ}+\varepsilon_{am}} \cdot \frac{m_{MZ}}{2}\cos(\omega t) \tag{4.1}$$

which is basically the same expression of (3.21) when (3.22) is introduced, but generalized to take the amplitude error into account. Assuming to have $\varepsilon_{ph} = 0$ for a sake of simplicity, we can identify four cases for (4.1):

- if $\varepsilon_{am} = 0$, the two contributions perfectly cancel out each other and we obtain the maximum OSSR possible;
- if $\varepsilon_{am} > -m_{MZ}$ and $\varepsilon_{am} > 0$, then $m_{DML}/(m_{MZ}+\varepsilon_{am}) > 0$, so we have a subtraction. This means that there is not a perfect elimination, but we still get a partial cancellation. This implies that the OSSR slowly decreases and tends to an asymptotic value depending only on the two modulation indices m_{DML} and m_{MZ};
- if $\varepsilon_{am} > -m_{MZ}$ and $-m_{MZ} < \varepsilon_{am} > 0$, then $m_{DML}/(m_{MZ}+\varepsilon_{am}) < 0$, so we still have $m_{DML}/(m_{MZ}+\varepsilon_{am}) > 0$ and, as a consequence, a subtraction. However, this time the OSSR drop is much sharper and more rapid. The cause is the fact that we are going toward the condition where $m_{MZ} + \varepsilon_{am} \to 0$, which it's like to

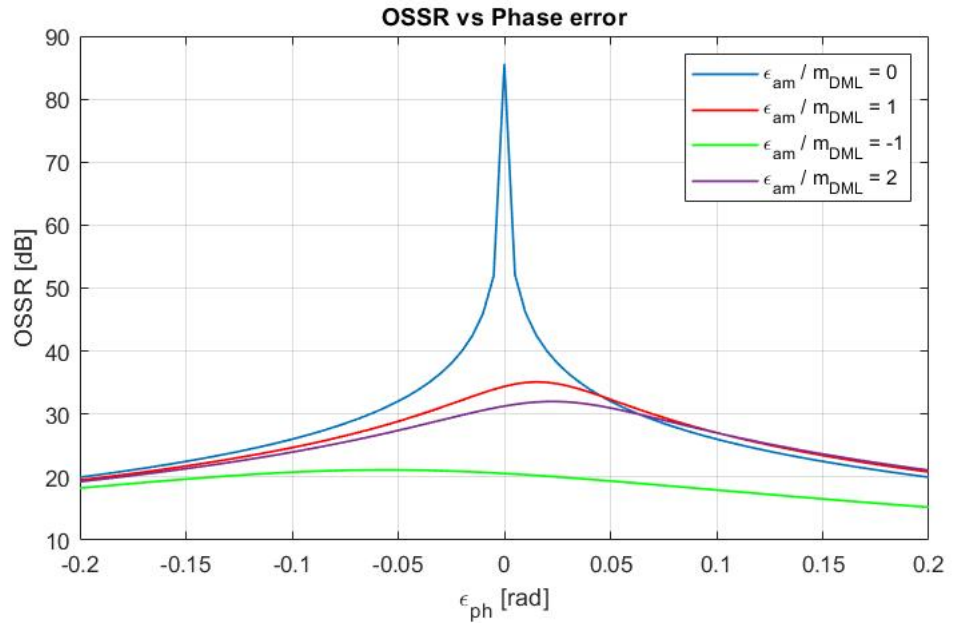

(a)

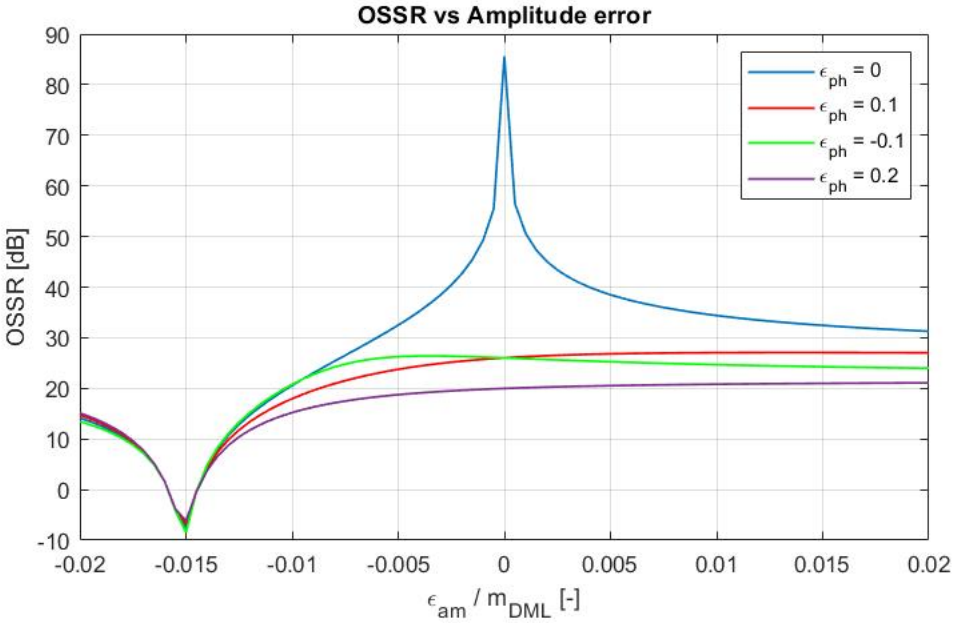

(b)

Figure 4.5: *OSSR surface cuts:* ***(a)*** *model performance varying the phase error with a fixed amplitude error;* ***(b)*** *model performance varying the amplitude error with a fixed phase error.*

say $m_{DML}/(m_{MZ}+\varepsilon_{am}) \to \infty$. Obviously, this implies that that the LSB is even enhanced instead of suppressed and, indeed, the OSSR becomes negative and the function absolute minimum;

- if $\varepsilon_{am} < -m_{MZ}$, then $m_{DML}/(m_{MZ}+\varepsilon_{am}) > 0$, so now we have a sum between the two contributions. Therefore, there is no LSB suppression, though we observe an increase of the OSSR until it gets to the same asymptotic regime previously described.

The asymptotic behaviour can be easily explained and the demonstration that it depends just on the indices m_{DML} and m_{MZ} is reported in Appendix B. This discussion made in the case $\varepsilon_{ph} = 0$ can be completely generalized when there is a phase error contribution too. Clearly, this new term has a certain impact on the asymptotic value of the OSSR, but Figure 4.5b shows that this effect is not so pronounced. However, in [4], there is a similar analysis with similar results, even if we can notice that the model for the DML-EAM modulator is slightly more stable. In fact, due to the different parameters definition, the negative depression of the OSSR cannot be seen, since it is shifted toward higher amplitude error values. Nevertheless, minimum errors cause a dramatic OSSR drop in this case too. Therefore, we get to the conclusion that a SSB signal generation is an extremely delicate process and we need to guarantee that the employed devices quality is good enough to have the proper precision.

4.3. Validation of the DMT generation procedure

After all the discussion about the single harmonic model and after demonstrating that it works properly, we can move to the analysis of the model for the DMT SSB signal generation, so that we can verify the potential validity of it. As previously done, we perform a comparison between the DML-EAM solution and our DML-MZ proposal. In this latter case, furthermore, we have to try to understand whether the laser choice has an impact on the output signal or not, which means a study both in terms of spectrum and in terms of time domain waveform. First of all, we must fix the fundamental parameters of the system, which are the components ones and the DMT signal ones. For what regards the lasers and the intensity modulators, we choose to use the same parameters employed in Section 4.1 apart for the CW power, that we set equal to 5 mW both for the DFB laser and for the VCSEL. Along with these ones, we fix also the parameters needed to keep the frequency responses into account: they are all reported in Table 4.5. In Table 4.6, instead, there is the list of the DMT signal parameters employed in the electrical waveform

generation. Due to the bit loading and power loading processes, note that in Table 4.6 we are fixing the constellations (and implicitly the power) just for the synchronization and training sections of the DMT frame.
With everything done, we can now apply the algorithm presented in Section 3.2, obviously referring to the MZ case. The starting point is the generation of the driving DMT DSB signals for the DML and the MZ in the electrical domain. The spectra of these signals in their final form (so after the digital SSB filtering, the subtraction, the clipping and the frequency response pre-compensation) are shown in Figure 4.6. In this picture we also report the spectrum of the basic SSB signal obtained with the classical algorithm (that is without any unusual kind of filtering or subtraction) before any pre-compensation. These graphs allow to visualize the effect of the various operations that we discussed in Section 3.2. In particular, for the DML signal spectrum it is evident the low frequencies depression with respect to the high frequencies enhancement. This is the combined result of the DML SSB filter application and the DML frequency response pre-compensation, as in both cases there is a reduction of the low frequencies amplitude with respect to the high frequencies. A posteriori, after the analysis of Section 4.1, it's easy to understand that this is done to combat the frequency dependence of the model parameters for the various components. Something similar happens for the MZ DMT signal spectrum, but the depression is less emphasized. This is because the suppression is just given by the frequency response pre-compensation, since the MZ SSB filter is a pure phase filter and, as a consequence, does not affect the spectrum amplitude. Together with the spectra, it is important also to consider the electrical signals in the time domain in order to check whether the small signal condition is verified or not. Figure 4.7 shows exactly this aspect of the DMT signals and it is straightforward to say that the working regime is correct. Actually, this statement is quite to the verge of the validity, but slightly exceeding in the non-linear region of the DML and MZ transfer functions does not necessary mean that we obtain negative effects. Moreover, we have to take into account that the pre-

Parameter	**Value**
f_i [GHz]	15
f_p [GHz]	5
γ [GHz]	100
B_{MZ} [GHz]	20
B_{EAM} [GHz]	20

Table 4.5: *Parameters for the DML and IM frequency responses.*

Parameter	Value	Meaning
B_{sig} [GHz]	20	Signal band
M_{PRBS} [-]	15	PRBS order
N_{tot} [-]	768	Total number of subcarriers
N_{sub} [-]	255	Used subcarriers number
CP [-]	16	Cyclic Prefix length
Δf_{sub} [MHz]	78.23	Subcarrier frequency spacing
T [ns]	12.78	DMT symbol duration
Δt [ps]	16.31	Time interval between two samples
f_{samp} [GHz]	245.32	Sampling frequency for the signal
N_{samp} [-]	784	Signal samples for the single DMT block
N_{synch} [-]	2	Number of synchronization symbols
M_{synch} [-]	64	QAM constellation order for the synchronization
N_{tr} [-]	16	Number of training symbols
M_{tr} [-]	4	QAM constellation order for the training

Table 4.6: *Parameters for the electrical DMT signals generation.*

compensation slightly increases the signal amplitude, so the actual modulation signals are correctly small signals. In Section 3.2 we said that a fundamental feature for the DMT driving signals is that they must be purely real signals. Nevertheless, Figure 4.7 shows that both waveforms exhibit both a real part and an imaginary part (even if very small compared o the real one) and this seems an inconsistency. That's not true at all. In fact, one has to keep in mind that the frequency pre-compensations for DML and MZ involve two complex functions and the imaginary part of the signals comes from this operation. Obviously, these contributions are cancelled at the time of the light modulation, going back to purely real signals. With this said, we can now analyze the dual modulator output results, considering that there are two main requirements in the two domains:

- in the frequency domain we want to obtain a power spectrum associated to a SSB signal;
- in the time domain we want to get a transposition of the original DMT signal as much accurate as possible (as to say that we want a high linearity degree).

In Figure 4.8 we report the output spectra for the DFB-MZ (Figure 4.8a), for the VCSEL-MZ (Figure 4.8b), for the DFB-EAM (Figure 4.8c) dual modulator architectures. The third one is used as a reference case. Figure 4.8d represents the comparison between the

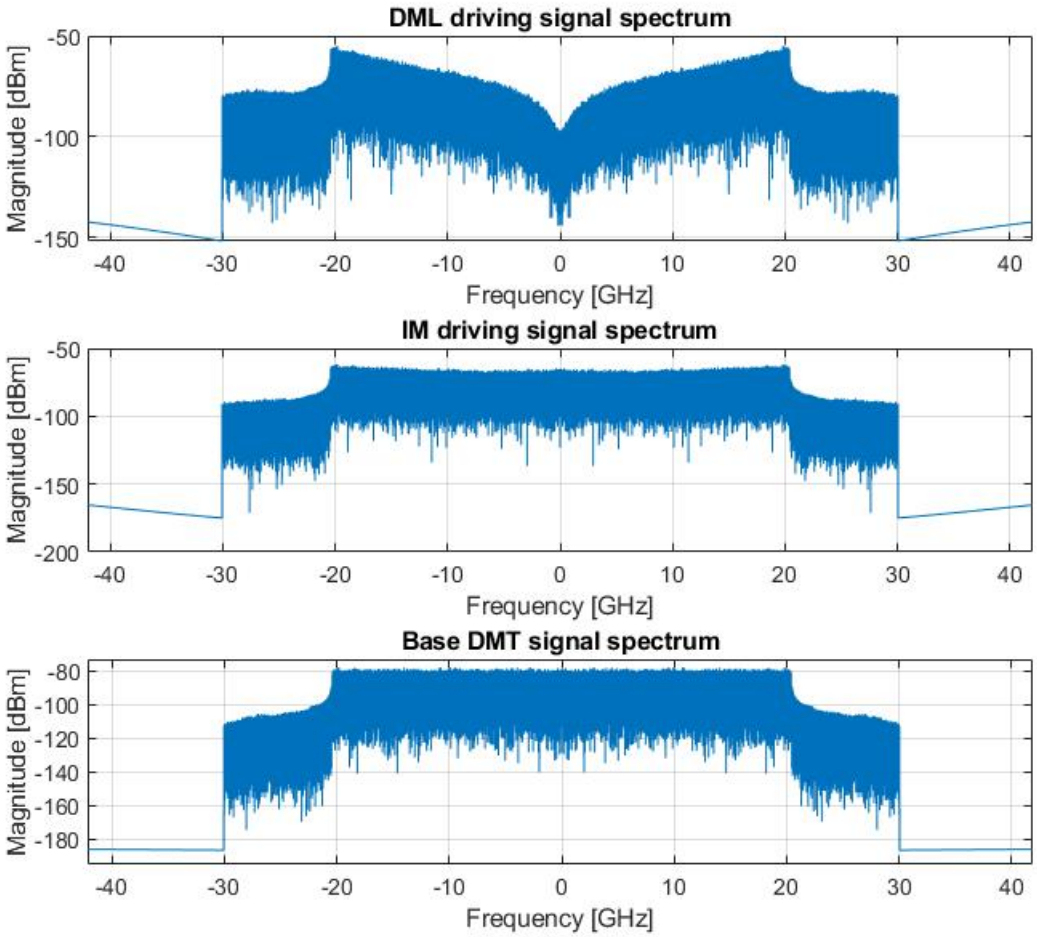

Figure 4.6: *DMT signals spectra. The last spectrum is related to the DMT signal obtained using the usual algorithm. We can notice that the pre-compensation operation boosts the DML and IM spectra.*

output spectrum for the VCSEL-MZ dual modulator and the output spectrum for the DFB-MZ dual modulator. This picture is shown in order to better understand the laser impact on the final signal. In fact, considering this outcome, a preliminary comment that can be made is that the laser choice does not basically affect the output spectrum: apart for the different linewidth broadening and a slightly higher noise floor at high frequencies, the spectrum shape and the LSB suppression are the same. This is something very good and it is mainly due to the DML SSB filter definition, that is able to guarantee the same working condition independently by laser employed in the dual modulator scheme realization. Anyway, in Figure 4.8a and Figure 4.8b it can be observed that we have for sure obtained what we wanted: the OSSR between the USB and the LSB is much

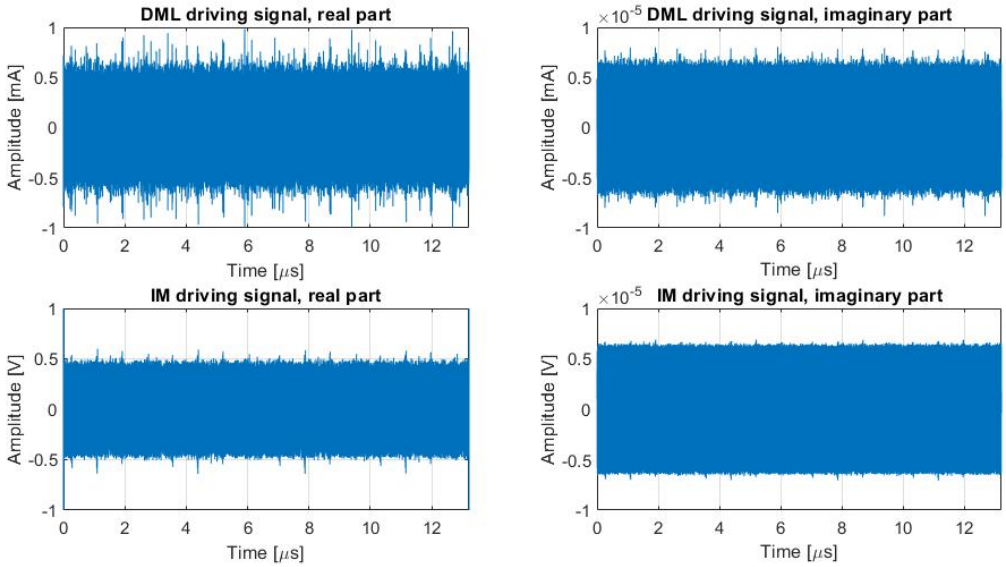

Figure 4.7: *DMT time domain driving signals for the DML and the intensity modulator. This image refers to the DFB-MZ dual modulator case, but the same conclusion can be achieved with the VCSEL-MZ modulator.*

lower than the values retrieved in the single harmonic case (as a consequence of the more complicated situation with a sinusoid superposition), but the approximately constant 20 dB value recovered is enough to say that the generated signal is a SSB signal with an excellent approximation. This OSSR result is even slightly larger than the one achieved with the DFB-EAM dual modulator, which, as shown in its figure and in [5], stands more or less at 17 dB. Along with this, we can notice that the spectrum quality with the MZ employment is a little better than the one achievable with an EAM. Indeed, the LSB suppression at low frequencies with this latter device is a bit worse than the one recovered with a MZ. This feature may be detrimental in the detection process. Going back to the DML-MZ modulator, the SSB spectrum shows that we are able to get a uniform suppression performance for a signal that is characterized by two very important aspects:

- it occupies quite a large bandwidth;
- it has very low components without the presence of any frequency gap, contrary to [5] where there is a 250 MHz gap left.

This conclusion is very important because it means that the theory developed in Section 3.2 not only works properly, but it returns even better results than the DFB-EAM dual modulator from the spectral point of view.
Together with this discussion, we also said that it is necessary to get a good transposi-

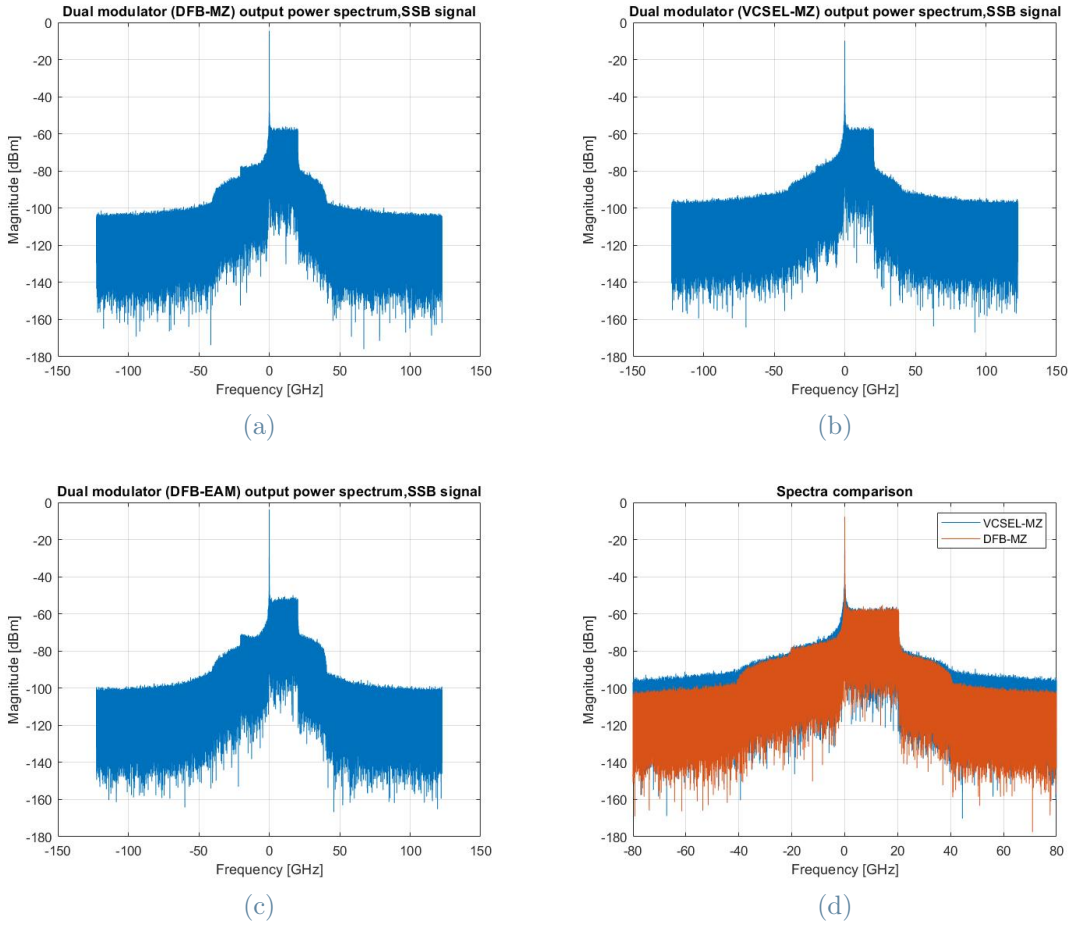

Figure 4.8: *Output spectrum for the* ***(a)*** *DFB-MZ modulator,* ***(b)*** *VCSEL-MZ modulator and* ***(c)*** *DFB-EAM modulator. In* ***(d)*** *we superimpose the spectra* ***(a)*** *and* ***(b)*** *to highlight the differences.*

tion of the DMT signal from the electrical domain to the optical domain. Therefore, we have to visualize the time domain signal in order to check whether This requirement is satisfied or not. Since the VCSEL employment is a little bit more critical than the DFB one because of the lower stability of the first one, we choose to represent the output field the VCSEL-MZ dual modulator and that's what we have in Figure 4.9. Note that we are taking for granted that the DML-EAM dual modulator scheme is able to fully satisfy this requirement. Figure 4.9 shows that there is obviously some distortion passing from the electrical to the optical signal and this is due to approximated linearity of the devices employed in the dual modulator architecture. Nevertheless, the fundamental DMT waveform is basically preserved and, at the same time, the amplitude is enhanced. This conclusion can be drawn even more so in the DFB case. Therefore, we can affirm that the time domain requirement is completely fulfilled too.

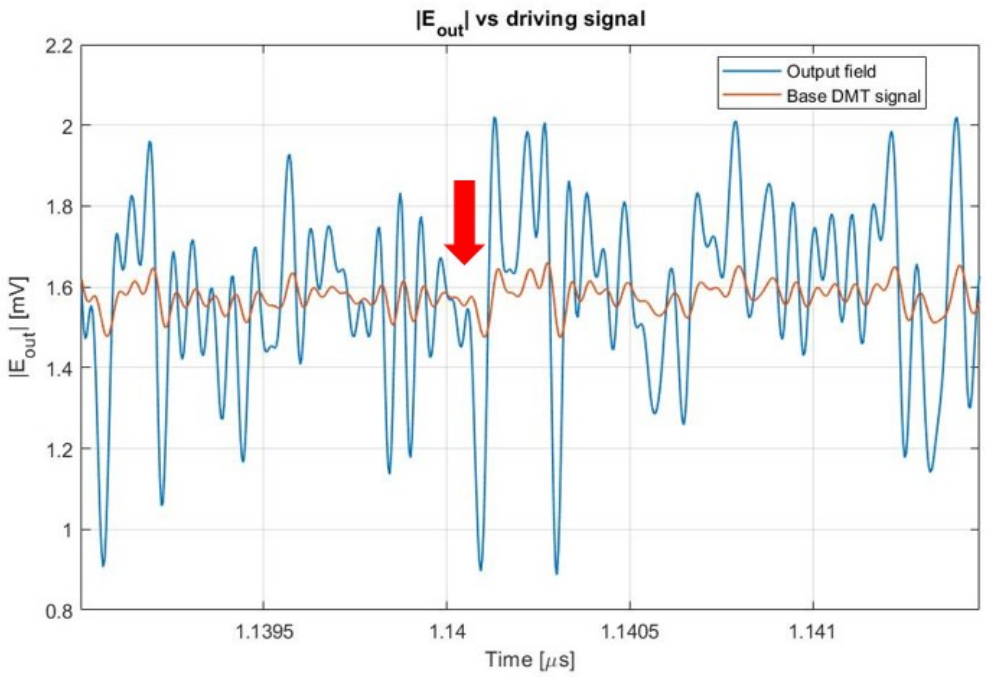

Figure 4.9: *Zoom of the VCSEL-MZ dual modulator output electric field. The red arrow points out a region where we have some distortion of the DMT signal to be transmitted.*

In conclusion, all this analysis focused on the optical DMT SSB signal generation demonstrates that, at least from a simulation point of view, the DML-MZ dual modulator scheme works correctly and shows overall a slightly better performance with respect to the DFB-EAM dual modulator. That's a good result, but, on the other hand, we have to admit that the DFB-EAM modulator is characterized by an integration advantage, something that for the DML-MZ dual modulator approach is hardly achievable nowadays. So, we are in a condition where we have two proposals, each one with its pros and its cons.

5 | Dual modulator application in the metro-access network

All the discussion in Chapter 4 is a good starting point, but it is concerned just on the generation aspect. Now, we have to move to the detection stage to study the dual modulator scheme performance in different conditions. We have already presented in Section 3.3 the detection and decoding procedure for the DMT signal and we are going to apply it now. In this study, we will compare all the possible dual modulator architectures involving a DFB laser or a VCSEL (as light source) and an EAM or a MZ (as intensity modulator), considering DSB and SSB signals and different parameters. Together with these schemes, we will take into account also the DML-OF architecture, already introduced and shown in Subsection 2.3.1. The chapter outline is the following one:

- in Section 5.1 we set the system parameters needed for the detection process and performance analysis;
- in Section 5.2 we study the transmitted capacity trend both for DSB and SSB signals as a function of the propagation distance, with a brief comment also on the signal OSSR and CSPR in the SSB case;
- in Section 5.3 we analyze the BER as a function of the propagation distance both for DSB and for SSB signals produced with the dual modulator architecture;
- in Section 5.4, still using a dual modulator scheme, we study the transmitted capacity as a function of the received power;
- in Section 5.5 we compare the performance of the VCSEL-MZ dual modulator with the DML-OF solution.

Parameter	Value
D_λ [ps/(nm · km)]	16
α_f [dB/km]	0.25
λ_L [nm]	1535.57
ρ [A/W]	0.7
B_{ph} [GHz]	15
NEC [pW/Hz$^{1/2}$]	20
M_{ch} [-]	4
BER_{tar} [-]	$4.6 \cdot 10^{-3}$
BER_{tol} [-]	$4 \cdot 10^{-4}$

Table 5.1: *Optical fiber, direct receiver and detection DMT signal parameters.*

5.1. Detection parameters

Before applying the DMT detection algorithm, we must fix the remaining system factors, which are

- the optical fiber parameters for the signal propagation (dispersion coefficient and specific attenuation);
- the direct receiver parameters;
- the DMT signal parameters needed to evaluate the capacity performance.

The values can be found in Table 5.1. Before proceeding, we have to make some comments about these quantities. First of all, every time we will have the signal propagation, we will assume to have a Standard Single Mode Fiber (*SSMF*), so the optical fiber values are referred to such kind of fiber. Then, we have made the laser carrier wavelength explicit, since we have to consider the chromatic dispersion caused by the signal propagation along the optical fiber. Finally, the signal parameter M_{ch} represents the QAM constellation order used in the channel estimation operation. This procedure has not been mentioned before because it was not relevant for the discussion, but it is always present in a system exploiting the DMT modulation and now it is a key point for the performance evaluation. In fact, it constitutes the basis for the subsequent bit loading and power loading aimed at the capacity optimization. In particular, the channel estimation corresponds to the first iteration of the generation and detection algorithms described in Section 3.2 and Section 3.3 and it is the only occasion where we fix the constellation (a 4-QAM) and the power for all the subcarriers. The main output of this simulator iteration is the SNR calculation

for each subcarrier, as the bit and power loading operations are performed using this parameter. Indeed, the SNR value for a certain subcarrier is compared to some thresholds to establish the best modulation to be used and the power quantity to be allocated for the considered frequency. The available constellations are the most different, from robust modulations like BPSK and 4-QAM to high capacity modulations like 128-Cross and 256-QAM. This Water Filling (WF) operation is repeated for every algorithm iteration until the real measured BER falls into an interval constituted by the target BER (BER_{tar}) plus or minus the BER tolerance (BER_{tol}).
Along with all the previous parameters, we should also fix the signal received power. This one can be tuned according to the wanted power level thanks to an Erbium Doped Fiber Amplifier ($EDFA$) and a Variable Optical Attenuator (VOA) before the receiver photodiode. However, the received power can vary depending on the considered situation, so we will specify it when it is most appropriate. The same concept is valid for the propagation distance too.
Before proceeding, we have to make one last preliminary comment. Since the simulations involve the electrical noise on the receiver side, the transmitted capacity and the CSPR associated to the optical signals are aleatory variables. In particular, the electrical noise acts such that the simulator iteration number and the final real BER are random and this impacts exactly on the signal parameters, making them vary even if we run more simulations with all the other system factors fixed. The variation is not so big (it is generally limited to the first decimal digit), but all the capacity (and capacity percent variation) and CSPR values reported in the following analysis have to be interpreted as mean values.
After this introduction, we can move to the real performance analysis for the different dual modulator schemes. In doing so, we will consider both SSB signals and DSB signals. These latter ones can be achieved by using the same dual modulator approach but in an EML scheme (so a CW laser and the IM modulator driven with the basic DMT signal, extracted applying the classical generation algorithm).

5.2. Capacity evaluation vs propagation distance

Considering that SSB signals are attractive because they can be employed in amplified and un-compensated networks, the first study that comes naturally is concerned on the capacity trend when we vary the propagation distance along the optical fiber. To do so, we use the parameters in Table 5.1 and we fix a constant received power $P_R = -3\ dB$ ($= 0.5\ mW$). Then, we have to fix the propagation distances. Keeping in mind that we are working in a metro and access context, a reasonable distance value that can be considered

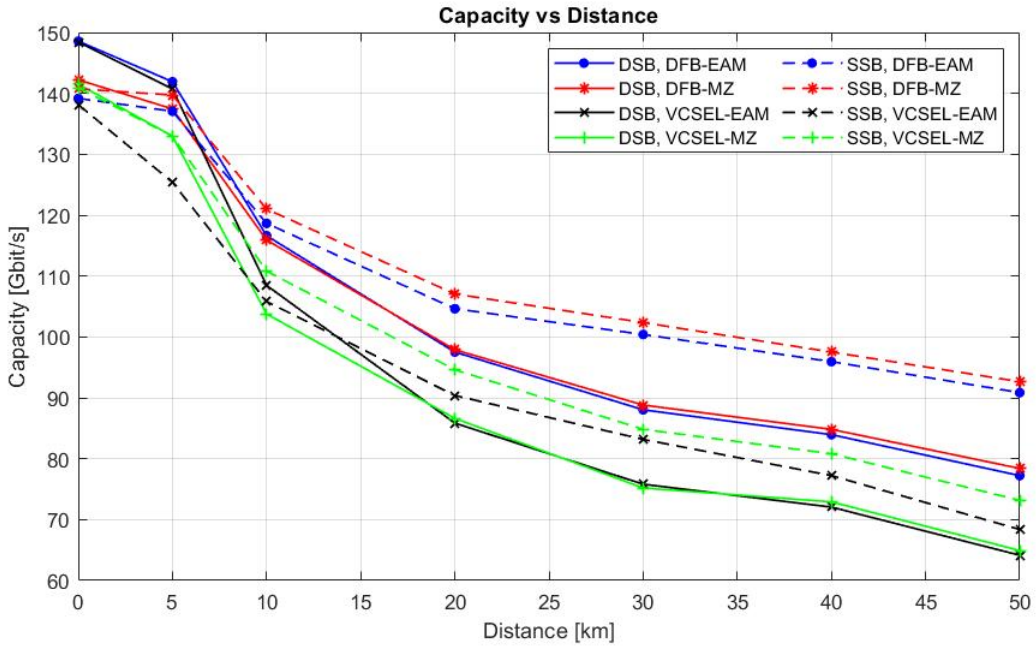

Figure 5.1: *Transmitted capacity as a function of the propagation distance for the four modulators and both signal types.*

is typically between 0 (B2B) and 50 km. For this reason, we can perform the analysis setting the distances $[0, 5, 10, 20, 30, 40, 50]$ km. With this said, we run the simulations and we represent as a function of the propagation distance

- the capacity trend (Figure 5.1);
- the OSSR trend (Figure 5.2);
- the CSPR trend (Figure 5.3).

Together with these graphs, we also report, again as a function of the propagation distance,

- the lost capacity percentage with respect to the B2B case (Table 5.2);
- the capacity gain percentage of a SSB signal with respect to the corresponding DSB one (Table 5.3).

In each figure we show the results for each dual modulator both for SSB and DSB signals (where it makes sense).
In Figure 5.1 we can observe that the DSB signals in the B2B condition correspond to the best situation we can strive for and, for this reason, it can be considered the reference case. This happens because, when we fold the negative part of the signal spectrum on the positive one, we double the power associated to each component and this implies

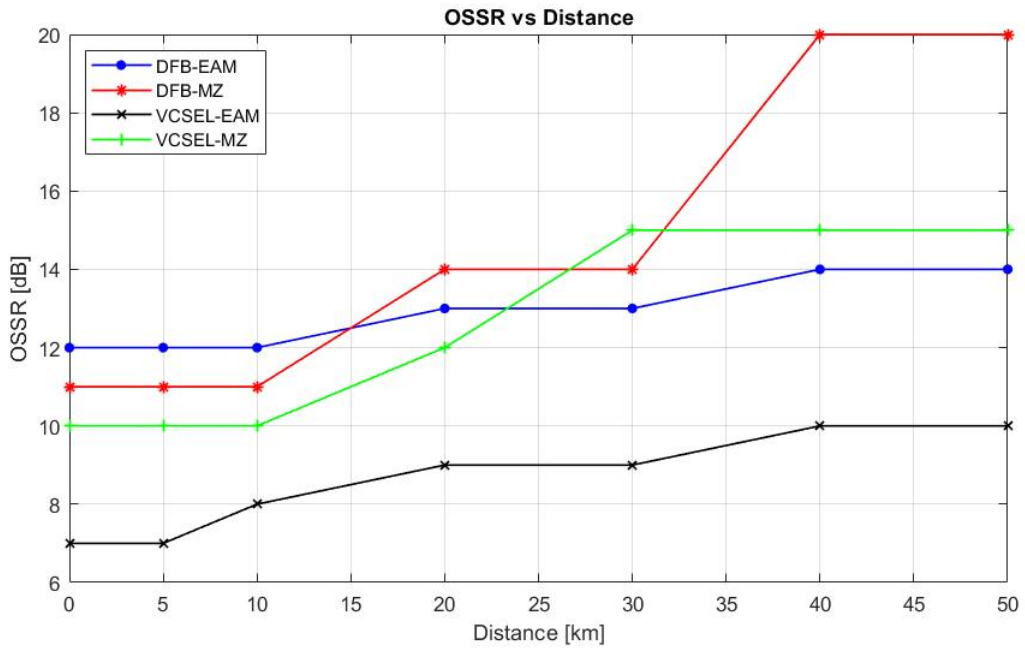

Figure 5.2: *Optimum OSSR for the SSB signal transmission as function of the propagation distance. The optimization is made with respect to the transmitted capacity.*

a maximization of the SNR. However, SSB signals are able to guarantee a comparable performance, even if a little lower. This interesting result can be easily explained by considering the SSB signal definition itself. In fact, what we basically do when we generate such kind of signal is a transfer of the power from negative frequencies to the positive ones. In the ideal case (that is with a full sideband suppression), we have a complete transfer and we get exactly the same situation as the DSB signal. In our real case, instead, the suppression is just partial and, as a consequence, we do not transfer the power completely. However, the optimization process has allowed to get very close to the ideal situation and this reflects in the high B2B capacity for the SSB signals too. On the other hand, it's immediately evident that this discussion is valid just in the B2B case. In fact, as soon as we let the signal propagate along the optical fiber, the SSB signal prevails over the DSB one and this becomes more and more evident as the propagation distance increases. In particular, for both signals kind we have a capacity drop, but this is much more pronounced for the DSB signals than for the SSB signals, as can be seen in Table 5.2. The reason of this event is the combination between the fiber chromatic dispersion and the frequency selective power fading. This latter one, in particular, is the most relevant cause. In fact, it produces dips both in the SNR function and in the photocurrent spectrum, as can be seen in Figure 5.4. These dips are due to the superposition of two corresponding frequency components that, because of the chromatic dispersion effect, have a π phase

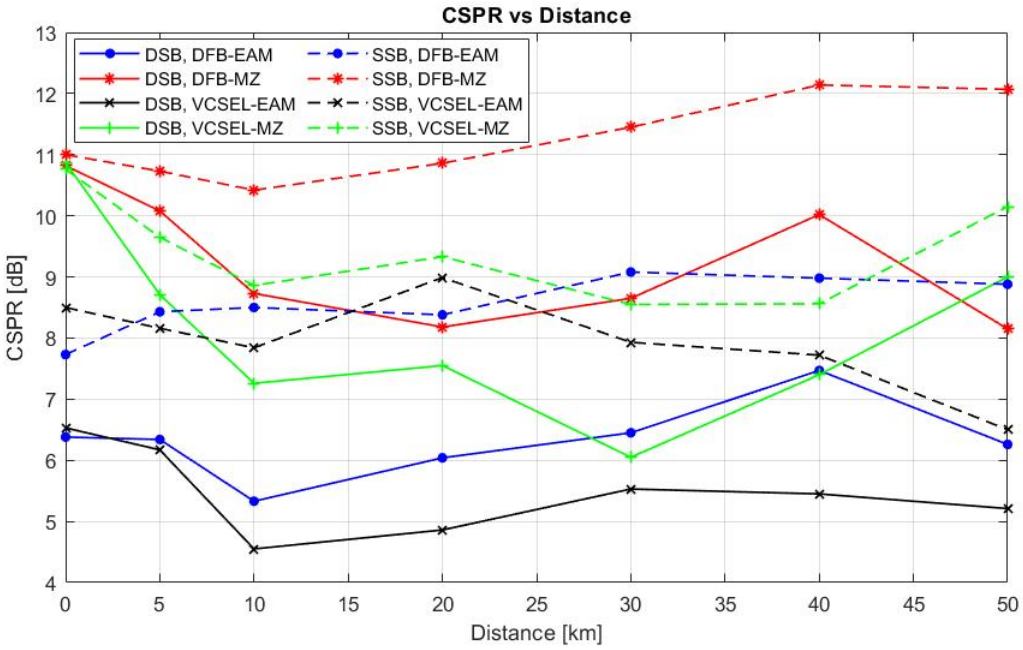

Figure 5.3: *Optimum CSPR for the signal transmission as function of the propagation distance. The optimization is made with respect to the transmitted capacity.*

shift, so they superimpose with a destructive interference. This event becomes more and more evident and originates more and more dips as the propagation distance increases. Note that the SSB signal shows the same issue, but the dips are much less pronounced than in the DSB case. This happens because in a DSB signal the two components have more or less the same power, so they completely cancel out. For a SSB signal, instead, we have the superposition between two contributions having a $10 - 20$ dB power difference, so the extinction is much less evident. Intuitively, this means that the DSB signal capacity transmission performance is much more affected, since we cannot optimally exploit (or even we cannot exploit at all) some subcarriers, which means a big inefficiency and capacity drop. Equally, the reach performance is affected too: with a SSB signal we can transmit the same amount of information as a DSB signal, but much further than this latter one.

Figure 5.1 also shows that the dual modulator schemes where we employ a DFB laser as DML have better performance than the ones using a VCSEL. This is something that could be expected considering the discussions of Section 4.3 about the output optical spectrum quality, but it's important to understand completely whether this is due just to this factor or if there is something else that is not working properly. For this reason, we consider, for example, the DML-MZ dual modulator architecture and we compare the performance among a DFB laser having the same linewidth broadening of the previous simulations, a

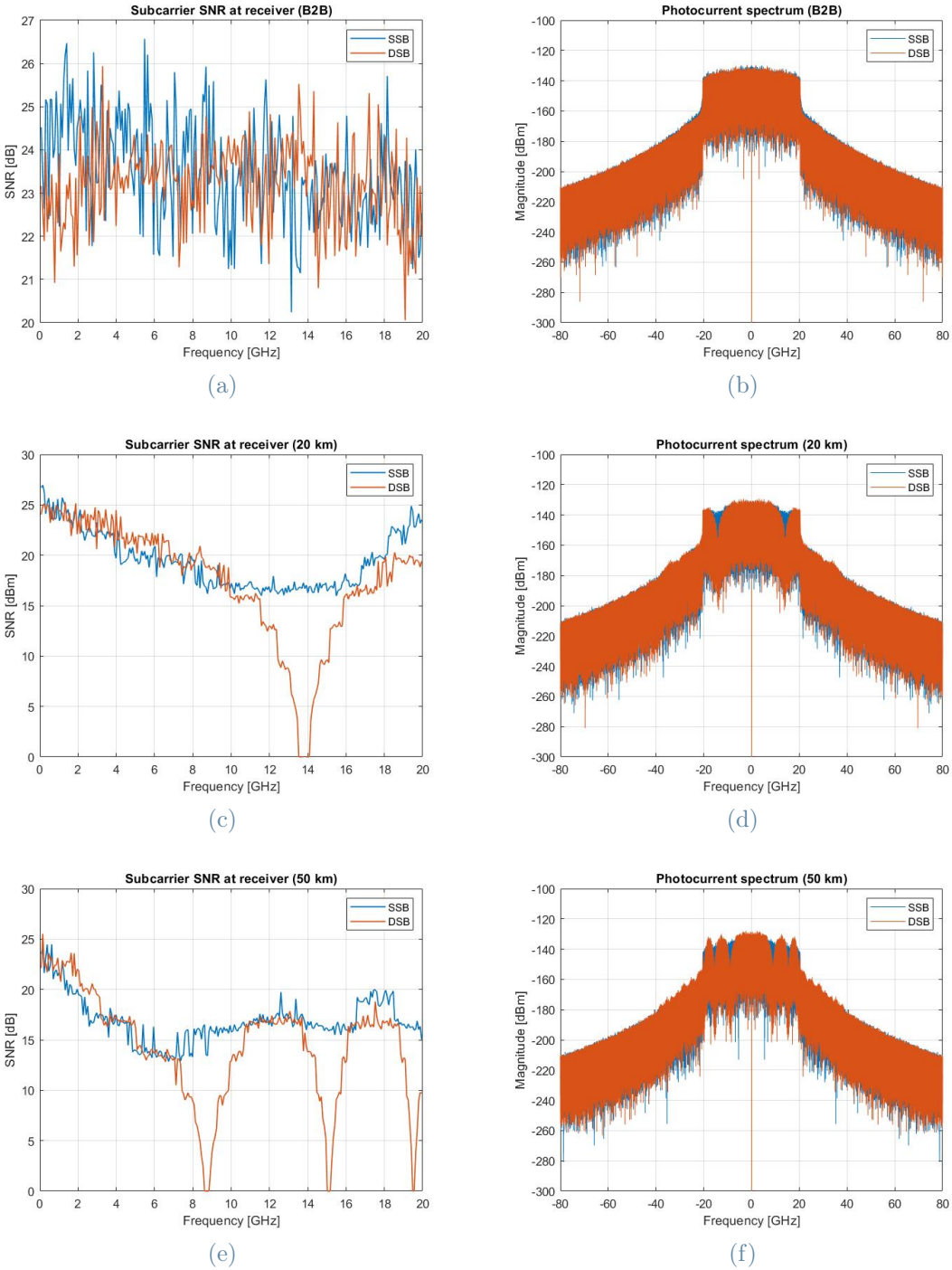

Figure 5.4: *Measured SNR per subcarrier and photocurrent power spectrum at the receiver in the DSB and SSB case:* ***(a)-(b)*** *in B2B;* ***(c)-(d)*** *after* 20 *km;* ***(e)-(f)*** *after* 50 *km.*

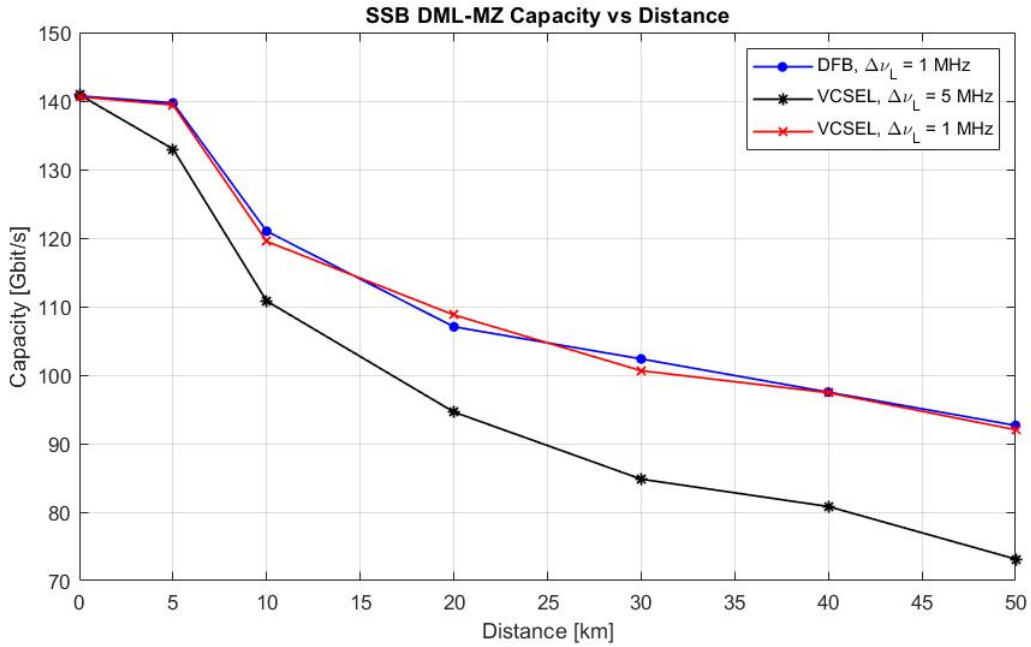

Figure 5.5: *Transmitted capacity as a function of the propagation distance for the DML-MZ modulator with a DFB laser ($\Delta\nu_L = 1\ MHz$), a VCSEL with ($\Delta\nu_L = 5\ MHz$) and a VCSEL with ($\Delta\nu_L = 1\ MHz$).*

VCSEL having $\Delta\nu_L = 5\ MHz$ (the one used in the simulations) and a VCSEL having $\Delta\nu_L = 1\ MHz$ (as the DFB laser). The result of this study in shown in Figure 5.5. We can for sure conclude that the performance deterioration has to be completely attributed to the broader VCSEL linewidth, that, even if it is not so wider with respect to the DFB one, is enough to cause the capacity worsening. Indeed, when the broadening is the same for both lasers, the capacity transmitted with a DFB laser and with a VCSEL is definitely comparable. This investigation is suggesting that, for the moment, DFB lasers are slightly better than the VCSELs. On the other hand, since Next-Generation VCSELs operating in the optical fiber C-band with higher bandwidth and lower noise are expected in the next years, the VCSEL employment may become a remarkable idea in the future.
From Figure 5.1, we can notice also that, once we have optimized the capacity, the performance of the two dual modulator schemes with the same DML and the same signal kind are similar. That's an interesting result especially for the SSB signal case, where we can also point a little advantage for the MZ solution out. This is likely due to the chirp absence for the MZ modulator in the PP configuration and to the model parameters magnitude, that helps with the small signal approximation (Tables 4.2 and 4.3). However, the transmitted capacity for each distance is very similar and the percent gain with respect to the DSB signal increases with the propagation length, as can be seen in Table 5.3. This is

	$C_{lost,\%}$ [%]							
	DFB-EAM		*DFB-MZ*		*VCSEL-EAM*		*VCSEL-MZ*	
D [km]	DSB	SSB	DSB	SSB	DSB	SSB	DSB	SSB
0 (B2B)	0	0	0	0	0	0	0	0
5	4.48	0.08	3.35	0.72	5.17	9.23	6.03	6.29
10	21.51	14.74	18.50	14.03	26.91	23.41	26.67	21.92
20	34.37	28.82	31.16	23.94	42.16	34.58	38.79	33.33
30	40.75	27.86	37.55	27.27	48.81	39.80	46.87	40.23
40	43.49	31.06	40.36	30.72	51.45	44.10	48.48	43.05
50	48.02	34.72	44.87	34.17	56.78	50.51	54.13	48.45

Table 5.2: *Lost capacity percentage with respect to the B2B case as a function of the propagation distance.*

a further confirmation that the optical SSB DMT generation algorithm for the dual modulator approach works very well also with different components and returns comparable results.

To conclude this comparison among the different dual modulator schemes based on the transmitted capacity, we can briefly discuss what we have obtained in percent variation terms in two cases of study:

- the percent lost capacity with respect to the B2B condition as a function of the propagation distance for all schemes, both with a DSB and a SSB signal;
- the percent capacity gain of a SSB signal transmission with respect to a DSB one as a function of distance for each architecture.

The results of these studies are reported in Table 5.2 and Table 5.3 respectively. For the first investigation, the percent variation has been computed by using the expression

$$C_{lost,\%} = 100 - \frac{C(D)}{C_{B2B}} \cdot 100 \tag{5.1}$$

where D represents the propagation distance. First of all, we can once again remark that, once we fix the DML, the results are very similar for the EAM and for the MZ, with a little advantage for the latter one. Considering, instead, the DML effect, we can notice that the DFB laser employment returns a better improvement with respect to the VCSEL, that,

	$C_{gain,\%}$ [%]			
D [km]	DFB-EAM	DFB-MZ	VCSEL-EAM	VCSEL-MZ
0 (B2B)	-6.33	-1.04	-6.91	-0.43
5	-3.42	+1.65	-10.91	0
10	+1.74	+4.39	-2.45	+6.78
20	+7.30	+9.35	+5.23	+9.22
30	+14.05	+15.26	+9.71	+12.81
40	+14.28	+14.96	+7.18	+10.85
50	+17.65	+18.18	+6.59	+12.68

Table 5.3: *Capacity percent gain for a SSB signal transmission with respect to the DSB case as a function of the propagation distance.*

we repeat, is due to the VCSEL broader linewidth. In particular, if we cascade a DFB laser and a MZ modulator, we obtain the best overall results, but we are not too far even using an EAM, especially when we look at the SSB signal performance. When we exploit a VCSEL, instead, we still get better results with a SSB signal than with a DSB one, but the improvement is lower. This confirms that, at least for the moment, the use of a DFB laser is slightly more advisable than a VCSEL, if we look from the capacity perspective. This percent variation analysis confirms also that SSB signals allow to increase the reach performance of the IM-DD network. In fact, SSB signals reach the same capacity drop values at much higher distances with respect to DSB signals (this is more evident when we exploit a DFB laser, but the same holds true also when we use a VCSEL). Considering that the B2B capacity is almost the same for DSB and SSB signals with a fixed dual modulator architecture, this means that SSB signals are able to transfer the same data amount but much further than DSB signals.
Basically the same discussion can be done by looking at the percent transmitted capacity gain when we transmit a SSB signal instead of a DSB one. The values has been computer by using the expression

$$C_{gain,\%} = \frac{C_{SSB}(D) - C_{DSB}(D)}{C_{DSB}(D)} \cdot 100 \tag{5.2}$$

where D still represents the propagation distance. We can notice that we start with a negative capacity gain (a loss) in the B2B condition, but then this variable turns to

positive and tends to increase with the propagation distance. In this case too, it is evident that the dual modulator schemes involving a DFB laser have the best trend, but we are able to almost resemble such behaviour with a VCSEL-MZ dual modulator. The VCSEL-EAM dual modulator, instead, is the one characterized by the worst performance due to its components.

5.2.1. OSSR and CSPR vs propagation distance

After discussing what happens in transmitted capacity terms, we can analyze what we have obtained for the other signal parameters in the SSB signal case. In particular, we have to consider the OSSR and the Carrier-to-Signal Power Ratio ($CSPR$). Once the DML is fixed, the two dual modulator architectures that can be built with an EAM and a MZ are quite similar also from the OSSR point of view. This can be seen in Figure 5.2 and it is more evident for low propagation distances. This image shows another remarkable outcome: in order to get the maximum capacity, it is not mandatory to operate with the maximum OSSR available, which is clearer especially for low propagation distances. This happens because we must take into account another signal parameter, which is the CSPR, defined as the ratio between the carrier power and the signal power. This factor is involved in the detection process and determines its performance in a certain sense. In fact, the best condition corresponds to a CSPR value in the interval $6-10\ dB$, otherwise the signal is either to small to be recognized (high CSPR value) or too close to the carrier power (low CSPR value). The CSPR optimal value as a function of distance in our simulations is shown in Figure 5.3, where with the term *optimal* we mean that it maximizes the capacity. Unfortunately, we can observe that the high OSSR requirement and the suitable CSPR requirement are in contrast one with the other. This is due to the dependence of these parameters by the modulation amplifications of the DMT signals driving the dual modulator elements:

- in order to obtain a high OSSR value, we need low-amplitude driving signals, so that we restrict to the very linear region of the components' transfer function. As a consequence, the LSB suppression is as optimal as possible. This implies that the signals amplifications cannot be too big. On the other hand, this working regime limits the optical signal amplitude a lot and, consequently, its power, so we get quite high values for the CSPR;
- in order to obtain a suitable CSPR value, we need to perform exactly the opposite discussion. In fact, we have to use high-amplitude driving signals, which means that we exceed in the non-linear region of the devices (not too much, otherwise we gener-

	G_{opt} interval [-]							
	DML (+EAM)		*DML (+MZ)*		*EAM*		*MZ*	
D [km]	DSB	SSB	DSB	SSB	DSB	SSB	DSB	SSB
0 (B2B)	-	5.5-6.5	-	1-1.3	9.5-12.5	7.5-8.5	9.5-10.5	1.6-2.3
5	-	5.5-6.5	-	1-1.3	9.5-12.5	7.5-8.5	10-12	1.8-2.3
10	-	5.5-6.5	-	1-1.3	9.5-11.5	7.5-8.5	9.5-10.5	1.8-2.4
20	-	5.5-6.5	-	1-1.3	9.5-10.5	7.5-8.5	9.5-10.5	1.3-1.9
30	-	5.5-6.5	-	1-1.3	9.5-10.5	7.5-8.5	9.5-10.5	1.2-1.8
40	-	5.5-6.5	-	1-1.3	6.5-8.5	7.5-8.5	7-9	1.4-1.8
50	-	5.5-6.5	-	1-1.3	7.5-10.5	7.5-8.5	7-9	1.2-1.7

Table 5.4: *Optimal electrical amplification intervals for the driving DMT signals supplied to the various components for the two signal kinds.*

ate too much distortion). Therefore, we must use big amplifications. On the other side, in this working regime we are creating non-negligible spurious components in the LSB that decrease the OSSR value.

The optimal modulation amplification intervals for the various devices used in the previous dual modulator schemes are reported in Table 5.4. The reason why the optimal amplification values vary so much is related to the driving signals generation process itself: the different steps or elements (especially the SSB filters) involved the procedure described in Section 3.2 return diverse signals with different amplitudes. However, it's easy to understand that these two conflicting parameters originate an optimum for the transmitted capacity. Figure 5.2 and Figure 5.3 show that this optimum favours the CSPR for low distances and the OSSR for high distances, that is quite intuitively: for low distances one wants to tend to best condition possible (the DSB signal one), while for high distances one wants to avoid the frequency selective power fading (so a SSB signal as good as possible is needed).

Another comment we can make is still about the CSPR. In particular, in Figure 5.3, we can see that the CSPR values are different depending on the IM modulator employed, but they are quite close one to the other. These values constitute a very good result, as they potentially allow to use the SSB signals generated by these dual modulator architectures in an IM-DD system including high level receivers, like a KK receiver. In fact, this kind of receiver implementing the KK algorithm needs a CSPR value between 5 dB and 10 dB

(with an optimum approximately at $6-7\ dB$) to properly reconstruct the incoming SSB spectrum. This can be a good addition for such system, since we are able to compensate the chromatic dispersion and, as a consequence, improve the transmitted capacity even more than what we have already obtained.

5.3. BER vs propagation distance

In order to deepen our analysis, we study the BER as a function of the propagation distance when the transmitted capacity is fixed. So, we basically perform the dual discussion with respect to Section 5.2, where we have considered a fixed target BER (plus or minus a tolerance) and the capacity as variable. Actually, the BER curves for the different cases could be recovered from Figure 5.1, but it is easier to visualize and briefly comment them. To achieve this goal, we consider just the channel estimation iteration, where the capacity is fixed and equal to more or less 40 $Gbit/s$. We have a 4-QAM modulation associated to each subcarrier, totaling 510000 transmitted bits. Apart for the the BER factors, the parameters employed in the simulations for the optical fiber and the direct receiver are the one reported in Table 5.1. The DMT signal parameters are the one reported in Table 4.6. Together with these ones, we still use a received power equal to $-3\ dBm$. With this said, we perform the simulations and we show the results in Figure 5.6. It's evident that, even if we are using a very robust modulation for each subcarrier, the SSB signal definitely prevails over the DSB signal. Indeed, we can deduce four conclusions:

- apart for the B2B condition and the 5 km propagation, the SSB signal performance is always much better than the DSB one and we are able to gain *at least* 3 orders of magnitude for each propagation distance;
- the BER becomes different from zero already after 10 km for the DSB signal, while for the SSB signal this happens after $20-30\ km$ and the number of errors is extremely low (about $5-10$ errors over the whole transmitted bits);
- the performance of all the dual modulator schemes are quite comparable for a DSB signal, while in the SSB case we can observe that the DFB laser works slightly better the VCSEL;
- once the DML is selected, for a DSB signal the IM modulator does not affect the outcome too much, while the MZ clearly outperforms the EAM when we employ a SSB signal.

These last points are very interesting, since they once again confirm that a DFB laser

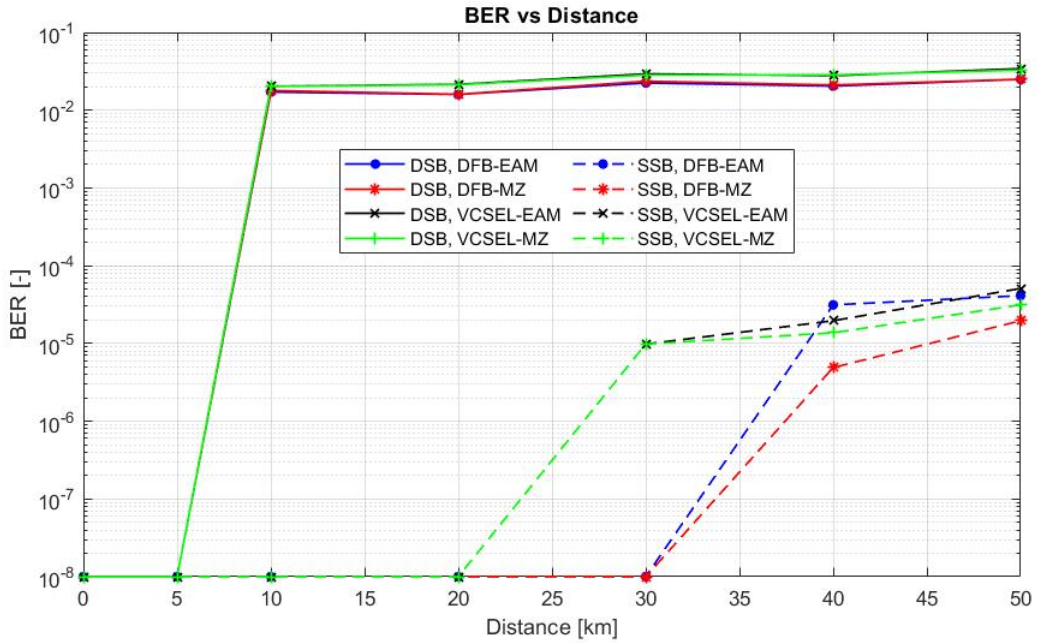

Figure 5.6: *Real BER as a function of the propagation distance. The value 10^{-8} represents a nominal zero, otherwise the log-scale would not be available.*

returns better results than a VCSEL laser (we repeat once again that this is due to the VCSEL broader linewidth) and a MZ works better than an EAM (because of the chirp lack for the first device). However, we have to point out that, with a SSB signal, the VCSEL is not too far from the DFB laser performance, even using a current VCSEL. Therefore, with a Next-Generation VCSEL the results are expected to improve and get closer to the DFB laser ones thanks to the reduced phase noise.

5.4. Capacity vs received power

Until now we have tackled a condition where we have fixed the received power and we have changed the signal propagation distance. Another interesting point of view can be the dual one, that is we fix the propagation distance and we vary the received power to study the transmitted capacity in various conditions. With respect to all previous cases, we perform this study just for the VCSEL-MZ dual modulator. This choice is determined by specific reasons both for the laser and for the intensity modulator. In particular, we consider the VCSEL because of three main key points:

- as we said, a VCSEL in tinier than a DFB laser, so it occupies less space on a chip when it is inserted/integrated;

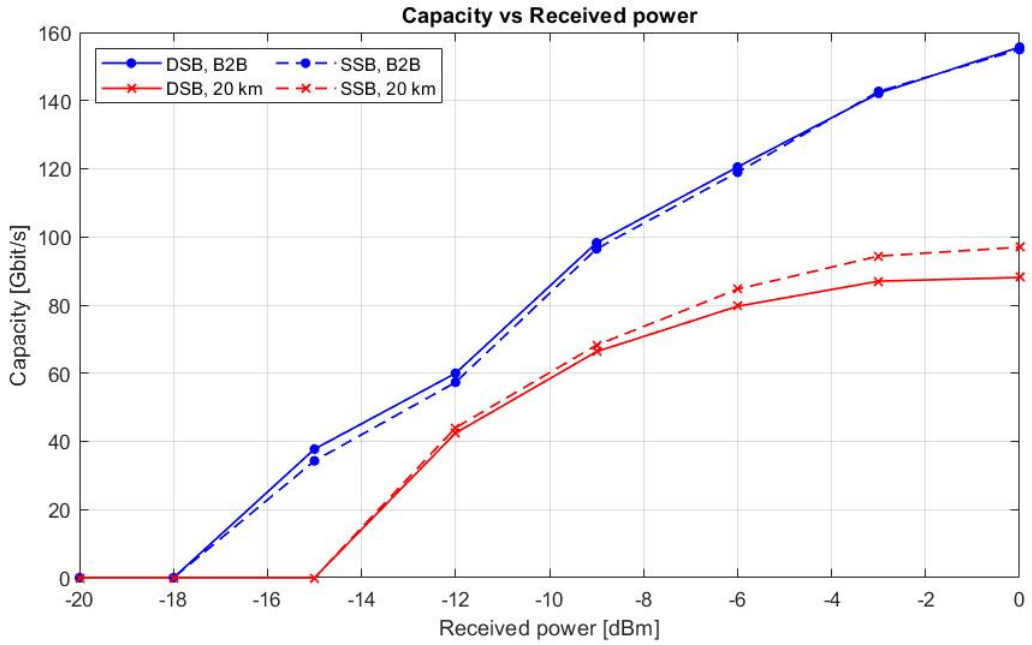

Figure 5.7: *Transmitted capacity as a function of the received power.*

- if the results with a VCSEL are remarkable, they are even more so for a DFB laser;
- if a current VCSEL already leads to a good improvement, a Next-Generation VCSEL having wider bandwidth and lower phase noise can increase this advantage even more.

The MZ choice, instead, is due to the analysis made in Section 5.2 and Section 5.3: when the dual modulator approach involves a VCSEL, the performance is considerably better when it is coupled with a MZ modulator than what is obtained with an EAM modulator. Clearly, we consider both the DSB and the SSB signal case of study, but we don't do that for every distance used in the previous sections. The conditions that will be analyzed are the B2B transmission (because it is the best one for both signals) and the 20 km propagation. We set this latter one since this is the distance where the the DSB signal loses almost the 40% of the transmitted capacity with respect to the B2B condition for the VCSEL-MZ dual modulator. Finally, the received power values that will be employed in the simulation are $[0, -3, -6, -9, -12, -15, -18]$ dBm. With this said, we can run the simulations and the outcomes are reported in Figure 5.7 and Table 5.5. We immediately notice that this study confirms what we have concluded in Section 5.2, as to say that in the B2B case the two signal kinds are not too far one from the other, but, after a 20 km propagation the SSB signal guarantees a better performance with respect to a DSB signal. However, we can observe that this statement is less and less correct as the received power

	B2B			20 km		
P_R [dBm]	C_{DSB} [Gbit/s]	C_{SSB} [Gbit/s]	G_{SSB} [%]	C_{DSB} [Gbit/s]	C_{SSB} [Gbit/s]	G_{SSB} [%]
0 (B2B)	155.70	154.99	- 0.46	88.11	96.88	+ 10.07
-3	142.15	142.69	+ 0.38	87.01	94.37	+ 8.46
-6	120.53	118.96	- 1.30	79.65	84.66	+ 6.29
-9	98.29	96.49	- 1.83	66.34	68.23	+ 2.85
-12	59.99	57.33	- 4.43	42.45	44.01	+ 3.67
-15	37.75	34.30	- 9.14	0	0	0
-18	0	0	0	0	0	0

Table 5.5: *Transmitted capacity values and percent variation (G_{SSB}) between DSB and SSB signals.*

decreases. That is something that could be intuitively explained. In fact, a received power decrease with a constant noise level implies a SNR drop independently by the type of signal exploited in the system. As a consequence, for low received power values, the SSB capacity trend resembles the DSB one even after a 20 km propagation (still remaining a little bit higher), as it can be noticed in Table 5.5. Moreover, Figure 5.7 shows that the capacity becomes zero when we set the received power equal to -15 dBm both for DSB and for SSB signals. However, even in this condition the SSB signal performs better than the DSB one. In fact, at the end of the channel estimation iteration, the measured real BER for the DSB signal is more or less $9.1 \cdot 10^{-2}$, while it is more or less equal to $2.8 \cdot 10^{-2}$ for the SSB one. Therefore, we almost have an order of magnitude between the two conditions.

5.5. Performance comparison between the VCSEL-MZ dual modulator and the VCSEL-OF SSB transmitter

Before the dual modulator development, the state of the art for the DMT SSB signal generation was constituted by the CW laser-IQ MZ modulator scheme and the DML-OF architecture. A brief discussion of the solutions can be found in Subsection 2.3.1 and the

architectures are represented in Figure 1.3 and 2.7. Examples of the DML-OF approach are reported in [30] and [31], where one can find experimental results obtained using a VCSEL as DML. This was done by employing a 17 GHz *bandwidth* VCSEL and a DMT signal having the same B_{sig}, N_{sub} and Δf_{sub} values fixed in Table 4.6. Moreover, the CP was set to the 2.1% of the whole DMT symbol length and the target BER was $4.6 \cdot 19^{-3}$, as for our simulations.
It is interesting to compare this solution with the dual modulator architecture, in particular the VCSEL-MZ one, in terms of capacity. The reference paper that we are going to consider is [30], since the direct detection approach is employed for the the DMT SSB signal detection, as we have done in our simulations. Before going on, we have to precise that a fair comparison is very difficult to be realized because of some features:

- the VCSEL-MZ dual modulator results come from a simulation, while the VCSEL-OF scheme data are experimental outcomes (so they are more reliable);
- the studied distance range in the paper is $0 - 10$ km, with just five distances considered, so we have to restrict the analysis to these conditions;
- the VCSEL has a 17 GHz bandwidth ([30]) against the MZ 20 GHz one in our simulation, so, being the available bandwidth wider, the dual modulator approach guarantees a better performance for sure, in absolute terms;
- the SSB optical signal generation procedure is completely different and this inevitably plays a role in the final performance.

For these reasons, an absolute terms comparison is quite critical to be performed. However, we can still compare the percent capacity loss variations for the two working schemes. Therefore, using the parameters reported in Table Figure 5.1 and fixing a received power equal to -3 dBm, we represent in Figure 5.8 the simulated transmitted capacity values for the VCSEL-MZ dual modulator (both for DSB and SSB signals) and the SSB experimental values for the VCSEL-OF scheme ([30]) just to visualize them, and then we base the comparison on the lost capacity percentage values, shown in Table 5.6. Note that we are not taking into account the DSB signal case for the VCSEL-OF scheme: the cause is the better performance of the SSB signal with respect to the DSB one in this approach too ([30]). In both discussions we set the propagation distance equal to $[0, 1, 3, 6, 10]$ km.
As we have said, the absolute transmitted capacity is much higher for the dual modulator approach than for the optical filter one due to the wider IM modulator bandwidth with respect to the VCSEL. However, by looking at Table 5.6, we can observe that the dual modulator scheme allows to have a lower capacity percent loss for low distances, while at higher distances the VCSEL-OF structure becomes better. This is true especially for

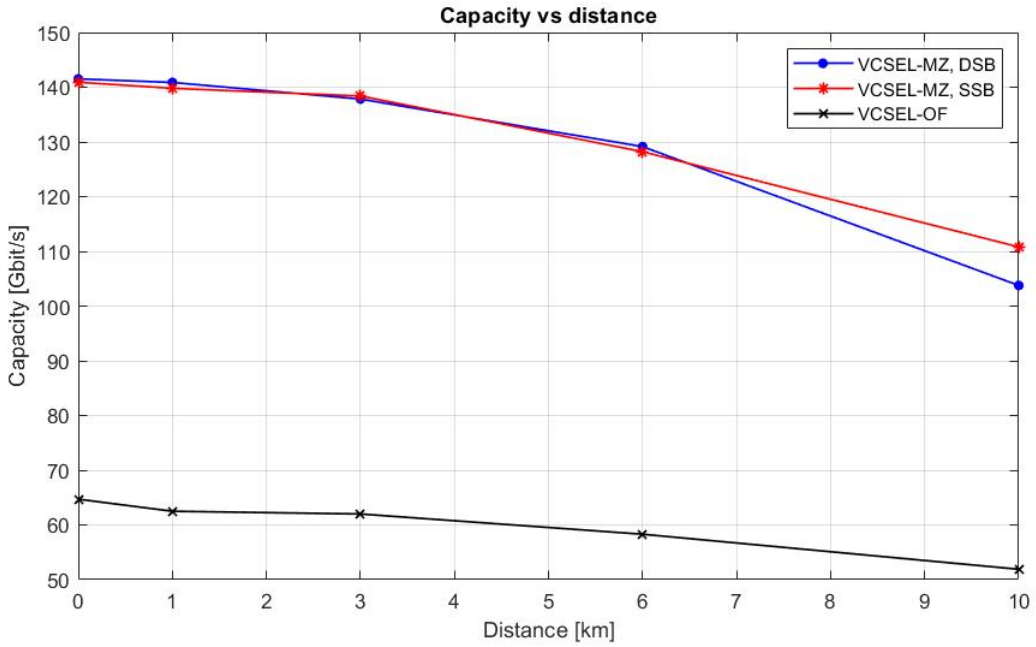

Figure 5.8: *Transmitted capacity comparison among the VCSEL-OF modulator and the VCSEL-MZ in the SSB and DSB case.*

the DSB signal, where the percent difference after a 10 km propagation is quite pronounced with respect to the VCSEL-OF architecture. The SSB signal generated by the VCSEL-MZ dual modulator, instead, is much better than the VCSEL-OF approach for low propagation distances and then the performance becomes almost the same at 6 km and 10 km.

All this discussion allows to get to an important conclusion. For the improvement of an IM-DD system performance, we start from the VCSEL-OF architecture for the DMT SSB signals generation. This solution works rather well and outperforms the DSB signal employment. However, the optical filter constitutes a big issue, since it is bulky, quite expensive and one must take care of its alignment and stabilization. For these reasons, we can try to replace it with an IM modulator, in particular a MZ modulator. This component is able to modulate the light intensity very well without adding any chirp contribution (under the proper working conditions). In this new scheme, keeping the laser in the CW regime and driving just the MZ modulator, we generate DSB signals and we are already able to improve the performance by a remarkable factor thanks to the available bandwidth increase. Nevertheless, DSB signals are affected by the frequency selective power fading issue, that deteriorates the VCSEL-MZ dual modulator performance much faster than the VCSEL-OF architecture as the propagation distance increases (Table 5.6). Therefore, already having a VCSEL and an intensity modulator, we can drive both com-

	$C_{lost,\%}$ [%]		
D	**VCSEL-OF**, SSB	**VCSEL-MZ**, DSB	**VCSEL-MZ**, SSB
[km]	(C_{B2B} = 64.7 Gbit/s)	(C_{B2B} = 141.52 Gbit/s)	(C_{B2B} = 140.91 Gbit/s)
0 (B2B)	0	0	0
1	3.40	0.46	0.79
3	4.17	2.61	1.79
6	9.89	8.75	9.01
10	19.78	26.67	21.36

Table 5.6: *Capacity percent loss for the VCSEL-OF modulator and for the VCSEL-MZ modulator in the DSB and SSB case.*

ponents to realize and employ SSB signals, which return even a bigger advantage due to their resilience to the power fading. Along with this improvement, we can basically keep the lost capacity percentage unchanged with respect to the VCSEL-OF scheme, so the VCSEL-MZ dual modulator for the DMT SSB signals generation can be reasonably believed the best solution for the metro and access network improvement. This affirmation can be pushed even further by using a KK receiver at the detection stage, because it improves the detection process and, as a consequence, both the transmitted capacity and the capacity percent drop with respect to the basic direct detection.

Conclusions and future developments

In this thesis work we have started from a general approach, where we have analyzed a considerable amount of the main proposals for the future performance improvement of the metro and access optical network, currently based on the IM-DD working scheme and the employment of DSB signals. In doing so, we have considered solutions both on the transmitter side and on the receiver side, discussing the key points. Among all these works, we have focused on the dual modulator approach, since it is a very interesting prospect for what concerns the transmitter side. In fact, it is a very simple architecture, but its exploitation allows to generate DMT SSB signals, which can lead to a significant capacity and reach performance improvement of an IM-DD system with respect to the current state of the art. In order to understand this improvement extent, we have performed many simulations for the performance evaluations, completely confirming our statement. In fact, thanks to the various outcomes, we have clearly observed that SSB signals generated by the dual modulator scheme definitely prevail over DSB signals, especially when the propagation distance tends to increase. This is due to the SSB signals increased resilience to the frequency selective power fading associated to the optical fiber chromatic dispersion.
We have also investigated the impact of the DML and IM modulator choice, considering a DFB laser or a VCSEL as light source and an EAM modulator or a MZ modulator as intensity modulator to constitute the dual modulator structure. This has been done because the research has concentrated on the DFB-EAM dual modulator, as it seems to reconcile the best performance and the best integration ease. However, we have proposed the new DML-MZ architecture, with particular attention to the VCSEL-MZ dual modulator. To our mind, indeed, such kind of scheme has some advantages:

- working in the push-pull configuration, the MZ modulator does not introduce any chirp contribution in the output optical signal;
- VCSELs are tinier than DFB lasers;
- Next-Generation VCSELs operating in the optical fiber C-band with better performance than current VCSELs (higher bandwidth and lower noise) are expected in

the future.

After the theory development for the DML-MZ structure and its validation process, we have performed an extensive comparison among all the dual modulator solutions that can be built using a DFB laser, a VCSEL, an EAM and a MZ with a simulative approach. In particular, this operation has been based on many studies:

- the transmitted capacity evaluation as a function of the propagation distances;
- the OSSR and CSPR evaluation as a function on the propagation distance;
- the BER evaluation as a function of the propagation distance;
- the transmitted capacity evaluation as a function of the received power.

The final conclusions that can be deduced from these investigations are that

- the MZ actually guarantees a better performance than the EAM (especially when a VCSEL is used), even if the results are not too far. This is due to the MZ chirp lack in the chosen working condition;
- a DFB laser is currently more advisable than a VCSEL. This is true just because of the lower linewidth broadening of a DFB with respect to a VCSEL. However, if this latter one's linewidth was the same of the DFB, the dual modulator architectures involving a VCSEL would be characterized by a similar performance as the DFB based ones. This should be guaranteed by Next-Generation VCSELs.

After this discussion regarding just the dual modulator scheme, we have finally tried to perform a comparison between the VCSEL-MZ dual modulator and the VCSEL-OF solution, found in the literature. This latter approach employs an optical filter to suppress one of the two sidebands of the DMT DSB signal coming out from the VCSEL and, as a consequence, to realize a DMT SSB signal in an all optical way. This comparison has been a little bit difficult because of the different working concepts and elements, but in the end we have stated that the VCSEL-MZ solution prevails over the VCSEL-OF scheme from an overall performance point of view and is less critical from a components point of view. These conclusions allow us to say that the VCSEL-MZ dual modulator can be a very interesting solution for the IM-DD system performance improvement in the future.

This work is a good and solid basis, but it misses some features that are relevant. For this reason, finally, we can list some future developments for this study:

- add the quantization both of the Analog-to-Digital Converter (ADC) and of the Digital-to-Analog Converter (DAC);

- consider the non-linear effects that affect the signal during the propagation along the optical fiber and investigate their impact on the IM-DD system performance;
- move from a single channel condition into a WDM context;
- implement the DML-MZ dual modulator solution in the laboratory and test it, in order to compare simulation and experimental results;
- perform a better comparison between the VCSEL-MZ dual modulator solution and the VCSEL-OF scheme, as to say we can consider, for example, higher distances;
- compare the dual modulator approach with the IQ MZ modulator solution for the DMT SSB signal generation, both in terms of signal spectrum quality and in terms of IM-DD system performance;
- compare the dual modulator scheme performance in the SSB signal and direct detection case with the coherent detection, that is the best detection technique available;
- implement the KK algorithm, in order to analyze the performance gain with such receiver.

Bibliography

[1] Tianwai Bo, Zhongwei Tan, Hoon Kim, and Yi Dong. Recent advances in optical sideband transmitters. In *2021 19th International Conference on Optical Communications and Networks (ICOCN)*, pages 1–3. IEEE, 2021.

[2] Hoon Kim. Eml-based optical single sideband transmitter. *IEEE Photonics Technology Letters*, 20(4):243–245, 2008.

[3] Mohamed Essghair Chaibi, Thomas Anfray, Christophe Kazmierski, Christelle Aupetit-Berthelemot, and Didier Erasme. Generation of ssb optical signals with dual-eml modulated with wideband ofdm. In *CLEO: Science and Innovations*, pages SW1J–6. Optica Publishing Group, 2014.

[4] Tianwai Bo and Hoon Kim. Generalized model of optical single sideband generation using dual modulation of dml and eam. *Optics Express*, 28(19):28491–28501, 2020.

[5] Tianwai Bo, Byunggon Kim, Yukui Yu, Daeho Kim, and Hoon Kim. Generation of broadband optical ssb signal using dual modulation of dml and eam. *Journal of Lightwave Technology*, 39(10):3064–3071, 2021.

[6] Tianwai Bo and Hoon Kim. 147-gb/s transmission of optical single sideband dmt signal generated by dual modulation of dml and eam. In *Optical Fiber Communication Conference*, pages F2D–2. Optica Publishing Group, 2021.

[7] Mohamed Essghair Chaibi, Thomas Anfray, Khalil Kechaou, Christophe Gosset, Luiz Anet Neto, Guy Aubin, Christophe Kazmierski, Philipe Chanclou, Christelle Aupetit-Berthelemot, and Didier Erasme. Dispersion compensation-free im/dd ssb-ofdm transmission at 11.11 gb/s over 200 km ssmf using dual eml. *IEEE Photonics Technology Letters*, 25(23):2271–2273, 2013.

[8] Didier Erasme, Thomas Anfray, Mohamed Essghair Chaibi, Khalil Kechaou, Juan Petit, Guy Aubin, Kamel Merghem, Christophe Kazmierski, Jean-Guy Provost, Philippe Chanclou, et al. The dual-electroabsorption modulated laser, a flexible solution for amplified and dispersion uncompensated networks over standard fiber. *Journal of Lightwave Technology*, 32(21):3466–3476, 2014.

[9] Mohamed E Chaibi, Luiz Anet Neto, Christophe Kazmierski, Frédéric Grillot, and Didier Erasme. Dispersion uncompensated im/dd transmissions of 12ghz-wide multiband ofdm over 100km with a d-eml. In *2015 European Conference on Optical Communication (ECOC)*, pages 1–3. IEEE, 2015.

[10] Yi-Hsiang Wang, Chia-Chien Wei, Hidenori Taga, and Takehiro Tsuritani. Novel im/dd single-sideband ofdm generation featuring tolerance to dispersion-related fading and distortion. In *ECOC 2016; 42nd European Conference on Optical Communication*, pages 1–3. VDE, 2016.

[11] Nebras Deb and John C Cartledge. Employing a kramers–kronig receiver with a directly-modulated laser. *Optics Communications*, 479:126472, 2021.

[12] Ling Wang, Ming Chen, Long Zhang, Dongsheng Xi, and Hui Zhou. Precoded ovsb-ofdm transmission system using dml with kramers-kronig receiver. *Optical Fiber Technology*, 63:102523, 2021.

[13] Fan Li, Xinying Li, Junwen Zhang, and Jianjun Yu. Transmission of 100-gb/s vsb dft-spread dmt signal in short-reach optical communication systems. *IEEE Photonics Journal*, 7(5):1–7, 2015.

[14] MS Erkılınç, D Lavery, K Shi, BC Thomsen, RI Killey, SJ Savory, and P Bayvel. Bidirectional wavelength-division multiplexing transmission over installed fibre using a simplified optical coherent access transceiver. *Nature communications*, 8(1):1–10, 2017.

[15] M Sezer Erkılınç, Domaniç Lavery, Robert Maher, Milen Paskov, Benn C Thomsen, Polina Bayvel, Robert I Killey, and Seb J Savory. Polarization-insensitive single balanced photodiode coherent receiver for passive optical networks. In *2015 European Conference on Optical Communication (ECOC)*, pages 1–3. IEEE, 2015.

[16] M Sezer Erkılınç, Domaniç Lavery, Kai Shi, Benn C Thomsen, Polina Bayvel, Robert I Killey, and Seb J Savory. Polarization-insensitive single-balanced photodiode coherent receiver for long-reach wdm-pons. *Journal of Lightwave Technology*, 34(8):2034–2041, 2016.

[17] Antonio Mecozzi, Cristian Antonelli, and Mark Shtaif. Kramers–kronig coherent receiver. *Optica*, 3(11):1220–1227, 2016.

[18] Ruben S Luis, Georg Rademacher, Benjamin J Puttnam, Satoshi Shinada, Hideaki Furukawa, Ryo Maruyama, Kazuhiko Aikawa, and Naoya Wada. A coherent kramers-

kronig receiver for 3-mode few-mode fiber transmission. In *2018 European Conference on Optical Communication (ECOC)*, pages 1–3. IEEE, 2018.

[19] Cristian Antonelli, Antonio Mecozzi, and Mark Shtaif. Kramers–kronig pam transceiver and two-sided polarization-multiplexed kramers–kronig transceiver. *Journal of Lightwave Technology*, 36(2):468–475, 2018.

[20] Menno van den Hout, Sjoerd van der Heide, and Chigo Okonkwo. Kramers-kronig receiver with digitally added carrier combined with digital resolution enhancer. *Journal of Lightwave Technology*, 40(5):1400–1406, 2022.

[21] Tianwai Bo and Hoon Kim. Kramers-kronig receiver operable without digital upsampling. *Optics Express*, 26(11):13810–13818, 2018.

[22] Keji Zhou and Sheng Cui. Complex signal field retrieval based on improved kramers-kronig coherent receiver without digital upsampling. In *2020 IEEE 4th Information Technology, Networking, Electronic and Automation Control Conference (ITNEC)*, volume 1, pages 180–183. IEEE, 2020.

[23] Nelson J Muga, Romil K Patel, Isiaka A Alimi, Nuno A Silva, and Armando N Pinto. Dsp optimization for simplified coherent receivers. In *2020 22nd International Conference on Transparent Optical Networks (ICTON)*, pages 1–4. IEEE, 2020.

[24] Nelson J Muga, Romil K Patel, Isiaka A Alimi, Nuno A Silva, and Armando N Pinto. Self-coherent optical detection for access and metro networks. In *2019 21st International Conference on Transparent Optical Networks (ICTON)*, pages 1–4. IEEE, 2019.

[25] Qi Wu, Yixiao Zhu, and Weisheng Hu. Low-complexity and non-iterative ssbi decomposition and cancellation algorithm for ssb direct detection system. In *2022 Optical Fiber Communications Conference and Exhibition (OFC)*, pages 1–3. IEEE, 2022.

[26] Huan Chen, Tao Yang, Liqian Wang, Xue Chen, and Yueying Zhan. A structure-simplified and cost-effective coherent receiver for high splitting downstream transmission in next-generation pons. *Optics Communications*, 434:218–223, 2019.

[27] Mario Rannello, Marco Presi, and Ernesto Ciaramella. Pbs-free polarization-independent pon coherent receiver. *IEEE Photonics Technology Letters*, 32(21):1361–1364, 2020.

[28] Rodney S Tucker. High-speed modulation of semiconductor lasers. *IEEE transactions on electron devices*, 32(12):2572–2584, 1985.

[29] Luiz Anet Neto, Didier Erasme, Naveena Genay, Philippe Chanclou, Qian Deniel, Fatoumata Traore, Thomas Anfray, Rajaâ Hmadou, and Christelle Aupetit-Berthelemot. Simple estimation of fiber dispersion and laser chirp parameters using the downhill simplex fitting algorithm. *Journal of Lightwave Technology*, 31(2):334–342, 2012.

[30] Paola Parolari, Alberto Gatto, Christian Neumeyr, and Pierpaolo Boffi. Flexible transmitters based on directly modulated vcsels for next-generation 50g passive optical networks. *Journal of Optical Communications and Networking*, 12(10):D78–D85, 2020.

[31] Alberto Gatto, Mariangela Rapisarda, Paola Parolari, Christian Neumeyr, Paolo Martelli, and Pierpaolo Boffi. Beyond 50 gb/s directly-modulated long-wavelength vcsels for next-gen access network. In *2019 IEEE Photonics Society Summer Topical Meeting Series (SUM)*, pages 1–2. IEEE, 2019.

[32] Rubab Amin, Rishi Maiti, Caitlin Carfano, Zhizhen Ma, Mohammad H Tahersima, Yigal Lilach, Dilan Ratnayake, Hamed Dalir, and Volker J Sorger. 0.52 v mm ito-based mach-zehnder modulator in silicon photonics. *APL Photonics*, 3(12):126104, 2018.

[33] Robert A Griffin, Stephen K Jones, Neil Whitbread, Susannah C Heck, and Lloyd N Langley. Inp mach–zehnder modulator platform for 10/40/100/200-gb/s operation. *IEEE Journal of Selected Topics in Quantum Electronics*, 19(6):158–166, 2013.

[34] Michael R Watts, William A Zortman, Douglas C Trotter, Ralph W Young, and Anthony L Lentine. Low-voltage, compact, depletion-mode, silicon mach–zehnder modulator. *IEEE Journal of Selected Topics in Quantum Electronics*, 16(1):159–164, 2010.

[35] Md Samiul Alam, Xueyang Li, Maxime Jacques, Essam Berikaa, Ping-Chiek Koh, and David V Plant. Net 300 gbps/λ transmission over 2 km of smf with a silicon photonic mach-zehnder modulator. *IEEE Photonics Technology Letters*, 33(24):1391–1394, 2021.

[36] Ling Liao, Dean Samara-Rubio, Michael Morse, Ansheng Liu, Dexter Hodge, Doron Rubin, Ulrich D Keil, and Thorkild Franck. High speed silicon mach-zehnder modulator. *Optics express*, 13(8):3129–3135, 2005.

[37] Tatsurou Hiraki, Takuma Aihara, Takuro Fujii, Koji Takeda, Yoshiho Maeda, Takaaki Kakitsuka, Tai Tsuchizawa, and Shinji Matsuo. Integration of a high-

efficiency mach-zehnder modulator with a dfb laser using membrane inp-based devices on a si photonics platform. *Optics Express*, 29(2):2431–2441, 2021.

A | DML chirp induced phase

This appendix contains the demonstration of (3.7). The starting point is the DML phase definition as

$$\phi(t) = 2\pi \int_0^t \Delta f(t)\, dt \tag{A.1}$$

where the chirp frequency definition is

$$\Delta f(t) = \frac{\alpha_{DML}}{4\pi} \left\{ \frac{d}{dt} \{\ln[P(t)]\} + \kappa P(t) \right\} \tag{A.2}$$

with the power evolution given by (3.3). For this proof we need (3.8), (3.9), (3.10), the fundamental logarithm property and the first order natural logarithm approximation is, that respectively are

$$\log_a (bc) = \log_a (b) + \log_a (c) \tag{A.3}$$

$$\ln(1 + x) \simeq x + o(x^2) \tag{A.4}$$

Moreover, we have to keep in mind that a sine and a cosine having the same frequency but different amplitudes can be summed using the relation

$$A\cos(\omega t) + B\sin(\omega t) = C\cos(\omega t + \delta) \tag{A.5}$$

where

$$C = \sqrt{A^2 + B^2} \tag{A.6}$$

$$\delta = -\arctan\left(\frac{B}{A}\right) \tag{A.7}$$

Now, we have everything we need. By substituting (2.4) and (A.2) and using (A.3), we can develop (A.1) as follows:

$$\phi(t) = 2\pi \int_0^t \frac{\alpha_{DML}}{4\pi}\left\{\frac{d}{dt}\{\ln[P(t)]\} + \kappa P(t)\right\} dt =$$

$$= \frac{\alpha_{DML}}{2}\left\{\int_0^t \frac{d}{dt}\{\ln[P(t)]\}\, dt \, + \int_0^t \kappa P(t)\, dt\right\} =$$

$$= \frac{\alpha_{DML}}{2}\left\{\ln[P(t)] + \kappa \int_0^t P(t)\, dt\right\} =$$

$$= \frac{\alpha_{DML}}{2}\left\{\ln\{P_0 \cdot [1 + m_{DML}\cos(\omega t)]\} + \kappa \int_0^t P_0 \cdot [1 + m_{DML}\cos(\omega t)]\, dt\right\} =$$

$$= \frac{\alpha_{DML}}{2}\left\{\ln(P_0) + \ln[1 + m_{DML}\cos(\omega t)] + \kappa \int_0^t P_0\, dt + \right.$$

$$\left. + \kappa \int_0^t P_0\, m_{DML}\cos(\omega t)\, dt\right\} =$$

$$= \frac{\alpha_{DML}}{2}\left\{\ln(P_0) + \ln[1 + m_{DML}\cos(\omega t)] + \kappa P_0 t + \frac{\kappa P_0\, m_{DML}}{\omega}\sin(\omega t)\right\} \tag{A.8}$$

Considering that $m_{DML} << 1$, we can use (A.4) to get that

$$\phi(t) = \frac{\alpha_{DML}}{2}\left\{\ln(P_0) + \ln[1 + m_{DML}\cos(\omega t)] + \kappa P_0 t + \frac{\kappa P_0\, m_{DML}}{\omega}\sin(\omega t)\right\} \simeq$$

$$\simeq \frac{\alpha_{DML}}{2}\left\{\ln(P_0) + m_{DML}\cos(\omega t) + \kappa P_0 t + \frac{\kappa P_0\, m_{DML}}{\omega}\sin(\omega t)\right\} =$$

$$= \frac{\alpha_{DML}\, m_{DML}}{2}\cos(\omega t) + \frac{\alpha_{DML}\,\kappa P_0\, m_{DML}}{2\omega}\sin(\omega t) +$$

$$\frac{\alpha_{DML}\,\kappa P_0}{2} t + \frac{\alpha_{DML}}{2}\ln(P_0) =$$

$$= \frac{\alpha_{DML}\, m_{DML}}{2}\cos(\omega t) + \frac{\alpha_{DML}\,\kappa P_0\, m_{DML}}{2\omega}\sin(\omega t) + \omega_c t + \frac{\alpha_{DML}}{2}\ln(P_0) \tag{A.9}$$

where we have used (3.10). Finally, applying (A.6) and (A.7) to the harmonic terms sum,

we obtain

$$\phi(t) \simeq \frac{\alpha_{DML}\, m_{DML}}{2}\cos(\omega t) + \frac{\alpha_{DML}\,\kappa P0\, m_{DML}}{2\omega}\sin(\omega t) + \omega_c t + C$$

$$= \frac{\alpha_{DML}\, m_{DML}}{2}\sqrt{1+\left(\frac{\kappa P_0}{\omega}\right)^2}\cdot\cos\left[\omega t - \arctan\left(\frac{\kappa P_0}{\omega}\right)\right] + \omega_c t + \frac{\alpha_{DML}}{2}\ln(P_0)$$

$$= m_{PM}\,\cos(\omega t + \beta_{PM}) + \omega_c t + \frac{\alpha_{DML}}{2}\ln(P_0) =$$

$$= m_{PM}\,\sin\left(\omega t + \beta_{PM} + \frac{\pi}{2}\right) + \omega_c t + \frac{\alpha_{DML}}{2}\ln(P_0) =$$

$$= m_{PM}\sin(\omega t + \phi_{PM}) + \omega_c t + \frac{\alpha_{DML}}{2}\ln(P_0) \tag{A.10}$$

where (3.8) and (3.9) have been employed. The obtained expression is exactly (3.7).

B | OSSR asymptotic regime

This supplementary appendix contains the proof that, in presence of an amplitude error, the DML-MZ dual modulator shows an OSSR that tends to a specific value depending just on the amplitude modulation indices m_{DML} and m_{MZ}.
Assuming to have no phase error, Equation (3.21) can be generalized to take into account an amplitude error for the ratio $m_{MZ}\,/\,m_{DML}$ as follows:

$$E_{out} \simeq \sqrt{\frac{P_0}{2}} \cdot \Bigg[1 + \pi m_{MZ} \cos(\omega t + \phi_{PM} + \Delta) + j m_{PM} \sin(\omega t + \phi_{PM}) + \\ + \frac{m_{DML}}{2}\left(1 - \frac{m_{MZ}}{m_{MZ} + \varepsilon_{am}}\right)\cos(\omega t)\Bigg] \tag{B.1}$$

So, in this new case we have two cosinusoids that make the real part of the field up (we neglect the DC component of the field as it is not relevant for the SSB signal generation due to the Hilbert transform definition). Hence, we need to sum these harmonics up, keeping in mind that they have the same frequency but different amplitude and phases. The result is a cosinusoid still having the same frequency, but the amplitude and the phase depend on the two contributions. Ignoring the phase discussion (which has its importance on the OSSR drop anyway), we can focus on the amplitude of the resulting sinusoid. By using the known formulas, we get that this is equal to

$$A(\varepsilon_{am}) = \sqrt{(\pi m_{MZ})^2 + \left[\frac{m_{DML}}{2}\left(1 - \frac{m_{MZ}}{m_{MZ} + \varepsilon_{am}}\right)\right]^2} = \\ = \sqrt{\pi^2 m_{MZ}^2 + \frac{m_{DML}^2}{4} + \frac{m_{DML}^2}{4}\frac{m_{MZ}^2}{(m_{MZ} + \varepsilon_{am})^2} - \frac{m_{DML}^2}{2}\frac{m_{MZ}}{m_{MZ} + \varepsilon_{am}}} \tag{B.2}$$

If we consider the third and fourth term of (B.2), we clearly note that they tend to zero when the absolute value of the amplitude error ε_{am} increases enough, so we can neglect them. Moreover, considering that $\pi^2 \simeq 10$ and, due to the parameters definition, $m_{MZ} \simeq m_{DML}$ for the chosen modulations frequency, we can approximate (B.2) with the

expression

$$A = \sqrt{\pi^2 m_{MZ}^2 + \frac{m_{DML}^2}{4}} = \pi m_{MZ} \cdot \sqrt{1 + \frac{m_{DML}^2}{4\pi^2 m_{MZ}^2}} \simeq$$
$$\simeq \pi m_{MZ} \cdot \left(1 + \frac{m_{DML}^2}{8\pi^2 m_{MZ}^2}\right) = \pi m_{MZ} \cdot (1 + \delta) \tag{B.3}$$

Obviously, we can generalize this formula as

$$A(\varepsilon_{am}) \simeq \pi m_{MZ} \cdot [1 + \delta(\varepsilon_{am})] \tag{B.4}$$

Therefore, asymptotically we get to a condition where we actually have the correct amplitude, but this is modified by a little term depending just on the amplitude modulation indices m_{DML} and m_{MZ}. This latter contribution, even if small, is enough to see the rapid OSSR drop highlighted in Section 4.2. However, at the same time it is not big enough to cause an OSSR reduction until values close to zero or even zero itself.
For what concerns the phase, we could demonstrate something very similar. We don't go though all the calculations, but we just report the final result:

$$\Phi(\varepsilon_{am}) = \arctan\left\{\tan\left(\phi_{PM} - \frac{\pi}{2}\right) - \frac{m_{DML}}{2\pi m_{MZ}\sin(\phi_{PM})} + \right.$$
$$\left. + \frac{m_{DML} m_{MZ}}{2\pi m_{MZ}(m_{MZ} + \varepsilon_{am})\sin(\phi_{PM})}\right\} \simeq$$
$$\simeq \arctan\left\{\tan\left(\phi_{PM} - \frac{\pi}{2}\right) + \beta(\varepsilon_{am})\right\} \rightarrow \arctan\left\{\tan\left(\phi_{PM} - \frac{\pi}{2}\right) + \beta\right\} \tag{B.5}$$

that is completely similar to what we have obtained for the amplitude[1]. Note that all this analysis is made without any assumption on the sign of the sum $m_{MZ} + \varepsilon_{am}$, so the conclusions are totally general, as long as the error absolute value is big enough.

[1]This calculation is actually the result of the sum between two sines, as the operations is easier. So, the $\pi/2$ that appears in (B.5) is due to the fact that the resulting sinusoid is a sine and its role is to go back to a cosine.

List of Figures

List of Tables

List of acronyms

Alphabetic order

ADC: Analog-to-Digital Converter
AWG: Arbitrary Waveform Generator
BER: Bit Error Rate
BS: Beam Splitter
B2B: Back-to-Back
B-PD: Balanced Photodiode
C: Capacity
CP: Cyclic Prefix
CW: Continuous Wave
DAC: Digital-to-Analog Converter
DCA: Decomposition and Cancellation Algorithm
DFB: Distributed Feedback (laser)
DFT: Discrete Fourier Transform
DML: Directly Modulated Laser
DMT: Discrete Multitone
DSB: Dual Sideband
DSP: Digital Signal Processing
EAM: Electro-Absorption Modulator
EDFA: Erbium Doped Fiber Amplifier
EML: Externally Modulated Laser
EVM: Error Vector Magnitude
E/O: Electro-Optical (conversion)
FFT: Fast Fourier Transform
ICI: Inter-Carrier Interference
IFFT: Inverse Fast Fourier Transform
IL: Insertion Loss
IM: Intensity Modulator

IM-DD: Intensity Modulation - Direct Detection
IP: In-Phase
ISI: Inter-Symbol Interference
KK: Kramers-Kronig
LO: Local Oscillator
LSB: Lower Sideband
MZ: Mach-Zehnder
NEC: Noise Equivalent Current
OCT: Orthogonal Circulant Matrix
OF: Optical Filter
OFDM: Orthogonal Frequency Division Multiplexing
OOK-NRZ: On-Off Keying - Non Return-to-Zero
OOK-RZ: On-Off Keying - Return-to-Zero
OSSR: Optical Sideband Suppression Ratio
O/E: Opto-Electrical (conversion)
PAM: Pulse Amplitude Modulation
PAPR: Peak-to-Average Power Ratio
PBS: Polarizing Beam Splitter
PD: Photodiode (or Photodetector)
PhD-CD: Phase Diversity - Coherent Detection
PP: Push-Pull (configuration)
PRBS: Pseudo-Random Bit Sequence
PSK: Phase Shift Keying
P2P: Point-to-Point
P/S: Parallel-to-Serial
Q: Quadrature
QAM: Quadrature Amplitude Modulation
RF: Radio-Frequency
RMS: Root Mean Square
SE-PD: Single Ended - Photodiode
SNR: Signal-to-Noise Ratio
SQRT: Square Root (algorithm)
SSB: Single Sideband
SSBI: Signal-Signal Beat Interference
SSBI-C: Signal-Signal Beat Interference - Cancellation
SSMF: Standard Single Mode Fiber
S/P: Serial-to-Parallel

USB: Upper Sideband
VCSEL: Vertical Cavity Surface Emitting Laser
VOA: Variable Optical Attenuator
VSB: Vestigial Sideband
WDM: Wavelength Division Multiplexing
WF: Water Filling (principle)